ANALYSIS OF THE RADICAL POLYMERIZABILITY OF DIALLYL MONOMERS

by

Nurcan Şenyurt Tüzün

B.S. in Chem. Boğaziçi University, 1996

M.S. in Chem. Boğaziçi University, 1997

Submitted to the Institute for Graduate Studies in
Science and Engineering in partial fulfillment of
the requirements for the degree of
Doctor
of
Philosophy

Boğaziçi University
2002

ACKNOWLEDGEMENTS

ABSTRACT

ANALYSIS OF THE RADICAL POLYMERIZABILITY OF DIALLYL MONOMERS

In this study, the radical cyclopolymerization mechanism of diallylamine and diallyl ether monomers and their derivatives has been investigated by computational modeling. The calculations were performed by the Density Functional Theory using the B3LYP/6-31G* basis set. In the first part of the study, a correlation has been built between the stucture of the monomer and the polymerizability. The experimentally measured ^{13}C NMR chemical shifts of the diallylamine monomers, which were in line with their polymerizabilities, could be successfully correlated to the descriptors derived from calculations. The charges, bond orders, reaction barriers have successfully reproduced the polymerizability trend. In the second and third parts of this study, the regioselectivities and stereoselectivities of ring closure reactions of diallylamine and derivatives have been explained by considering steric and electronic factors. Diallylamine monomers formed 5-membered rings even though the thermodynamically more stable 6-membered rings would be expected to form. It has been shown that the 5-membered rings have lower barriers for cyclization. The fourth part of the study includes the modeling of diallylether monomers and their derivatives. The fast and efficient polymerizability of diallylether monomer has been investigated by considering the similarities and differences between this compound and its amine analogue. In the last part of the study, the competing reactions, homopolymerization and H-transfer reactions, as well as standard cyclopolymerization reactions have been considered. The efficiencies of the competing reactions have been investigated in their relation to the standard cyclopolymerization reactions. Comparison of free energies of activation for cyclopolymerization and competing reactions has shown that competing reactions are less efficient in the case of cationic monomers.

ÖZET

DİALİL MONOMERLERİNİN RADİKAL POLİMERLEŞME EĞİLİMLERİNİN İNCELENMESİ

Bu çalışmada, dialilamin ve dialileter monomer ve türevlerinin, radikal siklopolimerizasyon mekanizması ile gerçekleştirdiği halkalı polimerlerin oluşma tepkimeleri hesapsal yöntemlerle incelendi. Monomer yapısının bu mekanizma üzerindeki etkisi araştırıldı. Modelleme "Density Functional Theory" ile B3LYP/6-31G* seviyesinde gerçekleştirildi. Çalışmanın ilk kısmı monomerin kimliği ile polimerizasyon etkinliği arasında bir ilişkinin geliştirilmesi konusunu kapsamaktadır. Deneysel olarak, iyi polimerleşme özelliği gösteren dialil türevlerinde vinil karbonların ^{13}C NMR sinyalleri ile polimerleşebilme özellikleri arasında bir ilişki saptanmıştır. Bu çalışmada monomerlerin yük dağılımları, bağ mertebeleri, geçiş konumları oluşturmak için gerekli aktivasyon enerjileri ile ^{13}C NMR sinyalleri arasında bir bağlantı oluşturulmuştur. Çalışmanın ikinci ve üçüncü kısımlarında dialilamin ve türevlerinin polimerizasyon tepkimelerinde oluşan halkaların yöresel ve sterik seçiciliklerinin nedenleri araştırıldı. Heteroatom ve zincirin üstündeki sübstitüyentlerin halka oluşturma mekanizmalarına etkileri ele alındı. Termodinamik yönden 6 üyeli halkaların polimer zincirini kararlı kılmaları beklenirken 5 üyeli halkaların oluşması kinetik tercihlerle açıklanmıştır. Beş üyeli halkaların aktivasyon enerjileri daha düşük olduğundan siklik polimerlerde 5-üyeli halkalar oluşmaktadır. Çalışmanın dördüncü kısmı dialileter ve türevlerinin siklopolimerizasyon tepkimelerinin modellemesini içermektedir. Bu kısımda amin/eter gruplarının siklopolimerizasyon tepkimelerinde olası benzerlik ve farklılıkları göz önünde bulundurularak dialileterlerin deneysel olarak gözlemlenen hızlı ve yoğun siklopolimerzasyon tepkimelerinin nedenleri araştırıldı. Çalışmanın son kısmı siklopolimerizasyon tepkimesi esnasında yer alan yan tepkimelerin - homopolimerizasyon, H-transferi- modellemesini içermektedir. Bu kısımda siklizasyon ile yarıştığı bilinen yan tepkimelerin serbest enerjileri ile siklizasyon tepkimesinin açığa çıkardığı serbest enerjiler kıyaslanarak katyonik monomerlerde yan tepkimelerin daha az etkili olduğu gösterildi.

TABLE OF CONTENTS

LIST OF FIGURES

LIST OF TABLES

LIST OF SYMBOLS/ABBREVIATIONS

A	Electron affinity
E	Energy of the sytem
E_b	Electrostatic energy of the positive background
E_c^{VWN}	Vosko-Wilk-Nusair correlation energy
E_T	Kinetic energy
E_V	Potential energy
E_J	Coulomb energy
E_{XC}	Exchange-correlation energy
$E[N, v(\mathbf{r})]$	Electronic energy as a functional of the number of electrons and external potential
$f(\mathbf{r})$	Fukui function
$f^+(\mathbf{r})$	Fukui reactivity index for a nucleophilic attack
$f^-(\mathbf{r})$	Fukui reactivity index for an electrophilic attack
$f^0(\mathbf{r})$	Fukui reactivity index for a radical attack
$\mathbf{F}$	Fock matrix
G	Free Energy
$G^{\neq}$	Free Energy of Activation
h	Planck's constant
$\mathbf{H}$	Hamiltonian operator
H_0	Zero-order Hamiltonian
I	Vertical ionization potential
k	Boltzmann constant
k_c	Rate constant for cyclopolymerization
k_i	Rate constant for homopolymerization
N	Number of electrons
s	Local softness
S	Global softness
$\mathbf{S}_{ij}$	Overlap matrix
$T[\rho]$	Kinetic energy of interacting electrons

$T_s[\rho]$	Kinetic energy of non-interacting electrons
U_{xc}^{λ}	Potential energy of exchange correlation
v	External potential
v($\mathbf{r}$)	Potential imposed by the nuclei at position $\mathbf{r}$
$V_{ee}[\rho]$	Interelectronic interactions
χ	Electronegativity
χ_{σ}	Electron spin
$\Delta\delta$	Chemical shift difference
ε	Dielectric constant
η	Hardness
λ	Interelectronic coupling-strength parameter
μ	Chemical potential
$v_{xc}(r)$	Exchange-correlation potential
$v_{eff}(r)$	External effective potential
$\rho(r)$	Electron density function
Ψ	Wavefunction
Ψ_0	Single-determinant wavefunction
$\Psi_0^{(1)}$	Higher order wavefunction
AM1	Austin Model
AO	Atomic Orbital
B88	Becke88 functional
BLYP	Becke's gradient-corrected exchange functional with Lee-Yang-Parr's gradient-corrected correlation functional
CI	Configuration interaction
CNDO	Complete Neglect of Differential Overlap
DES	Quantum chemical descriptors
DFT	Density Functional Theory
E_a	Activation energy
ΔE_x^{B88}	Becke's gradient correction

$\Delta H^{\neq}$	Enthalpy difference
HOMO	Highest Occupied Molecular Orbital
IRC	Intrinsic Reaction Coodinate
LDA	Local density approximation
LUMO	Lowest Unoccupied Molecular Orbital
LYP	Lee-Yang-Parr correlation functional
MNDO	Modified Neglect of Diatomic Overlap
MO	Molecular Orbital
MP	Møller-Plesset (MP) Perturbation Theory
NAO	Natural Atomic Orbital
NBO	Natural Bond Orbital
NDDO	Neglect of Differential Diatomic Overlap
NHO	Natural Hybrid Orbital
NLMO	Natural Localized Molecular Orbital
NMB	Natural Minimal Basis
NMR	Nuclear Magnetic Resonance
PCM	Polarized Continiuum Model
PM3	Parametric Method Number 3
q_k	Electronic population of atom k
$\Delta S^{\neq}$	Entropy Difference
SCRF	Self-Consistent Reaction Field
TS	Transition State

1. INTRODUCTION

Butler's discovery of polymerization of diallyl compounds via an alternating intramolecular-intermolecular mechanism (Figure 1.1), later named "cyclopolymerization", led to a new field in polymer chemistry [1,2,3]. The discovery has been classified as the eighth major structural aspect of synthetic polymer chemistry [4]. The mechanism served interesting features because the monofunctional counterpart of diallyl monomers, the allyl monomer, has always been considered as a poor monomer for polymerization, whereas the difunctional monomer could be successfully polymerized [5]. Furthermore, the cyclopolymerization mechanism offered synthetic control of properties related to physical and chemical properties of polymers. Since its first discovery, a large number of work has been devoted to cyclopolymerization and the attention on cyclopolymerization has increased over the years. The growing interest is a consequence of the advantageous properties of polymers such as high water solubility, high molecular weight, excellent electrical properties. Commercialization of the resulting polymers was rapid. The most common applications are in the mining industry, paper and textile manufacturing, wastewater-treatment, electrolysis, cosmetics and health care industries and in biological, medical and food applications [4]. The first cyclopolymer that has been manufactured commercially is poly(N,N-dimethyldiallylammonium chloride) and it is the most widely studied diallyl monomer [6]. There are 120 patents related to the applications of poly(N,N-dimethyldiallylammonium chloride) or its copolymers [4].

The cyclopolymerization reaction of diallyl monomers occurs by alternating intramolecular cyclization and intermolecular propagation steps shown in Figure 1.1. The mechanism can be visualized mainly in 4 different steps (Figure 1.1).

i. Initiation

ii. Cyclization

iii. Intermolecular Chain Propagation

iv. Termination

Initiation

Cyclization

exo   endo
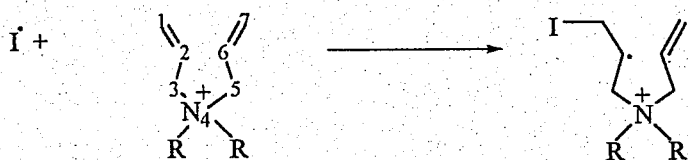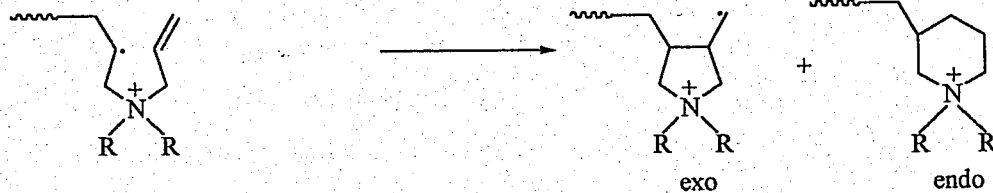
Intermolecular Propagation by the Ring

$= $ ~~~$\dot{M}$
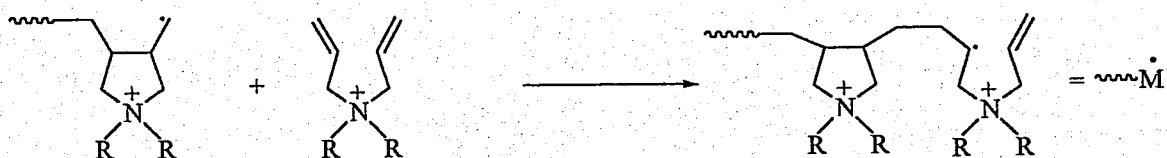
Intermolecular Propagation by the Uncyclized Polymer Chain
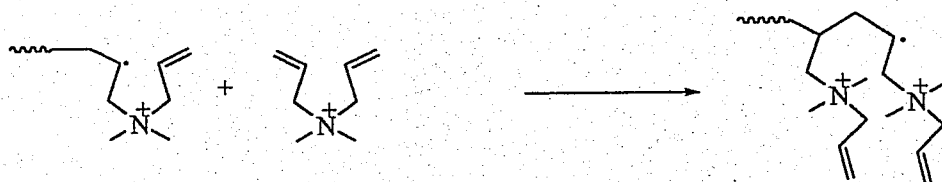
Chain Transfer

Termination
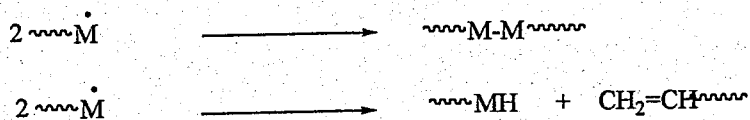
(I= Initiator, M=Monomer)

Figure 1.1. Cyclopolymerization mechanism and competing reactions

The radical polymerization reaction starts by activation of the initiator followed by the attack of the radicalic initiator at C_1. This forms a growing polymer with a secondary radical center at C_2 (Initiation, Figure 1.1). This monomer can attack intermolecularly to another monomer (Homopolymerization, Figure 1.1) and the pendant double bonds can further react to form water insoluble cross-linked polymers. However, Butler discovered that the polymerization of diallylammonium monomers undergo cyclization rather than linear polymerization and form water soluble linear polymers [1, 2, 3]. The growing chain with secondary radical at C_2 attacks intramolecularly to form either a 5-membered (exo) or a 6-membered (endo) ring depending on the site of attack (Cyclization, Figure 1.1). The polymerization then proceeds by further propagation involving intermolecular attack of the growing radical on another monomer (Intermolecular Propagation, Figure 1.1).

In the cyclization step of the polymerization reaction, 5- or 6-membered rings can form depending on the site of attack, C_6 or C_7. The formation of 6-membered (endo) ring was generally expected since a 6-membered ring is more stable than a 5-membered (exo). In addition, formation of the 6-membered ring would involve a secondary radical intermediate in the propagation step, whereas the 5-membered ring generates a primary radical, which is less stable. However, predictions based on thermodynamic control can be misleading because experimental results did not confirm these expectations and kinetic products are often found. [7-10].

The importance of cyclopolymerization lies not only in the properties of the final product but also on its mechanism. The difunctional monomers can be polymerized to high molecular weights although the monofunctional counterparts exhibit very low degrees of polymerization. In general, allyl monomers have a low tendency to polymerize and display a low degree of polymerization [11]. They can only be polymerized with difficulty and they yield polymers of medium molecular weight. The low polymerizability of allyl monomers is attributed to chain transfer processes (Chain Transfer, Figure 1.1) [12]. In the polymerization of allyl monomers, the growing chain involves a secondary radical that is reactive toward H-abstraction. H-abstraction produces a resonance stabilized allyl radical (Equation 1.1), which is less active and has less tendency to initiate a new polymer chain. Thus, chain transfer reactions lower polymerization efficiencies (Chain Transfer, Figure 1.1).

$$CH_2=CH-\overset{\cdot}{C}H-R \leftrightarrow \overset{\cdot}{C}H_2-CH=CH-R \qquad (1.1)$$
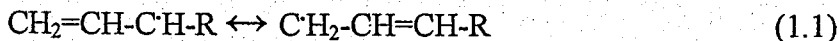
The effect of chain transfer reaction has been confirmed by deuterating the allylic carbon of allyl acetate monomer. This resulted in almost three-times higher rate of polymerization and higher molecular weight products compared to polymerization of non-deuteriated allyl acetate [5].

One of the most important aspect in synthetic polymerization is tailor making of final products. The initial strategy is to design the microstructure of polymers. It is of fundamental importance to start polymerization with monomers that are good candidates for the resulting polymers of desired physical or chemical properties. Thus, foreseeing the reactivity of monomers is a valuable information to save efforts.

In the first part of our study (Section 3), we have predicted the reactivities of a set of diallylamine and diallylammonium monomers, namely, N,N-diallylammine (1), N,N-diallylammonium cation (2), diallyl dimethyl ammonium cation (3), 4-(N,N-diallylamino) pyridine (4), and 4-(N,N-diallylamino) pyridine cation (5) (Figure 1.2). The purpose of this part of the study was to investigate the correlation between the polymerizability trend of diallylamine and diallylammonium monomers and some of their descriptors derived from quantum chemical calculations. The ultimate goal indeed was to build up a sound means of predicting the polymerizability of N,N-substituted-diallyl monomers prior to their synthesis. It was further desirable to provide guideful information to experimentalists in their endeavor to polymerize derivatives of diallyl monomers.
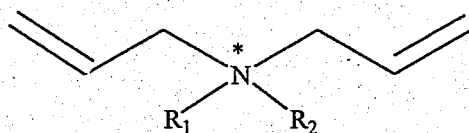
Monomer	R₁	R₂	Charge (*)
1	H	-	0
2	H	H	+1
3	CH₃	CH₃	+1
4	C₅NH₄	0	0
5	C₅NH₅	0	+1

Figure 1.2. Diallylamine and diallylammonium monomers studied in Section 3

In tailor making of final products, control over reaction rate, regioselectivity, stereoselectivity and the degree of cyclization is of fundamental interest in cyclopolymerization. This can be done only by a clear understanding of the factors that govern each step of the cyclopolymerization. In the following sections, we have approached cyclopolymerization in a mechanistic way. In Sections 4-6, main emphasis has been focused on cyclization.

In cyclopolymerization, complete cyclization without any pendant unsaturation is ideal. There are two approaches to facilitate high cyclization. In the first approach, the rate of cyclization can be enhanced, so that cyclization dominates over homopolymerization. In the second approach, intermolecular homopolymerization is suppressed. Use of dilute solutions in cyclopolymerization is based on this idea. In Section 4, the cyclization step of cyclopolymerization has been discussed in details to understand structural factors that influence polymerizability and to determine how it is related to the ease of cyclization. The regioselectivity and stereoselectivity have also been considered. With this purpose, the set of monomers in Figure 1.3 have been considered.
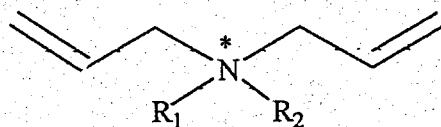
Monomer	R₁	R₂	Charge (*)
1	H	-	0
2	H	H	+
3	CH₃	CH₃	+
6	CH₃	-	0
7	CH₃	H	+

Figure 1.3. Diallylamine and diallylammonium monomers studied in Section 4

In this set of monomers, the influence of a change of nitrogen substitution upon the efficiencies of radical cyclization has been explained and rationalized.

Experimentalists have tried different means of controlling ring size, reaction yield and cyclization efficiency, k_c/k_i, where k_c and k_i are the rate constants for cyclopolymerization and homopolymerization, respectively. In diallyl monomers, usage of monofunctional moieties that do not homolymerize is reported to facilitate cyclization by suppressing homopolymerization [13]. However, high cyclization efficiency was not always accompanied by an increase in polymerization. Thus, it became important to use monomers which have both high cyclization efficiency and high polymerization capability. In that respect, compounds 6 (N-methyl-N,N-diallylamine), 8 (N-methyl- N-allyl-2-(methoxycarbonyl)allylamine) and 9 (N-methyl-N-methallyl-2-(methoxycarbonyl)allylamine) (Figure 1.4) have drawn considerable attention. Kodaira et al. have reported that 8 has both high cyclization efficiency and high cyclopolymerizability [14,15]. Monomers 6 and 8 have been found to undergo five membered cyclization whereas 9 formed six membered rings along with decreased polymerization tendency as compared to 8 [14-16]. These observations were attributed to steric and/or electronic factors due to the ester and methyl substitution on the C=C double bonds. In Section 5, a mechanistic study of the intramolecular cyclization reactions for 6, 8 and 9 is reported.

The steric and electronic effects of methyl and acetate substitution on the double in the cyclization efficiency of N-methyl-N,N-diallylamine is discussed. The regioselectivity of ring closure has also been considered. The computational findings have been compared with the experimental polymerizabilities.
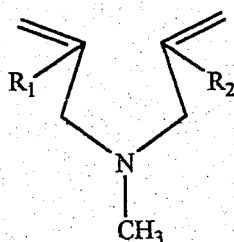
Monomers	R_1	R_2
6	H	H
8	$COOCH_3$	H
9	$COOCH_3$	CH_3

Figure 1.4. The monomers studied in Section 5

In most of the cases, the polymerization of non-symmetrical diallyl monomers was governed by the non-allyl counterpart [17]. The non-allyl monofunctional counterpart of methyl α-(allyloxymethyl)acrylate (11) (Figure 1.5), namely alkyl α-propoxymethylacrylate is reported to have high homopolymerization [18]. In that respect, monomer 11 was not expected to have a high polymerizability due to the principle mentioned above, but the experiments did not confirm these predictions. Almost complete cyclization and high radical polymerizability of monomer 11 even in bulk was observed [18,19]. Although inconclusive, the high cyclization of 11 has been explained experimentally by the conformational preferences of the monomer favoring cyclopolymerization [19].

Monomer	R
10	H
11	COOCH$_3$
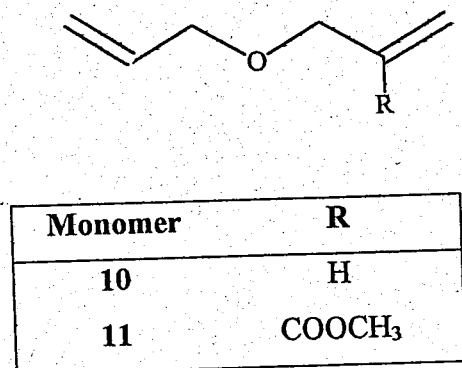
Figure 1.5. Diallylether monomers modeled in Section 6

In Section 6, the cyclization of monomers **10** and **11** in their cyclopolymerization mechanism has been discussed with a quantum mechanical approach to account for their cyclopolymerizabilities. We have explained the conformational preferences of the monomers prior to cyclization and have demonstrated their effect in cyclization. The regioselectivity and stereoselectivity of monomers have also been discussed. The effect of ester substitution has been inquired and finally, the experimental data has been compared with the calculations.

Although diallyl monomers are employed in various cyclopolymerization and cyclocopolymerization processes and great effort has been spent on tailor-making of the final products, all aspects of cyclopolymerization and factors that control different pathways and reactions of cyclopolymerization are not clear yet. In Sections 4-6 we have discussed the cyclization of diallyl monomers in their cyclopolymerization reaction, based on quantum mechanical calculations. The regioselectivities and stereoselectivities have been explained by considering steric and electronic factors. In Section 7, we have analyzed the cyclization and intermolecular propagation steps of the cyclopolymerization mechanism, based on kinetic and thermodynamic approaches. In addition to cyclization and intermolecular propagation reactions, the competing reactions and their ability to overcome the efficiency of standard cyclopolymerization steps have been modeled and discussed. Two representative monomers, N-diallylamine (**1**) and N,N-dimethyl-N, N-diallylamonium (**3**) are chosen for this study. This choice is based on the fact that the

[20]. Additionally, **1** has very low polymerizability while **3** has good polymerization efficiency [21]. In general, cationic monomers polymerize better than neutrals and this has been attributed to high chain transfer efficiency of neutral monomers [5]. In compound **3**, the effect of the positively charged allylic substituent has been discussed in comparison to the neutral compound **1**.

2. THEORY

The electronic structure methods use the laws of quantum mechanics. The energy and other related properties of a molecule may be obtained by solving the Schrödinger Equation

$$\mathbf{H}\Psi = E\Psi \qquad (2.1)$$

where, Ψ, the wavefunction describes the x, y and z spatial coordinates of the particles in the system, E is the energy of the sytem at that state and $\mathbf{H}$ is the Hamiltonian operator to derive the kinetic and potential energy of a sytem. Exact solutions are not computationally practical for large molecules. Approximations are introduced to electronic structure methods. The mostly encountered three major classes of electronic structure methods are:

- Semi-empirical methods, they use parameters derived from experimental data. Different semi-empirical methods are characterized by their different parameters.
- Ab initio methods, no experimental parameters are used.
- Density functional methods, the total energy of the system only depends on the electron density.

2.1. Semi-empirical Theory

The difficulty of performing ab-initio calculations on large molecules led to develop semi-empirical methods. In semi-empirical models, rather than solving all the integrals of the Schrödinger equation, parameters originating from experimental data are used. Semi-empirical models can be used to yield continuous energy surfaces. They are neither variational nor size consistent. More importantly, semi-empirical methods are inherently dependent on the choice of parameters. The parameterization is tested against a limited set of molecules to ensure its accuracy. This dependence on parameters can be minimized by using a large and varied training set of molecules to establish parameters. Like numerical iteration, this process is a continuing one. Parameters are introduced in order to reproduce

experimental equilibrium geometries, heats of formation, electric dipole moments and ionization potentials.

In solving Schrödinger equation, the number of off-diagonal one-electron integrals rapidly becomes very large and computationally burdensome. To handle this task, the approximation was made to set the overlap integrals to zero. With this assumption the secular determinant for the Hartree-Fock method reduces to

$$| \mathbf{F} - E | = 0 \qquad (2.2)$$

The Fock matrix, $\mathbf{F}$, here is the sum of the usual one-electron and two-electron positions. The latter presents a particularly difficult hurdle since the number of integrals of the form

$$\iint \Psi_i (1) \, \Psi_j (2) \, (1/r_{12}) \, \Psi_k (1) \, \Psi_l (2) \, \delta\tau (1) \, \delta\tau (2) \qquad (2.3)$$

are encountered where r_{12} is the distance between the particles. The overlap assumption sets these integrals to zero except in the case where i=j and k=l. The assumption led to the designation of CNDO [22], complete neglect of differential overlap. An additional assumption was that the off-diagonal resonance integral H_{ij} could be made proportional to the overlap integral i.e., although the overlap matrix disappears, values are still assigned to certain S_{ij} to allow evaluation of the H_{ij} and for later computation of charge distribution. A somewhat later upgrade in the parameterization was forthcoming under the tittle CNDO/2. Although the CNDO methods did not introduce electron-electron repulsions, they do not handle the question of the interactions between electrons with parallel and anti-parallel spins, especially when the electrons are on the same atom. NDDO (Neglect of Differential Diatomic Overlap) model is another semi-empirical model. This theory neglects differential overlap between atomic orbitals on different atoms [22]. The first practical NDDO method was introduced by Dewar and Thiel [23] in 1977, called "modified neglect of diatomic overlap" (MNDO). This model was parameterized on experimental molecular geometries, heats of formation, dipole moments and ionization potentials. The MNDO model is a very successful model, but it has also some limitations in reproducing hydrogen bonding successfully.

In this study, the semi-empirical PM3 model [24,25] which is the third parameterization of the original MNDO model is used. This is a NDDO method which utilizes more adjustable parameters for the core-core repulsion term. In PM3, all quantities that enter the Fock matrix and the total energy expressions have been treated as pure parameters. To accomplish this task of optimizing parameters an automatic procedure was introduced, allowing a parameter search over many elements simultaneously. This model employs minimal basis of Slater type orbitals. For hydrogen 1s, for first row elements 2s, 2p and for second row elements 3s and 3p orbitals are used.

Each atom is characterized through 13-16 parameters that are present in AM1 and additionally five parameters that define the one-center, two-electron integrals. In PM3, the parameters were optimized using an automatic optimization routine that used a large set of reference molecular data. It is the most precisely parameterized semi-empirical model but again it has some limitations. Lone-pair lone-pair repulsions are not always well represented in these methods and care must be taken.

2.2. Ab-initio Methods

The variational calculations of a system starts by writing a Hamiltonian operator for the system. Then a trial wavefunction, Ψ, is selected. The wavefunction must have variable parameters. The energy of the sytem is minimized by varying parameters. The term "ab-initio" means "from the beginning", indicating that the steps of writing Hamiltonian, selecting a trial wavefunction and minimization of parameters are performed. In ab initio method, the Hamiltonian and the wavefunction have been defined, the effective electronic energy can be found by use of the variational method. In the variational method, the best wavefunction is found by minimizing the effective electronic energy with respect to parameters in the wavefunctions.

Common levels of ab initio theory include Hartree-Fock. Hartree-Fock replaces the many electron problem by a one electron problem. The electron-electron repulsion is treated in an average way in these methods.

2.3. Density Functional Theory

Density Functional Theory (DFT) [26] is an approach to the electronic structure of atoms and molecules based upon a theory presented by Hohenberg and Kohn in 1964 which states that all the ground-state properties of a system are functions of the charge density. The DFT methods achieve significantly greater accuracy than Hartree-Fock theory at only a modest increase in cost. Although both methods account for the instantaneous interactions of pairs of electrons with opposite spin, DFT methods include the effects of electron correlation (electrons in a molecular system react to one another's motion and attempt to keep out of another's way) while Hartree-Fock calculations see this effect in an average sense (each electron sees and reacts to an averaged electron density) [27].

Density functional methods partition the electronic energy into several terms and compute them separately.

$$E = E_T + E_V + E_J + E_{XC} \qquad (2.4)$$

E_T is the kinetic energy term, E_V is the potential energy of the nuclear-electron attraction and nuclear-nuclear repulsion term, E_J is the electron-electron repulsion term (also called Coulomb energy), E_{XC} is the exchange-correlation term that includes the remaining part of the electron-electron interactions.

All the terms except the nuclear-nuclear repulsion, are functions of electron density, $\rho(r)$. E_{XC} can be divided into exchange and correlation functionals. E_{XC} accounts for the exchange energy arising from the antisymmetry of the quantum mechanical wavefunction and the dynamic correlation in the motions of the individual electrons.

In 1964, Hohenberg-Kohn provided the proof (DFT based methods ultimately derive from quantum mechanics research from the 1920's especially the Thomas-Fermi-Dirac model and may be regarded as an approximation to the exact theory) that DFT is in fact an exact theory for describing the electronic behavior of matter. The variational principle determines the ground state energy and electron density in terms of the electron density.

Further, the ground state electron density $\rho(r)$ determines the external potential, $v(r)$ and variationally determines the ground state properties of the system of interest.

The electronic energy can be expressed as a functional of the electron density:

$$E[\rho] = \int v(r)\rho(r)dr + T[\rho] + V_{ee}[\rho] \qquad (2.5)$$

where $T[\rho]$ is the kinetic energy of interacting electrons and $V_{ee}[\rho]$ is the interelectronic interactions.

The electronic energy may be written in the form of Kohn-Sham approach.

$$E[\rho] = \int v(r)\rho(r)dr + T_s[\rho] + J[\rho] + E_{xc}[\rho] \qquad (2.6)$$

This is based upon an orbital density description that removes the necessity of knowing the exact form of $T[\rho]$. Kohn-Sham proposed focusing on the kinetic energy of non-interacting system of electrons $T_s[\rho]$, as a functional of a set of single particle orbitals that give exact density.

$$T_s[\rho] = \sum_{i=1}^{N} \left\langle \Psi_i \left| -\frac{1}{2}\nabla^2 \right| \Psi_i \right\rangle \qquad (2.7)$$

$J[\rho]$ represents the electron-electron repulsion (Coulomb energy), and $E_{xc}[\rho]$ is the exchange-correlation energy functional with its functional derivative called the exchange-correlation potential, $v_{xc}(r)$.

$$E_{xc}[\rho] = T[\rho] - T_s[\rho] + V_{ee}[\rho] - J[\rho] \qquad (2.8)$$

$$v_{xc}(r) = \frac{\partial E_{xc}[\rho]}{\partial \rho(r)} \qquad (2.9)$$

$E_{xc}[\rho]$ is divided into two parts, namely an exchange functional, $E_x[\rho]$ and a correlation functional, $E_c[\rho]$.

$$E_{xc}[\rho] = E_x[\rho] + E_c[\rho] \qquad (2.10)$$

$E_x[\rho]$ and $E_c[\rho]$ functionals can be both local or gradient-corrected functionals. Local or gradient-corrected functionals are called traditional functionals. Local functionals depend only on electron density ρ, while gradient-corrected fuctionals depend on both ρ and its gradient, $\Delta\rho$.

A system of non-interacting electrons moving in an external effective potential $v_{\text{eff}}(r)$ is shown as;

$$v_{\text{eff}}(r) = v(r) + \frac{\partial J[\rho]}{\partial\rho(r)} + \frac{\partial E_{xc}[\rho]}{\partial\rho(r)} = v(r) + \int \frac{\rho(r')}{|r-r'|}dr' + v_{xc}(r) \qquad (2.11)$$

Now, an equation very similar to the Schrödinger Equation exists.

$$\left[-\frac{1}{2}\nabla^2 + v_{\text{eff}}(r) \right]\Psi_i = \varepsilon_i\Psi_i \qquad (2.12)$$

(2.6), (2.7), (2.8), (2.9), (2.10), (2.11) are Kohn-Sham Equations.

In order to evaluate the exchange-correlation functional some approximations are made. The first one is the local density approximation (LDA). It is based upon a model of uniform electron gas. In the uniform electron gas model, a large number of electrons uniformly spread out in a cube where there is a uniform distribution of the positive charge to make the system neutral. It assumes that the charge density varies slowly throughout the molecule so that a localized region of the molecule behaves like a uniform electron gas The energy expression is:

$$E[\rho] = T_s[\rho] + \int \rho(r)v(r)dr + J[\rho] + E_{xc}[\rho] + E_b \tag{2.13}$$

where E_b is the electrostatic energy of the positive background. Since the positive charge density is the negative to the electron density the equation reduces to:

$$E[\rho] = T_s[\rho] + E_{xc}[\rho] = T_s[\rho] + E_x[\rho] + E_c[\rho] \tag{2.14}$$

The exchange functional is given by:

$$E_x[\rho] = -C_x \int \rho(r)^{4/3} dr \tag{2.15}$$

$C_x = 0.7386$, this form was developed to reproduce the exchange energy of a uniform electron gas. However, it has weaknesses in describing molecular systems.

So, Becke formulated the gradient-corrected exchange functional

$$E_x = E_x^{LDA} - \beta \sum_\sigma \int \rho_\sigma^{4/3} \frac{x_\sigma^2}{1 + 6\beta x_\sigma \sinh^{-1} x_\sigma} dr \tag{2.16}$$

where χ_σ denotes the electron spin, $x_\sigma = \dfrac{|\nabla \rho_\sigma|}{\rho_\sigma^{4/3}}$ and β is an empirical constant ($\beta = 0.0042$) chosen to fit the exchange energies of the inert gas atoms. This functional is known as Becke88 (B88) functional.

The adiabatic connection formula is :

$$E_{xc} = \int_0^1 U_{xc}^\lambda d\lambda \tag{2.17}$$

where λ is an interelectronic coupling-strength parameter and U_{xc}^λ is the potential energy of exchange correlation at intermediate coupling strength. This formula connects the non-

interacting Kohn-Sham reference system (λ=0) to the fully interacting real system (λ=1). This formula has been approximated by Becke as [28]:

$$E_{xc} = \frac{1}{2}E_x + \frac{1}{2}U_{xc}^{LDA} \qquad (2.18)$$

since $U_{xc}^0 = E_x$, the exact exchange energy and $U_{xc}^1 = U_{xc}^{LDA}$. This exchange functional is called the Becke half-and-half functional.

The correlation functional used in this study is the Lee-Yang-Parr (LYP) correlation functional. The closed shell LYP functional is given by [29]:

$$E_c = -a\int \frac{1}{1+d\rho^{-1/3}}\left\{\rho + b\rho^{-2/3}\left[C_F\rho^{5/3} - 2t_w + (\frac{1}{9}t_w + \frac{1}{18}\nabla^2\rho)\right]e^{-c\rho^{-1/3}}\right\}dr \quad (2.19)$$

where,

$$t_w = \frac{1}{8}\frac{|\nabla\rho(r)|^2}{\rho(r)} - \frac{1}{8}\nabla^2\rho \qquad (2.20)$$

and a=0.04918, b=0.132, c=0.2533 and d=0.349.

DFT methods are defined by pairing an exchange functional with a correlation functional and can be named as traditional or hybrid functionals. Hybrid functionals include the exact term in the exchange functional, whereas traditional functionals do not.

BLYP (Becke's gradient-corrected exchange functional with Lee-Yang-Parr's gradient-corrected correlation functional) method is a traditional functional [30] whereas, B3LYP (Becke style three parameter functional in combination with the Lee-Yang-Parr correlation functional) method, the linear combination of LDA, B88, E_x^{exact} and LYP functionals, is a hybrid functional. [31]:

$$E_{xc} = E_{xc}^{LDA} + a_0(E_x^{exact} - E_x^{LDA}) + a_x \Delta E_x^{B88} + a_c \Delta E_c^{non-local} \qquad (2.21)$$

where ΔE_x^{B88} is the Becke's gradient correction, i.e. the second term at the right hand side of the equation 2.16 and the correction to the correlation ($\Delta E_c^{non-local}$) is provided by the Lee-Yang-Parr functional. But, LYP includes both local and non-local terms, then the correlation functional used is actually: $a_c E_c^{LYP} + (1 - a_c)E_c^{VWN}$ where E_c^{VWN} is the Vosko-Wilk-Nusair correlation energy. The parameters are specified by Becke by fitting the atomization energies, ionization potentials, proton affinities and first row atomic energies in the molecule set, a_0=0.20, a_x=0.72 and a_c=0.81. Hybrid functionals have proven to be superior to the traditional functionals.

2. 3. 1. Basis Sets

The basis sets used in quantum mechanical calculations are composed of atomic functions. The molecular orbitals are expressed as linear combination of a pre-defined set of one-electron functions called basis functions. The most convenient way is to use atomic orbitals as basis functions. Among the types of the basis sets (minimal basis sets, split valence basis sets, polarized basis sets, high angular momentum basis sets) the most popular one is the split valence basis set which is developed by Pople and his group [32] termed as K-MNG. 4-31G, 5-31G, 6-31G. In split valence basis sets, each inner shell is represented by a single basis function taken as a sum of K Gaussian functions and each valence orbital is split into two parts, an inner part described by M Gaussians and an outer part described by N Gaussians. Split valence basis sets allow orbitals to change size not the shape. Polarized basis sets remove this limitation by adding orbitals with angular momentum beyond the ground state configuration for each atom. In this study 6-31G*, also known as 6-31G(d) polarization basis set is used where d functions are added to heavy atoms.

2. 4. Møller-Plesset (MP) Perturbation Theory[33]

The Hartree-Fock theory fails to adequately represent electron correlation. In the self consistent field method, the electrons are assumed to move in an average potential of the other electrons. The position of electron is not influenced by the presence of a neighboring electron. However, this is not the exact picture. The electrons are correlated and they tend to avoid each other more than the Hartree-Fock theory finds. This lowers the energy. Configuration interaction (CI) is the most popular way of including electron correlation in the molecular orbital calculations. According to CI, better description of overal wavefunction is possible by a linear combination of the ground and excited wavefunctions. In general, the CI wavefunction can be written as

$$\Psi = c_0 \Psi_0 + c_1 \Psi_1 + c_2 \Psi_2 + \dots \tag{2.22}$$

Ψ_0 is single-determinant wavefunction. It is obtained by solving the Hartree-Fock equation. Ψ_1, Ψ_2... are wavefunctions, which are expressed as determinants. These wavefunctions represent configurations in which one or more of the occupied orbitals are replaced by virtual orbitals. The energy is then minimized by determining the coefficients by a variational approach.

Møller and Plesset proposed an alternative way to deal with the electron correlation problem [34]. In this method, the true Hamiltonian is defined by the sum of zero-order Hamiltonian, H_0 and a perturbation, v.

$$H = H_0 + \lambda v \tag{2.23}$$

λ is a parameter that can vary between 0 and 1. The eigenfunctions and eigenvalues E_i of H are expanded, the wavefunction and eigenvalues in terms of perturbation is

$$\Psi_i = \Psi_i^{(0)} + \lambda \Psi_i^{(1)} + \lambda^2 \Psi_i^{(2)} \dots \tag{2.24}$$

$$E_i = E_i^{(0)} + \lambda E_i^{(1)} + \lambda^2 E_i^{(2)} \dots \tag{2.25}$$

$E_i^{(1)}$ is the first order correction to the energy, $E_i^{(2)}$ is the second-order correction and so on. These energies can be calculated from the eigenfunctions as follows:

$$E_i^{(0)} = \int \Psi_i^{(0)} H_0 \Psi_i^{(0)} d\tau \tag{2.26}$$

$$E_i^{(1)} = \int \Psi_i^{(0)} v \Psi_i^{(0)} d\tau \tag{2.27}$$

$$E_i^{(2)} = \int \Psi_i^{(0)} v \Psi_i^{(1)} d\tau \tag{2.28}$$

$$E_i^{(3)} = \int \Psi_i^{(0)} v \Psi_i^{(2)} d\tau \tag{2.29}$$

The wavefunction to a given order must be determined to find the corrections to the energy. To improve the Hartree-Fock energy it is necessary to use Møller-Plesset perturbation at least to second order. This level is referred to as MP2 and involves the integral $\int \Psi_0^{(0)} v \Psi_0^{(1)} d\tau$. The higher order wavefunction, $\Psi_0^{(1)}$, is expressed as linear combinations of solutions to the zero-order Hamiltonian.

$$\Psi_0^{(1)} = \sum_j c_j^{(1)} \Psi_j^{(0)} \tag{2.30}$$

The $\Psi_j^{(0)}$ in equation 2.30 will include single, double, etc., excitations obtained by promoting electrons into the virial orbitals obtained from a Hartree-Fock calculations. The second order energy is given by:

$$\sum_i^{occupied} \sum_{j>i} \sum_a^{virtual} \sum_{b>a} \frac{\iint d\tau_1 d\tau_2 \chi_i(1) \chi_j(2)(1/r_{12})[\chi_a(1)\chi_b(2) - \chi_b(1)\chi_a(2)]}{\varepsilon_a + \varepsilon_b - \varepsilon_i - \varepsilon_j} \tag{2.31}$$

The Møller-Plesset perturbation theory is size independent but not variational and sometimes gives energies that are lower than the true energy. Especially, MP2 is the most popular way of incorporating electon correlation in quantum mechanical calculations.

2.5. Reactivity Descriptors

Reactivity and its relation to structure and properties have been of importance to theoretical chemists. Although the accurate electronic wave function potentially contains all the necessary information, the computation of the wave function and consequently properties is a complex numerical task even by the standards of modern computation. In this context, the density functional theory (DFT), based on the basic variable of three-dimensional electronic density, has introduced simplifications [35, 26]. Many of the well known, empirical but important, chemical concepts such as the chemical potential (μ), electronegativity (χ), hardness (η) and softness (S) appear naturally within the framework of DFT. This not only provides them with a new status, but also gives a rigorous way for estimating their actual values. In general, these quantities correspond to the linear responses of the electron density with respect to changes in external potential (v) and number of electrons (N). These global parameters help understanding the behavior of a system and lead to widely applicable and useful principles such as the principle of maximum hardness. In a more local approach, the parameters mentioned above also emerge as a useful tool for rationalizing, interpreting and predicting diverse aspects of chemical bonding and reaction mechanism.

If electronic energy is defined as a functional of the number of electrons and external potential, E [N, v(r)], these perturbations can be obtained by a series of derivatives of the energy. Perturbations due to changes in the number of electrons are defined as "global" properties [36] and are related to overall molecular stability. Perturbations due to changes in external potential are called as "local" properties [36] and determine the site selectivity of a molecule for a specific reaction type.

2.5.1. Global Descriptors

The chemical potential (μ) is a global property that determines the extent of a reaction.

$$\mu = \delta E \, [N, v(r)] \, / \, \delta N \qquad (2.32)$$

Electronegativity (χ) is defined as the negative of chemical potential:

$$\chi = -\mu \qquad (2.33)$$

Hardness is a global property described as the resistance to change in electron distribution [37] which determines the stability of a molecule. It is expressed as

$$\eta = \delta\mu / \delta N = \delta^2 E\,[N, v(\mathbf{r})] / \delta N^2 \qquad (2.34)$$

where $v(\mathbf{r})$ is the potential imposed by the nuclei at position $\mathbf{r}$. A finite difference approximation yields

$$\eta = (I\text{-}A) / 2 \qquad (2.35)$$

where I is the vertical ionization potential and A the electron affinity. Furthermore, in the molecular orbital theories where the Koopman's theorem is valid,

$$\eta = (\varepsilon_{LUMO} - \varepsilon_{HOMO})/2 \qquad (2.36)$$

where ε_{LUMO} and ε_{HOMO} are the LUMO and HOMO orbital energies of the species, respectively. Therefore hardness is proportional to the HOMO-LUMO gap and large η should imply stability for the chemical species.

Global softness (S) is expressed as the inverse of global hardness:

$$S = 1 / \eta \qquad (2.37)$$

2.5.2. Local Descriptors

Local softness (s) describes local perturbation in terms of electron density ($\rho(r)$) with respect to a global change in chemical potential, μ:

$$s(r) = \delta\rho(r) / \delta\mu \qquad (2.38)$$

The Fukui function, $f(r)$, is a space-dependent local function and "*it measures how sensitive a system's chemical potential is to an external perturbation at a particular point*" [26]. It also gives information about a quantity related to the electron density of an atom or molecule in its frontier regions [26, 38]:

$$f(r) = (\delta\mu / \delta v(r))_N = (\delta\rho(r) / \delta N)_{v(r)} \qquad (2.39)$$

These two local properties are related to each other [39] through global softness, S:

$$s(r) = f(r) S \qquad (2.40)$$

Since, however, $\delta\rho(r) / \delta N$ is a discontinuous function of N, it will have one value from the right, one from the left and an average at some integral value of N:

$$f^+(r) = [\delta\rho(r) / \delta N]^+ \qquad \text{(as N goes from } N_0 \text{ to } N_0 + \delta) \qquad (2.41)$$

$$f^-(r) = [\delta\rho(r) / \delta N]^- \qquad \text{(as N goes from } N_0 - \delta \text{ to } N_0) \qquad (2.42)$$

$$f^0(r) = 1/2 \, [f^+(r) + f^-(r)]^0 \qquad \text{(average)} \qquad (2.43)$$

where $f^+(r)$ is the reactivity index for a nucleophilic attack, $f^-(r)$ for an electrophilic attack and $f^0(r)$ for a radical attack. Within the finite difference approximation, these relationships can be written as

$$f^+(r) = \delta\rho_N(r) - \delta\rho_{N-1}(r) \tag{2.44}$$

$$f^-(r) = \delta\rho_{N+1}(r) - \delta\rho_N(r) \tag{2.45}$$

$$f^0(r) = \tfrac{1}{2}[\delta\rho_{N+1}(r) - \delta\rho_{N-1}(r)] \tag{2.46}$$

A more convenient way of calculating the $f(r)$ functions is to use the condensed Fukui functions obtained from the previous equations, when integrated over the kth atomic region for the nucleophilic, electrophilic and radical attacks, respectively.

$$f^+ = q_k(N+1) - q_k(N) \tag{2.47}$$

$$f^- = q_k(N) - q_k(N-1) \tag{2.48}$$

$$f^0 = \tfrac{1}{2}[q_k(N+1) - q_k(N-1)] \tag{2.49}$$

Here q_k is the electronic population of atom k in the molecule under consideration. It is known that these descriptors are generally used to probe the regio-selective nature of a reaction.

2.6. Polarized Continiuum Model (PCM)

Chemical problems in the liquid state are diverse and there are different approaches to treat these problems of solvent effects:

i.   virial equations of state, correlation functions
ii. Monte Carlo or molecular dynamics simulations
iii. Continuum treatments
iv. Molecular treatments

Continuum models typically form a cavity of some sort containing the solute molecule and the solvent outside the cavity is thought of as a continuous medium. The solvent is categorized by a limited amount of physical data, such as the dielectric constant. The electric field of the charged particles comprising the solute interact with this background medium, producing a polarization in it, which in turn feeds back upon the solute's wavefunction.

A simple continuum model is the Onsager cavity model, often called the Self-Consistent Reaction Field, or SCRF model [40]. This represents the charge distribution of the solute in terms of a multipole expansion. SCRF usually uses an idealized cavity (spherical or ellipsoidal) to allow an analytic solution to the interaction energy between the solute multipole and the multipole which this induces in the continuum.

Polarizable Continuum Model (PCM) is a much more sophisticated continuum method [41-43]. The PCM method places a solute in a cavity formed by a union of spheres centered on each atom. PCM also includes a more exact treatment of the electrostatic interaction with the surrounding medium, as the electrostatic potential of the solute generates an 'apparent surface charge' on the cavity's surface. The computational procedure divides this surface into small tesserae, on which the charge (and contributions to the gradient) are evaluated. Typically the spheres defining the cavity are taken to be 1.2 times the van der Waals radii. A technical difficulty caused by the penetration of the solute charge density outside this cavity is dealt with by a renormalization. The solvent is characterized by its dielectric constant, surface tension, size, density, and so on. Procedures are provided not only for the computation of the electrostatic interaction of the solute with the apparent surface charges, but also for the cavitation energy, and dispersion and repulsion contributions to the solvation free energy.

2.7. Natural Bond Orbital Analysis

The Natural Bond Orbital (NBO) analysis [44-48] gives a simple and intuitive picture of the wavefunction, ideal for making theory meaningful and useful. The analysis provides useful information such as charges, bond types, hybrid directions, resonance weights, bond orders and other familiar valence descriptors. NBO analysis is based on a

method for optimally transforming a given wavefunction into localized form, corresponding to the one-center ("lone pair") and two-center ("bond") elements of the chemist's Lewis structure picture.

The concept of "natural" orbitals was first introduced by Löwdin to describe the unique set of orthonormal 1-electron functions $\theta(r)$ that are *intrinsic* to the N-electron wavefunction $\Psi(1, 2, ..., N)$. Mathematically, the $\theta(r)$s can be considered as *eigen*orbitals of Ψ (or, more precisely, of Ψ's first-order reduced density operator), and they are therefore "best possible" (most rapidly convergent, in the mean-squared sense) for describing the electron density $\rho(r)$ of Ψ hence they are "natural" in the sense of Löwdin, having optimal convergence properties for describing the electron density.

In a system of two H atoms,

$$\Psi_2 = \Psi(H_A, H_B) \tag{2.50}$$

The orbital description of Ψ_2 is nearly identical to that for for the corresponding localized wavefunctions

$$\Psi_{1A} = \Psi(H_A) \text{ and } \Psi_{1B} = \Psi(H_B) \tag{2.51}$$

The natural orbitals of Ψ_2 will be found to differ qualitatively from those of Ψ_{1A} or Ψ_{1B}, because Ψ_2 must incorporate superposition symmetry [49] between H_A and H_B. This results in making orbitals look more delocalized. Thus, the natural orbitals, as originally defined include bogus "delocalization effects" that have no physical significance. To remove the effects associated with symmetry adaptation, a localized criterion for analogous maximum-occupancy (natural) character in localized 1-center and 2-center regions of the molecule can be formulated [44, 50]. The set of high occupancy NBOs, each taken doubly occupied, is considered to represent most accurate possible "natural Lewis structure" of the molecule.

The NBOs are one of a sequence of natural localized orbital sets that include natural atomic (NAO), hybrid (NHO), and (semi-)localized molecular orbital (NLMO) sets, intermediate between basis AOs and canonical molecular orbitals (MOs).

$$AOs \rightarrow NAOs \rightarrow NHOs \rightarrow NBOs \rightarrow NLMOs \rightarrow MOs \qquad (2.52)$$

All of these natural localized sets are complete and orthonormal. They are able to *exactly* describe any property of Ψ. As compared to standard AOs, the NAOs give a much more condensed description of Ψ, ("minimal basis") with only a small number having appreciable occupancy. Thus, a "minimal" description in terms of core and valence-shell NAOs is often found adequate for chemical purposes, providing a compact representation of Ψ that is intimately related to standard valence concepts. In other word, the condensation of occupancy in the natural localized orbitals leads to partitioning into high and low occupancy orbital types. The small set of most highly-occupied NAOs, is referred to as the "natural minimal basis" (NMB) set. The NMB (core + valence) functions are distinguished from the weakly occupied "Rydberg" (extra-valence-shell) functions. Rydberg functions complete the span of the NAO space, but they make little contribution to molecular properties. Likewise, in the NBO space, the highly occupied NBOs of the natural Lewis structure can be distinguished from the "non-Lewis" antibond and Rydberg orbitals that complete the span of the NBO space.

Each bonding NBO σ_{AB} can be written in terms of two directed valence hybrids (NHOs) h_A, h_B on atoms A and B, with corresponding polarization coefficients c_A, c_B,

$$\sigma_{AB} = c_A\, h_A + c_B\, h_B \qquad (2.53)$$

This is in accordance with the simple bond orbital picture. The polarization coefficients vary depending on covalent and ionic character of the bond, such that it may be covalent with ($c_A = c_B$) or ionic ($c_A \gg c_B$) or in between this limit. Each valence bonding NBO must in turn be paired with a corresponding valence antibonding NBO to complete the span of the valence space.

$$\sigma_{AB}^* = c_B\, h_A - c_A\, h_B \qquad\qquad (2.54)$$

The "Lewis"-type (donor) NBOs (2.53) are thereby complemented by the "non-Lewis"-type (acceptor) NBOs (2.54) that are formally empty in an idealized Lewis structure picture. Weak occupancies of the valence antibonds (2.54) show departures from an idealized localized Lewis structure picture, i.e., true "delocalization effects." The energetic stabilization due to such $\sigma \rightarrow \sigma*$ donor-acceptor interactions can be estimated by 2nd-order perturbation theory. For example, for a $\sigma_i \rightarrow \sigma_j^*$ interaction, the stabilization energy E(2) associated with delocalization is estimated as:

$$E(2)=\Delta E_{ij}=q_i\, (\, F\, (i,j^*)^2)\, /\, (\, \varepsilon_{j^*} - \varepsilon_i\,) \qquad\qquad (2.55)$$

Where q_i is the donor orbital occupancy, F is the orbital Hamiltonian (Fock or Kohn-Sham operator), $F\,(i,j^*)$ is the off-diagonal NBO Fock matrix elements, $\varepsilon_i = <\sigma_i\,|\,F\,|\,\sigma_i>$, $\varepsilon_{j^*} = <\sigma_j^*\,|\,F\,|\,\sigma_j^*>$ are the respective orbital energies of donor and acceptor NBOs. Thus, by considering the valence antibonds (2.54) therefore leads to far-reaching extension of elementary Lewis structure concepts to encompass leading delocalization corrections in simple NBO perturbative estimates such as Eq. (2.55).

The NBO methods and terminology are increasingly recognized as standard in theoretical presentations. High numerical stability and rapid convergence insure maximum reliability and efficiency of the theoretical description. The NBO program is implimented in many programs that calculate electronic structure, such as Gaussian, Jaguar, Gamess, PQS and QChem.

3. PREDICTING POLYMERIZABILITIES OF DIALLYLAMINE AND DIALLYLAMMONIUM MONOMERS

Making an educated guess on the reactivity of monomers to obtain a specific polymer product is an important task, because foreseeing the reactivity of monomers is a valuable information to save efforts. In the literature, there are reports on the reactivity of allyl and vinyl compounds, and very few on diallyl compounds.

Kinetic studies on the reactivity of allyl monomers ($CH_2=CHCH_2X$) by Zubov *et al.* [11] have shown a correlation between the radical polymerizability and the nature of the functional group X of the monomer in radical polymerization. They report that the rate of polymerization depends on the nature of the functional group in the allylic position; the more electron-withdrawing the allylic group, the less efficient the hydrogen abstraction from the allylic CH_2 [11]. The polymerization efficiency of the monomers is correlated to pK values of the allylic substituent. The pK value is defined as the inverse logarithm of the dissociation constant of the acid derived from the corresponding conjugated base.

The behaviour of vinyl and acrylic monomers with the chemical structure $CH_2=CR_1R_2$ in polymerization is influenced by the polar character of the olefinic double bond and the resonance effects associated with the electronegativity of the substituents [51,52]. In another study on vinyl compounds, the π electron density is reported to affect the ^{13}C NMR chemical shift of the α and β ($H_2C_\beta=C_\alpha R_1R_2$) carbons [53]. This is also related to the reactivity of the vinyl compounds: a lower electron density on the β-carbon of the monomer leads to an easier electron transfer from the propagating polymer radical to the monomer [54]. This results in a higher reactivity of the monomer.

Later in 1992, Gollard *et al.* have studied the kinetic behavior of the free radical polymerization of N-[4-(methacryloyloxy)phenyl]-2-(4-methoxyphenyl)acetamide and N-[4-[[(4-methoxyphenyl)acetyl]oxy]phenyl]methacrylamide ($H_2C_\beta=C_\alpha(CH_3)COR$) [53]. The charge densities calculated by the semi-emipirical PM3 and AM1 methods have been

related to the reactivity of monomers. The less negative charge density of the β-carbon has enhanced the reactivity of the monomer.

In a study of N, N-disubstituted methacrylamides ($H_2C_\beta=C_\alpha RR'$) and related compounds, ^{13}C NMR chemical shifts of the C=C double bonds are summarized. It has been reported that the $\delta_{C\alpha}$ and $\delta_{C\beta}$ values shift to a higher and lower magnetic field, respectively, with a linear relationship when polymerization efficiency of monomers increase with the increasing electron-attracting power of the substituents [17]. This showed that the difference in ^{13}C NMR chemical shifts ($\Delta\delta$) of C_α and C_β reflect the influence of substituents more effectively than their absolute values.

Vaidya and Mathias have reported a structure-reactivity relationship for the homopolymerizability of various diallylamine and diallylammonium monomers [21]. Their aim was to develop easily applied techniques to predict polymerizability. Mathias et al. have polymerized various diallylamines (Figure 3.1) and built up a correlation between ^{13}C NMR chemical shift differences of the vinyl carbons and their polymerizability. The same study includes a relationship between the quantum mechanical (MINDO/3) structural and energetical features of these compounds and their polymerizabilities.
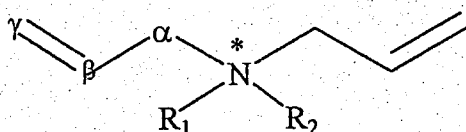
Monomer	R_1	R_2	Charge (*)
1	H	-	0
2	H	H	+1
3	CH_3	CH_3	+1
4	C_5NH_4	0	0
5	C_5NH_5	0	+1

Figure 3. 1. Diallylamine and diallylammonium monomers analyzed in Section 3

It was shown that as the electron-withdrawing ability of the allylic substituent increases, the β-carbon and γ-carbon peaks shift upfield and downfield, respectively (Figure 3.1). This implies that β and γ peaks get closer as the electron-withdrawing ability of the allylic substituent increases. Table 3.1 shows a decrease in chemical shift difference, Δδ (Δδ=δγ−δβ), between allylic carbons with increasing electron-withdrawing ability of allylic substituents. A smaller chemical shift difference reflects polarization away from the double bond and the connecting CH₂ groups. This reduces chain transfer of hydrogens on the connecting CH₂ groups and high molecular weight polymers are produced. The Δδ values were correlated to the polymerizabilities of the monomers such that monomers with Δδ less than 7.5 ppm were easily polymerized, while those with Δδ values higher than 17 ppm polymerized poorly. The Δδ value from 7.5 to 17 ppm is the transition region from good polymerizability to poor polymerizability. Similar results were observed for ester vs. ether derivatives of α-hydroxymethyl acrylates, with the former displaying smaller chemical shift differences and giving much higher molecular weight polymers than the latter [55].

Table 3.1. The polymerizability and chemical shift difference ($\Delta\delta = \delta_\gamma - \delta_\beta$) data of diallylamines in Figure 3.1 [21]

Monomer	R_1	R_2	$\Delta\delta = \delta_\gamma - \delta_\beta$ (ppm)	Polymerizability
1	H	-	19.1	Very poor
2	H	H	3.1	Good
3	CH₃	CH₃	3.0	Very good
4	C₅NH₄	0	16.4	Very poor
5	C₅NH₅	0	12.4	Moderate

In the first part of our study, we have predicted the reactivities of a set of diallyamine and diallylammonium monomers. The purpose of this part of the study was to investigate the correlation between the polymerizability trend of diallylamines and some of their descriptors derived from quantum chemical calculations.

The following steps have been achieved throughout this study

i.   computational modeling of five diallylamines, namely N,N-diallylammine (**1**), N,N-diallylamine hydrochloride (**2**), diallyl dimethyl ammonium chloride (**3**), 4-(N,N-diallylamino) pyridine (**4**), and 4-(N,N-diallylamino) pyridine hydrochloride (**5**) (Figure 3.1);

ii. correlation of experimental polymerizability to calculated monomeric descriptors such as charge distribution, energy barrier for cyclization, bond order, local softness values, HOMO-LUMO gaps

iii. establishment of a mathematical relation between the polymerizability of the monomers, represented by the experimental value of their chemical shifts ($\Delta\delta$) and the descriptors derived from quantum chemical calculations. The ultimate goal indeed was to build up a sound means of predicting the polymerizability of N,N-substituted-diallylammonium halide monomers prior to their synthesis.

3.1.Methodology

3.1.1. Computational Modeling

The most stable conformer for each of the selected diallylamine monomers shown in Figure 3.1 was determined by carrying out a conformer search using the semi-empirical PM3 [24, 25] method using the SPARTAN 5.1.1 [56] package. The counterions of the cationic monomers are excluded in calculations. All possible stationary geometries for the structures located as minima along the potential energy surfaces were generated by free rotation around single bonds. The number of conformers for each compound is 3^n, where n is the number of C-C or C-N single bonds. Thus, one would have to deal with a very large number of conformers for a given compound. Analysis of the structures located as local minima along the potential energy surfaces revealed that appreciable changes in the geometry produced only slight changes in energy. Having decided not to consider the structure corresponding to the global minimum only, we were focused on those structures,

which lay within a pre-selected energy threshold. Accordingly, we decided to consider the distribution of structures among energy levels within 3 kcal/mol from the global minimum. The probability for each conformer to exist in the proposed energy range was calculated using the Boltzmann distribution. The population of states among energy levels was determined by:

$$N_i / N_j = e^{-(E_i - E_j) / kT} \qquad (3.1)$$

where, N_i and N_j refer to the population, E_i and E_j are the energies of states i and j, k is the Boltzmann constant and T is the temperature. The relative probability of each state was found by computing the ratio of N_i to N_T, where $N_T = \Sigma N_j = \Sigma e^{-E_j/kT}$. The next step was to calculate weighted averages for each descriptor by multiplying the relative probability of each energy state by the corresponding value of the descriptor. This was followed by summing up over all states, which lay within 3 kcal/mol from the global minimum. The monomeric descriptors discussed in what follows are Boltzmann averages derived from semi-empirical calculations.

In the intramolecular propagating step of the polymerization reaction (Figure 1.1), there is a long polymer chain at the first position. For simplicity and in order to reduce the computational cost, the long polymer chain is replaced by a hydrogen atom as if it had been initiated by H radical and will be referred to as "living monomer" (Figure 3.2).

Propagating Polymer Chain   Living Monomer
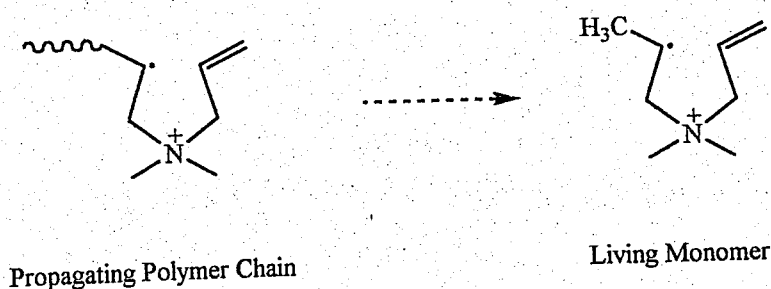
Figure 3.2. Model for the living polymer

To find the minimum energy conformer for this living monomer, a conformer search was performed along the potential energy surface for **2** by using SPARTAN 5.1.1 [57] package with the semi-empirical PM3 method. Different substituents were inserted on nitrogen atom and then optimized, starting with the global minimum of **2** geometry. These 3-dimensional structures were used as representative living monomers (Figure 3.3). To model the cyclization reaction and find the geometric, thermodynamic and kinetic parameters for the intramolecular cyclization reaction, these living monomers and the transition state structures for 5- and 6-membered cyclization reactions were located for all the monomers studied. All the plausible transition state structures, *cis-* or *trans-* orientations in the 5-membered ring and chair or boat conformations in 6-membered ring, were located. The nature of the transition state structures was confirmed by one imaginary frequency belonging to the forming bond. Nevertheless, the transition states with the minimum energy of activation were selected for each monomer since the reactions proceed along the lower barrier pathway. Figure 3.4 displays the 3-dimensional structures of the transition states of minimum energy of activation with Mulliken charges on C_1, C_2, C_6, C_7, N and some critical distances.

The local and global softness calculations were performed on the monomers by using Mulliken atomic charges. Although electrostatic charges were used to calculate the average charges in the monomers, it is common practice to use Mulliken charges to calculate local softness. The local softness values for C_6 are shown in Table 3.4.

In the intermolecular reaction, there is an attack from ring structure to another monomer. The difference in energies of the HOMO of the incoming radical and LUMO of allyl monomer have been analyzed in order to investigate an effective overlap between the two (Table 3.4). For the intramolecular reaction, the HOMO-LUMO energy differences of the representative living monomers have been also tabulated in Table 3.4.

Throughout the discussion, the numbering system in Figure 1.1 has been employed.

3.1.2. Mathematical Modeling

The correlation between the polymerizability of diallylamine monomers and their quantum chemical descriptors was established by constructing a non-linear regression model with one dependent and multiple independent variables. The dependent variable was defined as the chemical shift in β and γ carbons, depicted from the experimental work of others [21]. The independent variables were made of a set of monomer-specific descriptors estimated by PM3 calculations and corresponding to the two symmetric structures around β and γ carbons, respectively. Hence, two models were defined for each monomer as:

$$\delta_\beta = A_\beta + B_\beta f(DES_1)_\beta + C_\beta f(DES_2)_\beta + D_\beta f(DES_3)_\beta + ... \qquad (3.2)$$

$$\delta_\gamma = A_\gamma + B_\gamma f(DES_1)_\gamma + C_\gamma f(DES_2)_\gamma + D_\gamma f(DES_3)_\gamma + ... \qquad (3.3)$$

where, δ_β and δ_γ are the chemical shifts in β and γ carbons, respectively; $f(DES_1)_{\gamma,\beta}$, $f(DES_2)_{\gamma,\beta}$, $f(DES_3)_{\gamma,\beta}$,... are linear or non-linear functions of the quantum chemical descriptors defined by DES_i; and $A_{\gamma,\beta}$, $B_{\gamma,\beta}$, $C_{\gamma,\beta}$, $D_{\gamma,\beta}$ are the parameters of the models, the subscripts referring to β and γ cases. The input data for the independent variables consisted of bond lengths, atomic charges, heats of formation and energy of activation. The statistical significance of each variable in terms of their contributions to the proposed correlation was tested within 95% confidence limits, and those variables with insignificant contributions were discarded from the model. Once the variables of the best representative model were selected, the model was tested for reliability by computing δ_β and δ_γ values of an arbitrarily selected diallylamine sample, using the estimated values of model parameters. All regression analyses were carried out by using the non-linear subroutine of a statistical package program [57].

3.2. Discussion

3.2.1. Descriptors Derived from Calculations

It has been shown experimentally that the polymerizability trend depends on the nature of the substituents attached to nitrogen atom [21]. The structural parameters, bond orders, charges, heats of formation, local softness values, energy barriers to polymerization reaction were considered as plausible descriptors for the polymerizability of diallylamines. Throughout the discussion that follows, these descriptors will be discussed. The numbering system is the same as the one adopted in Figure 1.1.

3.2.1.1 <u>Charges.</u> The average electrostatic charge on C_1 was found to decrease in the order: **1>4>5>3>2** (Table 3.2). Since the experimental polymerizabilities of the monomers are in the reverse order (Table 3.1) [21], it follows that the smaller the electron density distribution on C_1, the better the polymerizability.

Table 3.2. The Average Electrostatic Charges on Atoms calculated with PM3

	1	2	3	4	5
C_1	-0.20	-0.03	-0.04	-0.16	-0.09
C_2	-0.18	-0.21	-0.26	-0.18	-0.22
C_1-C_2	-0.02	0.18	0.22	0.02	0.13
C_6	-0.22	-0.22	-0.17	-0.20	-0.21
C_7	-0.17	-0.03	-0.05	-0.15	-0.09
C_7-C_6	0.05	0.19	0.12	0.05	0.12
N	-0.76	0.63	0.58	-0.64	-0.10

The trend in experimental polymerizability is perfectly reproduced in our calculations except for the exchange in the orders of **2** and **3**, in which the charges on C_1 are very close (–0.03 and –0.04, respectively). The long-range delocalization of charges depends on the substituents such that the charge on C_1 is more positive for the most electron-withdrawing allylic substituent. The situation is similar for C_7, which is

symmetric to C_1. The charge on C_7 reflects the polymerizability trend as in the case of C_1 and the orders of **2** and **3** are interchanged again due to very close values of charge distributions (-0.03 and –0.05, respectively).

The electron density on C_2 was also found to be an indicator of polymerizability. The calculated charges on C_2 are given in the following order of increasing electron-density: **3>5>2>4=1**. This order is in agreement with the experimental polymerizability trend, except for **2** and **5**, (whose orders are exchanged), in which electron distributions are almost equivalent (-0.21 and –0.22, respectively) (Table 3.2).

During the intramolecular cyclization, the electron rich center is more prone to be attacked by a radical. The electrostatic charge distribution has shown C_2/C_6 to be richer in negative charge distribution than C_1/C_7. This computational finding is in agreement with the experimentally observed 5-membered cycles instead of 6-membered ones during the cyclopolymerization.

Furthermore, the calculated charge difference between the vinyl carbons is an excellent replicator of the experimental polymerizability trend, shown in Table 3.1. As the electrostatic charge difference between C_1 and C_2 (C_1-C_2), and C_6 and C_7 (C_6-C_7) atom pairs increases, the polymerizabilities of the monomers of interest also increase. Hence, the difference of charges on double bond carbons was found to be higher for the monomers that polymerized well and lower for the poorly polymerizing monomers.

Another indicator of polymerizability is the electrostatic charge on the nitrogen atom (Table 3.2). The calculated electrostatic charges on nitrogen atoms in order of decreasing electron densities are as **1>4>5>3>2**. This trend mimics the experimental tendency for polymerizability of the monomers. Vaidya *et al.* have also correlated the electron-withdrawing ability of allylic substituents with their polymerizabilities [21]. The electrostatic charge on nitrogen is indicative of the electron-withdrawing ability of the monomer. The order of decreasing nitrogen charges in the studied monomers reflects the decreasing electron-withdrawing capacity, implying also a decreasing trend in polymerizability.

3.2.1.2 Energetics and Rate. The minimum energy structures for reactants and the transition states of the cyclization reaction are displayed in Figure 3.3 and Figure 3.4, respectively.
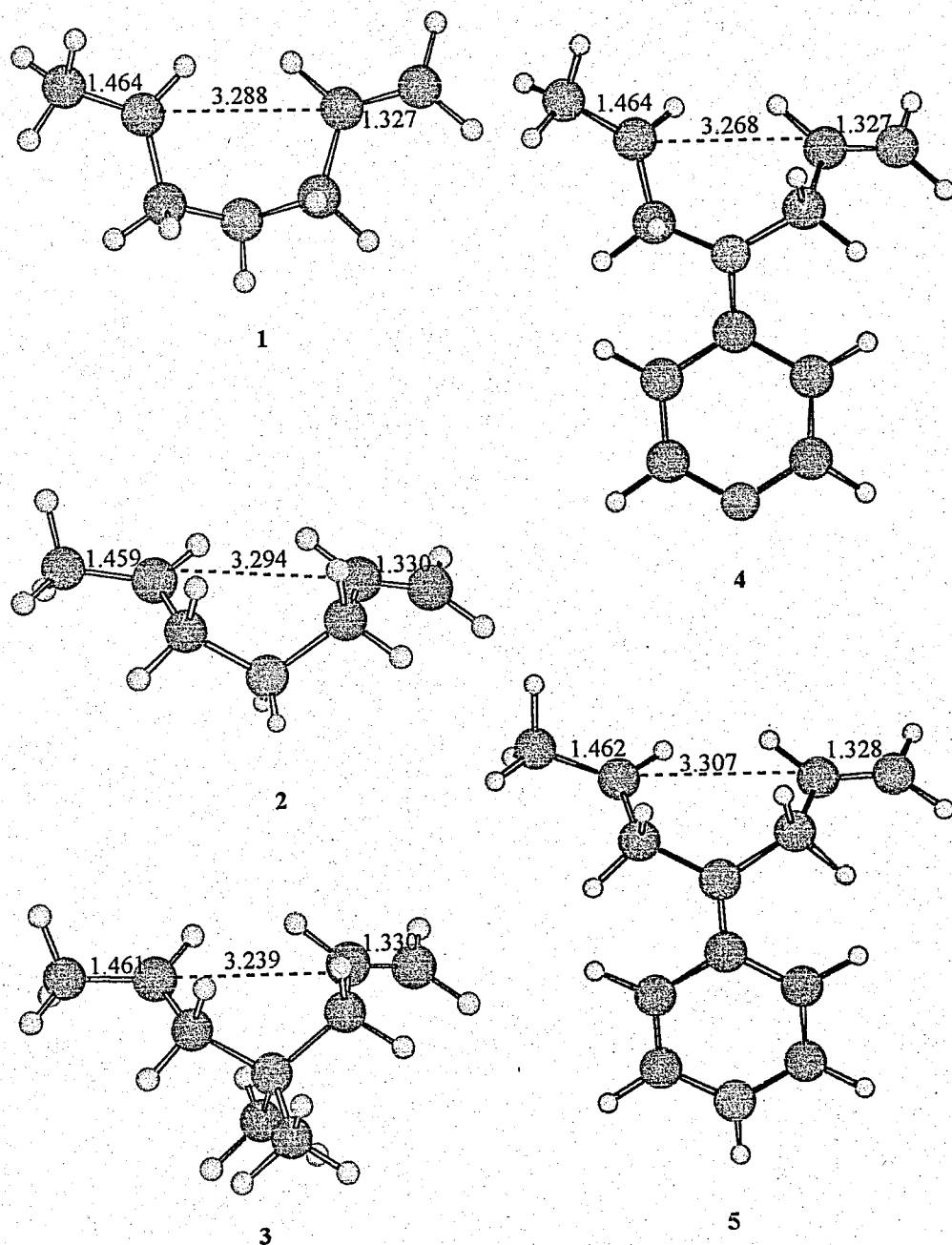
Figure 3.3. The 3-dimensional structures for the living monomers of **1-5** as models to reactants
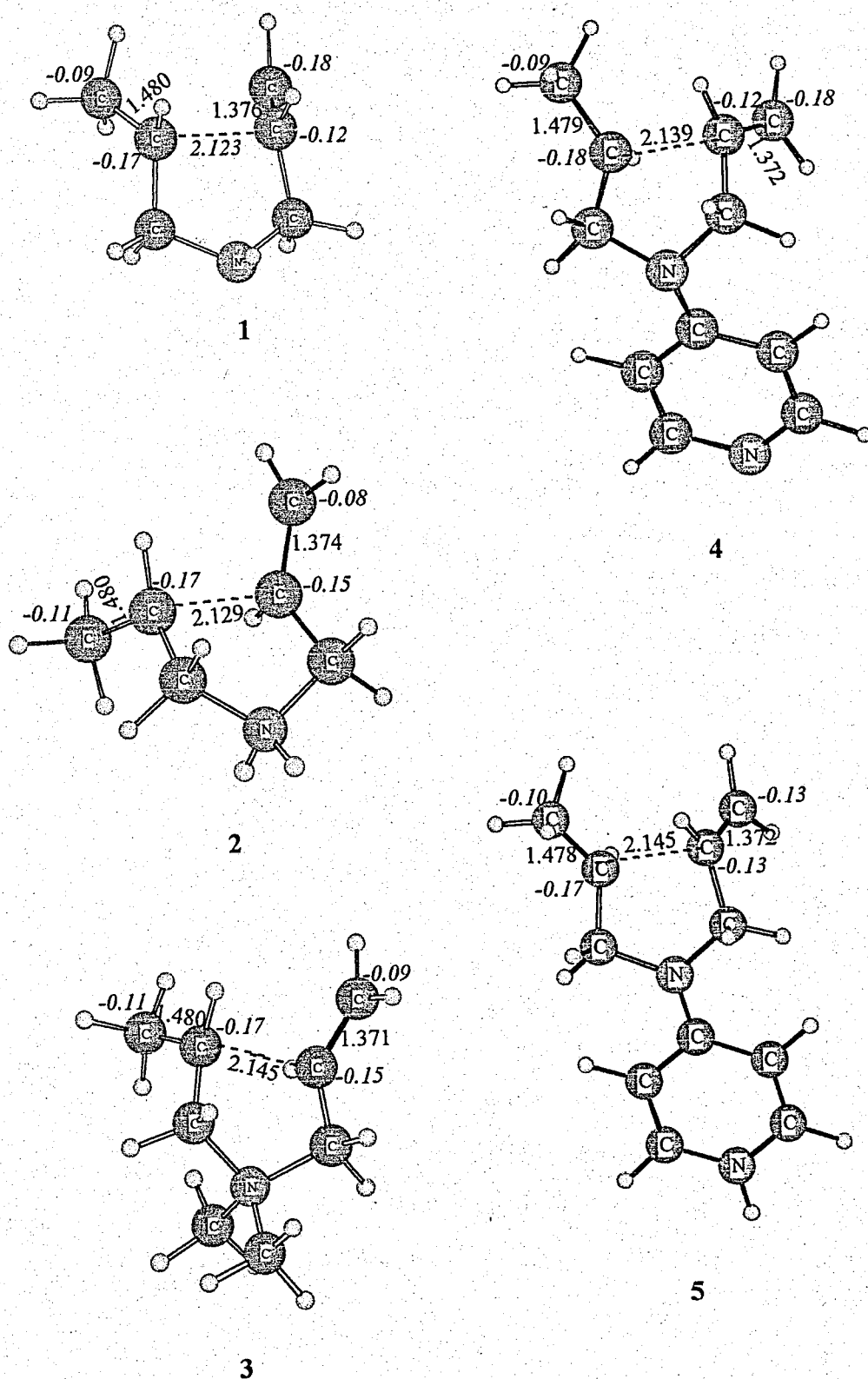
Figure 3.4. The 3-dimensional transition state structures of minimum activation energy for intramolecular cyclization reactions

In all of the monomers studied, the C—C distance for the forming bond in the transition state structures is ~2.1 Å. The plausible transition state structures for 5- and 6-membered rings leading to cyclization reactions have higher heats of formation for 6-membered ring formation. Except for **1**, all the monomers have the lowest heat of formation of transition state structure for 5-membered ring formation as reported by experiments [7-10] (Table 3.3). Additionally, it was reported experimentally that the rings had a *cis:trans* ratio of 6:1 [7- 9] and 3-4:1 [10] for **3** in different studies. With the semi-empirical PM3 calculations, the dominating ring streochemistry was *trans*, in contrast to experimental findings.

Table 3.3. Energetics and kinetics for the intramolecular cyclization reaction (T=298.15°K)

Energetic and Kinetic Data	1	2	3	4	5
E_a [a] (kcal/mol)	9.8	10.51	7.5	9.1	10.83
E_a+ZPE [b] (kcal/mol)	9.61	10.45	7.88	11.67	10.50
$\Delta H^\ddagger$ [c] (kcal/mol)	8.79	9.61	6.78	10.39	9.85
$\Delta H^\ddagger$ + ZPE [d] (kcal/mol)	8.60	9.55	7.16	12.96	9.52
$\Delta S^\ddagger$ [e] (cal/mol)	-9.38	-9.98	-13.02	-12.38	-7.49
$\exp(-E_a/RT)$	$6.54*10^{-8}$	$1.97*10^{-8}$	$3.18*10^{-6}$	$2.13*10^{-7}$	$1.15*10^{-8}$
$\exp(-(E_a+ZPE)/RT)$	$9.02*10^{-8}$	$2.18*10^{-8}$	$1.67*10^{-6}$	$2.79*10^{-9}$	$2.02*10^{-8}$
$\exp(-\Delta H^\ddagger/RT)$	$3.60*10^{-7}$	$9.02*10^{-8}$	$1.07*10^{-5}$	$2.40*10^{-8}$	$6.01*10^{-8}$
$\exp(-(\Delta H^\ddagger+ZPE)/RT)$	$4.96*10^{-7}$	$9.98*10^{-8}$	$5.64*10^{-6}$	$3.14*10^{-10}$	$1.06*10^{-7}$
$\exp(-E_a/RT)*\exp(\Delta S^\ddagger/RT)$	$5.83*10^{-10}$	$1.30*10^{-10}$	$4.53*10^{-9}$	$4.20*10^{-10}$	$2.65*10^{-10}$
$\exp(-(E_a+ZPE)/RT)*\exp(\Delta S^\ddagger/RT)$	$8.03*10^{-10}$	$1.44*10^{-10}$	$2.39*10^{-9}$	$5.48*10^{-12}$	$4.67*10^{-10}$
$\exp(-\Delta H^\ddagger/RT)*\exp(\Delta S^\ddagger/RT)$	$3.21*10^{-9}$	$5.94*10^{-10}$	$1.53*10^{-8}$	$4.73*10^{-11}$	$1.39*10^{-9}$
$\exp(-(\Delta H^\ddagger+ZPE)/RT)*\exp(\Delta S^\ddagger/RT)$	$4.42*10^{-9}$	$6.57*10^{-10}$	$8.04*10^{-9}$	$6.17*10^{-13}$	$2.44*10^{-9}$

[a] Ea= Activation Energy
[b] E_a+ZPE= Activation Energy with Zero-Point Energy
[c] $\Delta H^\ddagger$= Enthalpy Difference
[d] $\Delta H^\ddagger$ + ZPE= Enthalpy Difference with Zero-Point Energy
[e] $\Delta S^\ddagger$= Entropy Difference

The activation energies, calculated by using the energetics of transition states, were considered as indicators of barriers to cyclization reactions. The activation energies for **2, 3, 5** reproduced the polymerizability trend (Table 3.3). The trend was further improved when the zero point energies were taken into account, except for **1**, which did not fit into the expected trend. The enthalpy of activation, $\Delta H^{\ne}$, showed the same trend as the energy of activation. The entropies of activation, $\Delta S^{\ne}$, were also calculated to see their effect on the pre-exponential factor, A, in the rate equation. The rate of a reaction is described as:

$$Rate = A* e^{-Ea/RT} \tag{3.3}$$

The pre-exponential factor, A, is proportional to the entropy of activation exponentially, such that:

$$A= (kT/h)*e*e^{\Delta S_{\ne}/R} \tag{3.4}$$

where, k is the Boltzmann constant, h is the Planck's constant. The product of the pre-exponential factor with the exponential factor did not reproduce the expected trend qualitatively. It may be that the entropy does not play a significant role in predicting the rate of polymerization or the rigid rotor and harmonic oscillator approximations used in calculating the thermodynamic parameters are not adequate approximations for the molecules selected.

3.2.1.3 Bond Order.

The bond order of the forming bond between C_2 and C_6 atoms, in the intramolecular cyclization reaction of the propagating living monomer was in the order of 0.01103, 0.01038, 0.01028, 0.0995 and 0.0989 for **3, 2, 5, 4** and **1** (Table 3.4), respectively. These values indicate that the higher the bond order, the more eager the monomer is for bond formation and the more polymerizable it is.

3.2.1.4. Local Softness.

One of the descriptors of polymerizability was found out to be the local softness (s), tabulated in Table 3.4. The local softness values of C_6, which is the site of attack for the 5-membered ring formation in the cyclization reaction, showed that there was a 10-fold decrease from monomers of high polymerizability to low polymerizability.

This indicated the sensitivity of C_6 to a radical attack and hence reproduced the polymerizability trend.

Table 3.4 . Quantum mechanical descriptors

Descriptor	1	2	3	4	5
Bond Order for C_2--C_6	0.00989	0.01038	0.01103	0.00995	0.01028
f_{C6}	0.06	0.075	0.075	0.07	0.05
S	0.099	0.781	0.896	0.112	1.695
S_{C6}	0.0069	0.0585	0.0672	0.0067	0.0847
ΔE_I [a]	10.138	1.281	1.117	8.918	0.590
ΔE_{II} [b]	10.346	-0.039	-0.080	8.997	0.015

[a]: ΔE_I= $HOMO_{reactant}$ - $LUMO_{reactant}$
[b]: ΔE_{II}= $HOMO_{ring}$ - $LUMO_{monomer}$

3.2.1.5. HOMO-LUMO Gaps. The HOMO-LUMO difference in a chemical system can be considered as a measure of its resistance to changes in electronic configuration. Large HOMO-LUMO gaps are known to provide great stability and low reactivity to a chemical species. In the intramolecular propagating step of polymerization reaction, there is a transfer of the unpaired electron from the incoming radical to the olefinic bond. This transfer is accomplished by mixing of the α-odd electron with the LUMO of olefinic bond. The HOMO-LUMO energy differences for the propagating living monomer, ΔE_I, are much larger for monomers polymerizing poorly whereas this difference is quite small for good polymerizing monomers (Table 3.4).

In the intermolecular step during polymerization, the HOMO from the propagating radicalic ring structure, which is the donor of electron, will interact with another monomer, which is the acceptor. This HOMO-LUMO interaction may take place more efficiently when the energy gap between the two molecular orbitals, ΔE_{II}, is small. The gap between the HOMO of the 5-membered ring and the LUMO of the unattacked diallyl monomer reflected the polymerization trend perfectly. The gap is very small for monomers of high

polymerizability indicative of easier mixing of these orbitals. The gap is significantly larger for monomers of low polymerizability.

3.2.2 Correlation of Monomeric Descriptors with Polymerizability

The input data for estimating the parameters of the proposed models initially consisted of all the calculated descriptors of the five diallylamines in concern, and the experimentally determined chemical shifts in β and γ carbons. In the first step, a stepwise regression analysis was performed to exclude those descriptors (if any) with statistically insignificant contributions to the proposed models, represented by Equations 3.2 and 3.3. In accordance, it was found that the only significantly contributing descriptors were the electrostatic charges on C_1, C_2, C_6, C_7 and N. Furthermore, the model was found to improve statistically when the carbon-related charge variables were represented by two arithmetic means: as that of C_1 and C_7 (named C1C7) and C_2 and C_6 (named C2C6). The reduced set of input variables after elimination of non-contributing independent variables is presented in Table 3.5. Note that the variable N represents the charge on nitrogen.

Table 3.5. Final input data for estimating model parameters

Monomer	Dependent Variable		Independent Variables		
	δ_γ	δ_β	DES_1 (C1C7)	DES_2 (C2C6)	DES_3 (N)
1	117.6	136.7	-0.19	-0.20	-0.76
2	125.0	128.1	-0.03	-0.22	+0.63
3	125.4	128.4	-0.05	-0.22	+0.58
4	115.3	131.7	-0.16	-0.19	-0.64
5	118.3	130.7	-0.09	-0.22	-0.10

The output data for the proposed models (to predict δ_β and δ_γ) are presented in Table 3.6 in terms of charge descriptor functions and the estimated parameters.

Table 3.6. Model Outputs

Model	f(DES_n)			A	B	C	D
	DES_1	DES_2	DES_3				
I (γ-shift)	C1C7	C2C6^2	N	103.08	-134.61	111.39	19.68
II (β-shift)	C1C7^2	C2C6	N	91.16	315.60	-171.76	-0.50

Results of variance analysis, standard errors of estimate and regression coefficients for the predicted correlations are summarised in Table 3.7.

Table 3.7. Analysis of variance and correlation coefficients

Model	Sum of Squares		Mean Square		Corrected R^2	Standard Error			
	Regression	Residual	Regression	Residual		A	B	C	D
I (δ_γ)	72468.7	0.227	18117.2	0.227	0.989	4.99	21.84	95.03	2.20
II (δ_β)	86010.2	0.003	21502.6	0.003	1.00	0.97	6.33	4.56	0.14

In summary, the predicted correlation between the polymerizability of a diallyl monomer (in terms of the shift in γ- and/or the β-carbon) and the quantum chemical descriptors is defined by:

$$\delta_\gamma = 103.08 - 134.61(C1C7) + 111.39(C2C6)^2 + 19.68(N) \quad (r^2 = 0.989) \tag{3.5}$$

$$\delta_\beta = 91.16 + 315.60(C1C7)^2 - 171.76(C2C6) - 0.50(N) \quad (r^2 = 1.00) \tag{3.6}$$

where, N represents the electrostatic charge on the nitrogen atom of the concerned monomer.

In observing the values in Table 3.7, it appears that the second model (developed for the shift of β carbons) is a better predictor of polymerizability in terms of statistical

significance. However, the test of the two models on a diallylamine monomer outside our sample population, namely N, N, N-triethyl-N-allylammonium bromide showed that the predicted shifts by both models are highly close to the actual values. The results of this test and the input data for the monomer are presented in Table 3.8.

Table 3.8. The result of test and the input data for test monomer, N,N,N-triethyl-N-allylammonium bromide

Charges			Chemical Shifts			
			Predicted		Observed	
C1C7	C2C6	N	γ	β	γ	β
-0.03	-0.23	0.66	126.0	130.62	125.1	128.9

N-methyl-N-allylmethacrylamide has also been used as a test molecule although the main structure of the monomer is different from our samples. The model predicts the chemical shifts of the carbons on the methacryloyl side systematically lower than the actual values (Table 3.9). However, the chemical shift difference ($\Delta\delta$), that has been considered as an indicator of polymerizability reproduces the actual value [58].

Table 3.9. The result of test and the input data for test monomer, N-methyl-N-allylmethacrylamide

Charges			Chemical Shifts			
			Predicted		Observed	
C1C7	C2C6	N	γ	β	γ	β
-0.11	-0.24	-0.55	113.5	136.5	117.3	140.8

One more test has been applied by the N-methyl, N-N-diallylamine monomer (Table 3.10). Although the chemical shifts of C_γ and C_β were not available, the chemial shift difference of 11.1 correlates with the experimentally known poor polymerizability of the monomer [16].

Table 3.10. The result of test and the input data for test monomer, N-methyl, N-N-
diallylamine

Charges			Chemical Shifts		
			Predicted		$\Delta\delta$
C1C7	C2C6	N	γ	β	
-0.20	-0.16	-0.63	120.5	131.6.	11.1

3.3. Concluding Remarks

The aim of this part of the project was to correlate the experimental cyclopolymerizability trend of a series of diallylamine monomers by the descriptors derived from quantum mechanical calculations. Hence, it is possible to make predictions on monomers that have not been synthesized yet. The ^{13}C NMR chemical shifts of the studied diallylamine monomers, which have been correlated to the polymerizabilities [21], could be successfully correlated to the descriptors derived from calculations. The "weighted average" charges of vinyl carbons and nitrogen could successfully produce the polymerizability trend. The activation energies and the enthalpy differences between the transition state structures and the living monomers for the intramolecular cyclization reproduced the polymerizability trend successfully in general. The C_2--C_6 bond order, local softness values of C_6 and HOMO-LUMO gaps were also found to reflect the polymerizabilities of the monomers. The mathematical model has predicted ^{13}C NMR chemical shifts based on electrostatic charges derived from quantum mechanical calculations (PM3). Although the model has been developed with only 5 samples, the validation check has shown that the model is acceptable. Data on similar monomers are desired in order to extend the usage of the proposed model.

4. FACTORS CONTROLLING THE RATES OF CYCLIZATION IN RADICAL POLYMERIZATIONS OF DIALLYLAMINE AND DIALLYLAMMONIUM MONOMERS

In Section 3, descriptors are saught to determine the polymerizabilities of monomers. However, the results of this study have led us to study the cyclization reaction of cyclopolymerization in more detail.

The importance of cyclopolymerization lies not only in the properties of final product but also in its mechanism. The difunctional monomers can be polymerized to high molecular weights although the monofunctional counterparts exhibit very low degrees of polymerization. They can be polymerized to only low molecular weights in special complexing media [11]. It has been mentioned in section 1 that the low polymerizability of allyl monomers is attributed to chain transfer processes (Chain Transfer, Figure 1.1). In the polymerization of allyl monomers, the growing chain has a secondary radical that is reactive toward H-abstraction, thus chain transfer reactions lower polymerization efficiencies (Chain Transfer, Figure 1.1). On the other hand, the difunctional monomers can be polymerized efficiently. In cyclopolymerization, the growing radical attacks the second double bond that is in close vicinity and cyclizes. The resulting primary radical is sterically unhindered and highly reactive towards radical addition. Propagation is facile and faster than other reactions that terminate the polymerization. N, N-diallylamine (1), N, N-diallylammonium (2), and N, N-dimethyl-N,N-diallylammonium (3) (Figure 4.1) can all be cyclopolymerized, but the experimental polymerizabilities vary from very poor to very good for 1, 2 and 3, respectively [21].

Although the difunctionality of diallylamine (1) monomer makes it a suitable candidate for cyclopolymerization, chain transfer reactions are still competitive. Zubov *et al.* reported that both diallylamine and allylamine have very low rates of polymerization [11].
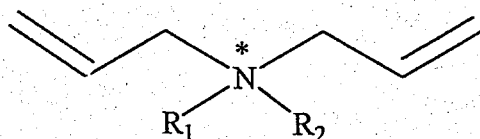
Monomer	R_1	R_2	Charge (*)
1	H	-	0
2	H	H	+
3	CH$_3$	CH$_3$	+
6	CH$_3$	-	0
7	CH$_3$	H	+

Figure 4.1. Diallylamine and diallylammonium monomers studied

In general, cationic diallyl monomers have higher polymerizabilities than neutral as in the case of 1 and 2. The poorest compound, 1, is reported to have very poor polymerization [11] although it is a difunctional monomer. However, its protonated form has good polymerizability [21]. Polymerization of cationic monomers may have some advantages over neutral in terms of cyclization or termination reactions. It has been proposed that the growing chain may be stabilized against disproportionation by the inductive effect of the ammonium cation, diminishing chain transfer [59]. In cationic monomers, the C_α-H bond attached to an ammonium group is quite unreactive towards abstraction by electrophilic radicals.

Allyltrimethylammonium chloride demonstrates the importance of cyclization in the polymerization. The monoallyl salt is reported to have poor polymerization tendency and to be polymerized only in a special complexing medium [12], whereas its difunctional analog N,N-dimethyl-N,N-diallylammonium (3) can polymerize very efficiently to high molecular weights with a high degree of polymerization and low chain transfer [20, 9, 60]

Among the monomers studied here, N,N-dimethyl-N,N-diallylammonium (3) is the most extensively studied. It is reported that 5-membered rings are formed in the

cyclopolymerization reaction of **3** with a *cis:trans* ratio of 6:1 [7-9] or 3-4:1[10] in different NMR studies. The *cis:trans* ratio for N-methyl-N, N-diallylamine (**6**) was also reported as 5:1 with ^{13}C NMR studies [16].

The intramolecular radical cyclizations of model systems for intermediates involved in polymerization of the monomers N, N-diallylamine (**1**), N, N-diallylammonium (**2**), and N, N-dimethyl-N,N-diallylammonium (**3**), N-methyl-N, N-diallylamine (**6**) and N-methyl-N, N-diallylammonium (**7**) have been explored in this section (Figure 4.1). We want to understand the factors that influence the polymerizability and to determine how it is related to the ease of cyclization. The influence of a change of nitrogen substitution upon the efficiencies of radical cyclization has been explained and rationalized.

4.1. Methodology

A model compound was used for cyclization of the growing polymer as in Section 3 (Figure 3.2). The polymer chain at C_1 in the actual system was replaced by a H atom, and this model radical was used to model the cyclization reactions. The model compounds for **1**, **2**, **3**, **6** and **7** will be designated by **1'**, **2'**, **3'**, **6'** and **7'**. In the model compounds, initiation has already taken place and the monomer is about to cyclize.

The DFT method [26] employing the B3LYP [31] functional with the 6-31G* basis set has been used to carry out the full optimization of the compounds of interest with the Gaussian 98 [61] package. Recently, the origins of stereoselectivity in intramolecular Diels-Alder cycloadditions have been modeled with success using the B3LYP methodology [62]. The stationary points were analyzed by vibrational frequency calculations. Various possible transition states for both 5-exo (Figure 4.2) and 6-endo (Figure 4.3) cyclizations were modeled. Both chair and boat conformations of 5-exo and 6-endo cyclization transition states were found. The transition states will be referred as chair/boat and substituents as axial/equatorial as in earlier calculations of cyclizations of 5-hexenyl. The transition structures were verified to be saddle points by the presence of one imaginary frequency corresponding to the reaction coordinate. An IRC [63, 64] calculation was performed on the transition state for the models of monomers studied and then the

structures for reactants and products were further optimized to locate corresponding stationary points. The reactants obtained in this way are called the "reactive rotamers"; these are the rotamers that are close in geometry to the transition state. The reactants were also fully optimized in their global minimum geometries. The reactive rotamer and the global minimum for **1'** and **2'** are shown in Figure 4.4, as representative of cationic and neutral monomers.
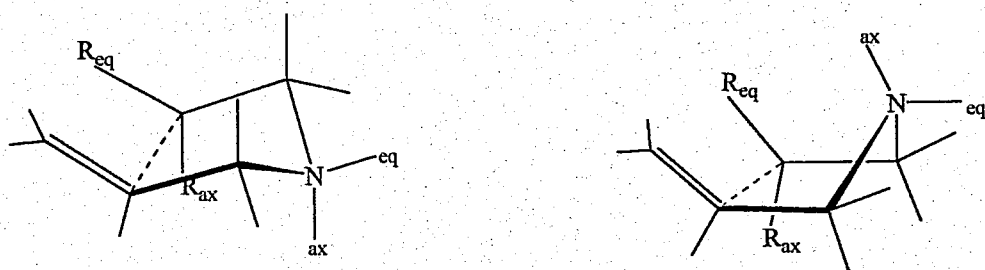
Figure 4.2. Chair and boat transition structures for 5-membered ring cyclization
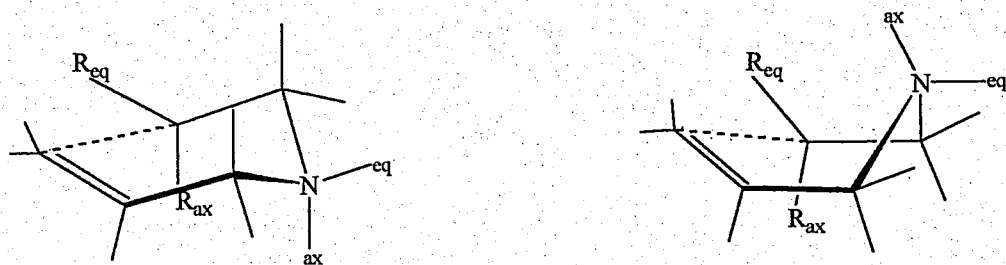
Figure 4.3. Chair and boat transition structures for 6-membered ring cyclization

4.2. Discussion

The global minima of the radical intermediate models are in extended conformations (Figure 4.4).
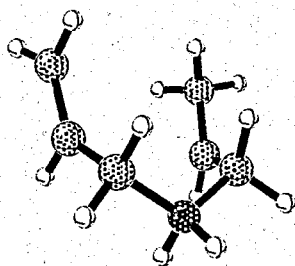
Reactive rotamer of intermediate radical derived from N, N-diallylammonium (**2′**)
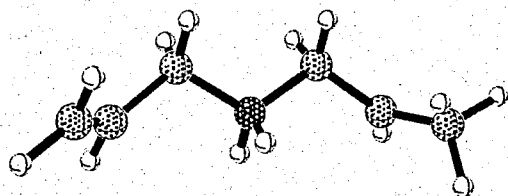
Global minimum of intermediate radical derived from
N, N-diallylammonium (**2′**)
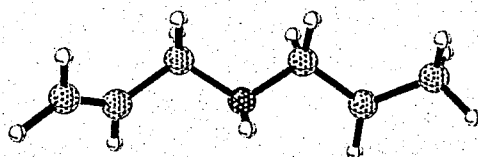
Global minimum of intermediate radical derived from
N, N-diallylamine (**1′**)

Figure 4.4. Reactive rotamer and global minimum of **1′** and **2′**

The reactant molecules have all anti conformations about C-N bonds. In cationic reactants (**2′**, **7′** and **3′**) the NCC=C dihedral angles are 90-110°, as are the NCC-C dihedrals involving the radical centers. In neutral models, the NCC=C and NCC-C dihedrals are −160° and 125°, respectively (Figure 4.4). Thus, in the cationic intermediates, the p-orbital on the radical center is parallel to the C_3-N_4 bond, whereas in the neutral case it is almost at a right angle with that bond. The parallel orientation provides the suitable

geometry for a delocalization of electrons in p-orbital into σ^*_{C-N} and may act as a stabilizing effect on that conformer. The effect of this interaction may be traced from the C_3-N_4 and C_5-N_4 bond lengths. In the neutral intermediates, these bonds are equal in length (1.46 Å in 1' and 6') whereas in cationic monomers the C_3-N_4 bond is always longer by 0.02-0.03 Å than C_5-N_4 bond.

Butler had indicated that cyclopolymerization might be facilitated by $\pi-\pi$ interaction of the two double bonds in 1,6-dienes. However, the reported spectroscopic evidence has been inconclusive [6, 65] The conformational study on compounds 1'-3', 6' and 7' has shown extended structures with no significant $\pi-\pi$ interactions between the double bonds in their global minima. However, the reactive rotamers that have quasi cyclic structures are 1-3 kcal/mol higher in energy (Table 4.1).

The cyclization transition structures for 1'-3', 6' and 7' are very similar in many ways to those of the cyclization of hexenyl radical reported earlier [66-73]. These reports have demonstrated the preference of 5-exo over 6-endo cyclization. Formation of 5-membered rings is also anticipated from the generalized "Baldwin Rules" for the relative facilities of ring closure [74].

The activation energies for 5- and 6-membered transition states are shown in Table 4.1. The 5-exo transition states are lower in energy than 6-endo by 3.0-5.6 kcal/mol even though the 6-membered ring products are more stable than the 5-membered. The large energy difference between 5-exo and 6-endo transition states is consistent with the experimental preferences for formation of five-membered rings in the polymerization of these monomers. $\Delta\Delta G^{\neq}$, the difference in free energy of activation for 5-exo and 6-endo cyclization for 1'-3', 6' and 7' are 4.0, 5.9, 3.3, 3.9 and 4.3 kcal/mol, respectively, in favor of 5-membered ring formation. This is mainly an enthalpic effect, although the entropy of activation is also slightly more favorable for the 5-exo cyclizations (Table 4.1). The $\Delta\Delta S^{\neq}$ values between exo and endo cyclizations are 0.6-0.8 e. u. for 1'-3', 6' and 7'.

Table 4.1. The energies of activation (E_a) (kcal/mol), free energies of activation ($\Delta G^{\neq}$) (kcal/mol) and the entropies of activation ($\Delta S^{\neq}$) (e.u.) for 5-exo and 6-endo transition states.

Energy	1'	2'	3'	6'	7'
E_a (E_{TS}-$E_{reactive\ rotamer}$)	5.4	5.4	3.7	3.7	4.3
E_a ($E_{TS-5-exo}$-$E_{reactant}$)	7.2	8.6	6.2	5.0	6.4
E_a ($E_{TS-6-endo}$-$E_{reactant}$)	10.9	11.6	10.3	10.6	10.2
ΔE_{rxn}	-10.9	-10.9	-13.1	-13.6	-12.0
$\Delta G^{\neq}$ (5-exo)	9.7	11.7	8.2	7.3	8.7
$\Delta S^{\neq}$ (5-exo)	-10.0	-12.3	-8.9	-9.4	-9.6
$\Delta G^{\neq}$ (6-endo)	13.7	15.0	12.5	13.2	12.6
$\Delta S^{\neq}$ (6-endo)	-10.8	-13.0	-9.6	-10.0	-10.2

In Figure 4.5, the transition structure obtained for the 5-membered cyclizations of N, N-dimethyl-N, N-diallylammonium (3') is shown.
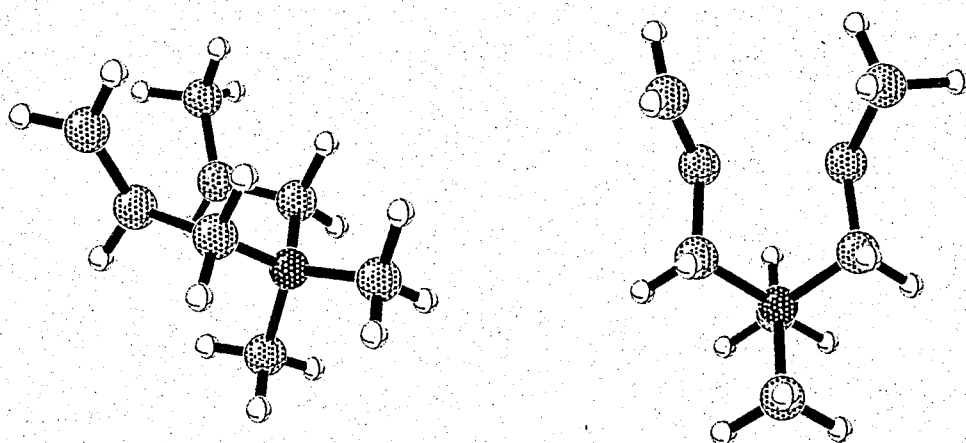
Figure 4.5. The 5-exo transition state for cyclization of 3' (side and top views)

All the transition states displayed similar features and are very similar to transition states of the 5-hexenyl ring closure reaction [66]. The 5-exo transition states are chair-like as in 5-hexenyl case. In the transition structure for cyclization of 3', the bonding distance is 2.29 Å, slightly shorter than the 2.34 Å in earlier calculations of 5-hexenyl [66]. The

double bond, C_6-C_7, lengthens to 1.37 Å. The C_2-C_6-C_7 angle is 110°, similar to 106° of 5-hexenyl. Likewise, the C_1-C_2-C_6 angle is 109°. In the 5-membered transition states, the ~109° attack angle is readily obtained while maintaining the overlap of the p-orbitals forming the π bond. In the 6-endo, the orientation of the reacting centers does not allow very efficient overlap.

In 5-exo transition states, the bonding distances are shorter and C_6=C_7 bond lengths are longer than in 6-membered (Figure 4.6). Similar observations were reported by Jursic in the cyclizations of 5-hexenyl radicals using B3LYP [73].
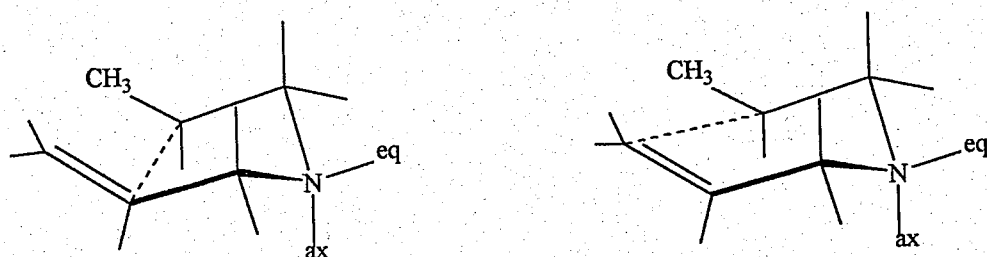
| Compound | 5-exo | 6-endo | 5-exo | 6-endo |
	C---C	C---C	C=C	C=C
1'	2.17	2.36	1.40	1.36
2'	2.27	2.36	1.37	1.36
3'	2.29	2.37	1.37	1.36
6'	2.25	2.35	1.37	1.36
7'	2.27	2.37	1.37	1.36

Figure 4.6. The C---C bonding distances and the C=C bond lengths of 5-exo and 6-endo transition structures

The 5-exo transition states may have *cis* or *trans* isomers depending on the orientation of the methyl group and the double bonds as shown in Figure 4.7.

cis-chair   *cis*-boat

trans-chair   *trans*-boat
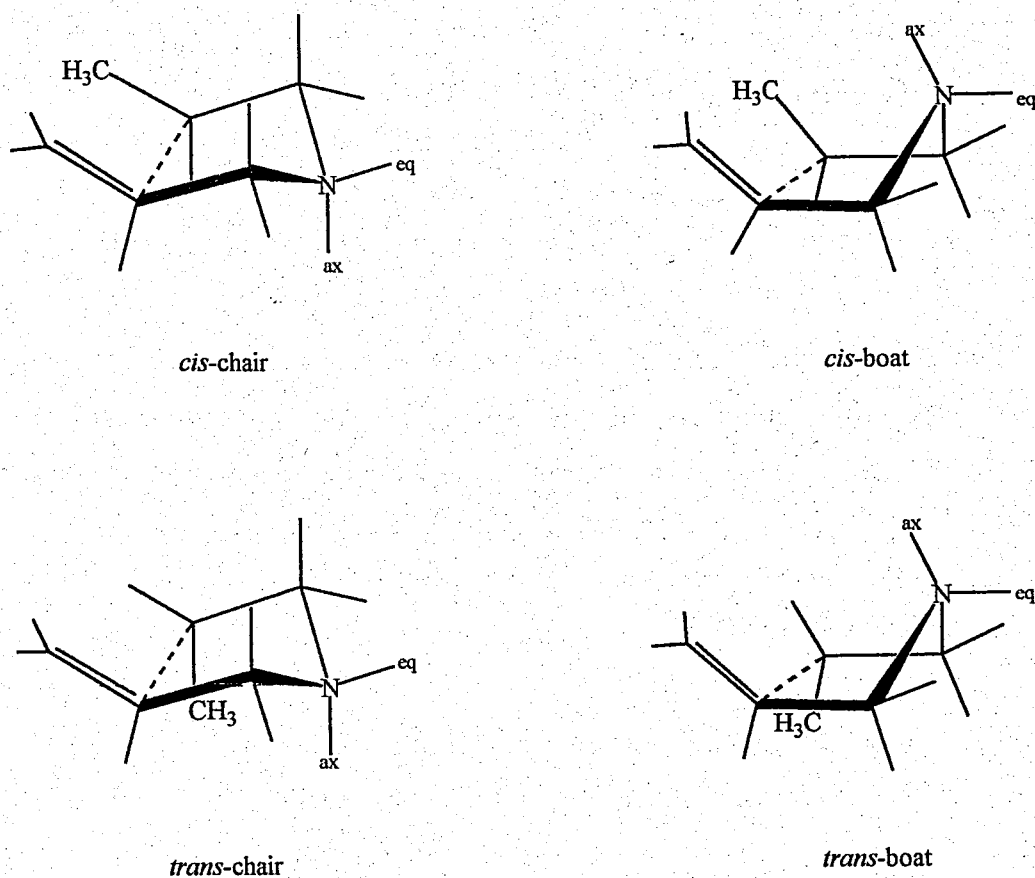
Figure 4.7. The *cis* and *trans* conformations of 5-exo transition state

The lowest energy corresponds to *cis*-chair conformer with the equatorial substitution on nitrogen. C_1 is in a pseudo-equatorial position and cis to the double bond. The transition state resembles a cyclohexane, and C_1 behaves as a substituent on the cyclohexane ring. Equatorial substitution will be favored for simple steric reasons. Likewise, substituents on nitrogen also prefer the equatorial conformation. In the hexenyl analogs, this was reported to be favored both experimentally and by calculations [66]. Structure **3** was reported to give dominantly *cis* products with a *cis:trans* ratio of 6:1 [7, 8, 9] or 3-4:1[10] in different NMR studies. The activation energy for the 5-membered minimum energy *cis* structure of **3'** is 6.2 kcal/mol whereas for the *trans* it is 7.4 kcal/mol. The calculated *cis:trans* ratio of **3** at 25 °C is 4.9:1, in between the two experimental values. The ratio is 1.6:1 for **6**, which is lower than the experimental ratio of 5:1.

In the 6-endo transition states, the chair is more stable than the boat (Figure 4.3). Equatorial substitution is favored here, as in the 5-exo cases. Except for unsubstituted **1**, all the monomers preferred equatorial CH_3 on carbon or nitrogen.

4.2.1. The N-alkyl and N, N -gem-dialkyl Effects

N-methylation of diallylamine (**1**) lowers the activation energy for cyclization of the radical derivative from 7.2 to 5.0 kcal/mol, i.e. 2.2 kcal/mol. Similar conversion of diallylammonium to the N-methyl derivative lowers the activation energy from 8.6 to 6.4 kcal/mol, again by 2.2 kcal/mol (Table 4.1). The methylation of N-methyl derivative, **7**, lowers the activation energy for cyclization reaction by only 0.2 kcal/mol (Table 4.1). The mono-alkyl effect here is larger than the better known gem-dialkyl effect [75-91].

The rate enhancement of cyclization reactions by geminal substitution on the atom joining reactive functionalities is called the "gem-dialkyl effect" [75-91]. Jung and co-workers have demonstrated numerous examples of the effect of geminal substituents on cyclization rates. In their work on substituted 2-furfuryl methyl fumarates [88], they observed that the rate of cyclization increased by methyl substitution (Figure 4.8). They reported that dimethyl substitution had a greater effect than monomethyl substitution. In our calculations, one methyl substitution increases the predicted rate by a factor of 160 (**2'** vs. **7'**) while the rate constant is only doubled by substitution of a second methyl (**3'** vs. **7'**).

Various explanations of the gem-dialkyl effect have been offered. The Thorpe-Ingold effect [92] was an explanation based on the idea that the two reacting centers are moved closer together by alkyl substitution. This is accompanied by a compression of the internal angle caused by the alkyl groups. This effect has generally been found to be negligible [79, 85, 92].

(1)
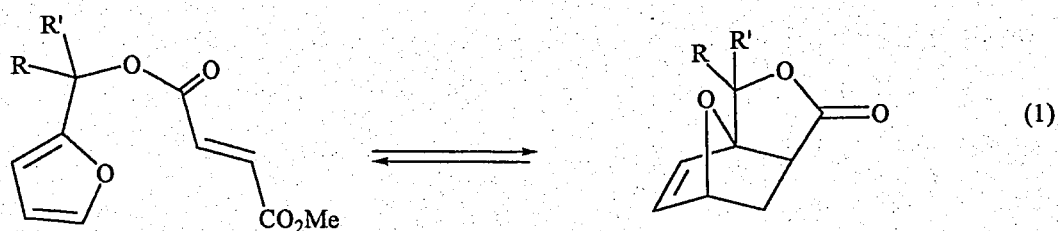
R	R'	k_1 (in CD_3CN)	$k_{relative}$
H	H	2×10^{-7}	1
H	Me	1.1×10^{-6}	5.5
Me	Me	3.4×10^{-4}	1700

(2)
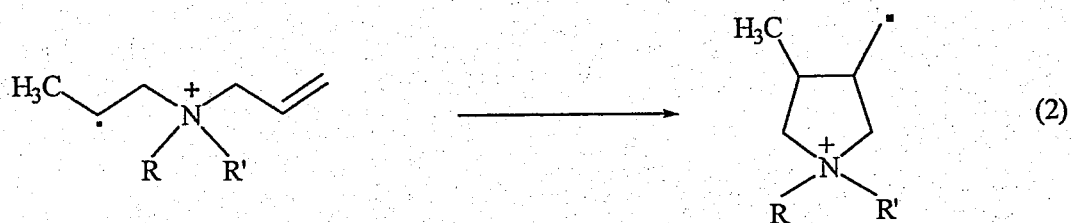
R	R'	k_{cyc}	$k_{relative}$
H	H	1.0×10^{-9}	1
H	Me	1.6×10^{-7}	160
Me	Me	3.1×10^{-7}	310

Figure 4.8. The rate constants and the relative rate constants for cyclizations of (1) 2-furfuryl methyl fumarates [88] (experimental) and (2) of cyclizations studied in this work (calculated)

An alternative explanation for the increased rate on substitution is based on the higher population of the reactive rotamer, called the "reactive rotamer effect" by Bruice and Pandit [93]. Their explanation is based on the idea that the cyclization rate depends on the concentration of the reactive rotamer. They propose that substitution of alkyl groups for hydrogen increases this concentration. The reactive rotamer is the folded conformation of

the reactant, which is very close in geometry to the transition state structure. Figure 4.9 shows the situation schematically. For a cyclization to occur, the reactive units, X and Y, must be in the gauche conformation rather than the more stable anti conformation. If one of the two carbons of the C-C bond is substituted with one or two alkyl groups, then the anti form is destabilized and becomes closer in energy to the gauche. Therefore, the population of the gauche conformer will increase with alkyl substitution. The increase in the reactive rotamer population will enhance the rate of cyclization with respect to the non-alkylated molecule.

anti   gauche

anti   gauche
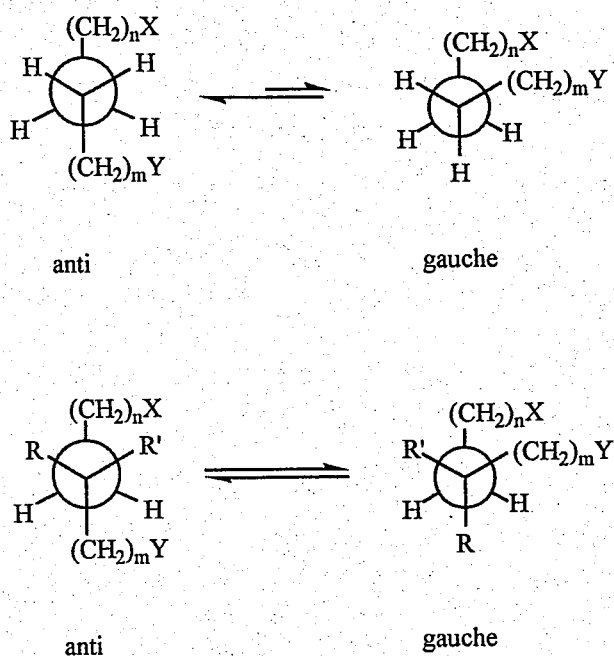
Figure 4.9. Effect of substituent on the conformational equilibrium

According to the "facilitated transition state hypothesis" by Parrill and Dolata [94], the rate acceleration for a cyclization is due to lowering of rotational energy barriers by substitution. In particular, the barrier corresponding to achieving the transition state is the focus of their explanation. Substitution of H by an alkyl group increases the energy of both staggered and eclipsed conformations of the reactant, but the increase in energy is much more pronounced in the staggered case corresponding to reactants. Thus, substitution lowers the energy difference between the reactant (staggered) and transition state (eclipsed). The ground state is destabilized relative to the transition state.

4.2.2. Interpretation of the Energy Barriers Based on the Equatorial-dialkyl Effect

The applicability of each of these explanations to the cases studied here has been evaluated. First, the C-N-C angles in reactants were inspected for a significant Thorpe-Ingold effect. There is a compression of this angle from 116° in **2'** to 112° in **7'** and 107° in **3'**. Although the Thorpe-Ingold trend is as predicted, this angle compression is not accompanied by a decrease in bonding distance (Table 4.2). The Thorpe-Ingold compression is not a significant factor in activation energy lowering.

Table 4.2. Geometric parameters in the 5-exo transition state structures

Monomer	1'	2'	3'	6'	7'
C----C Bonding Distance (Å)	2.25	2.27	2.29	2.27	2.28
C-N-C Angle (°)	113	116	107	112	112

In our study, two rotamers are analyzed for compounds **1'-3'**, **6'** and **7'**. One of these is the global minimum, which has a very extended conformation, unsuitable for cyclization, and the other is the folded rotamer obtained from the IRC calculation. To form product, only rehybridization and bond formation must occur (Figure 4.4).

In the reactive rotamer, the C_2-C_3-N_4-C_5 dihedral angle is ~60° in all the compounds. The rotamers where the C_2-C_3-N_4-C_5 dihedral is 180° were also computed to see the energy difference between the anti and gauche conformers around the C_3-N_4 bond in the reactive rotamer. The energy difference ($HF_{C-C-N-C=60°}$ - $HF_{C-C-N-C=180°}$) is 1.4 kcal/mol for **2'**, 0.7 kcal/mol for **3'** and 0.3 kcal/mol for **7'**. Substitution of an alkyl group for H on nitrogen decreases the energy difference between the anti and gauche conformers around the C_3-N_4 bond. The reactive rotamers for compounds **2'**, **3'** and **7'** are 3.2, 2.5 and 2.1 kcal/mol higher in energy than their corresponding ground state structures. Hence, alkyl substitution tends to increase the population of the reactive rotamer.

Figure 4.10 shows how substitution influences the activation energy of the reaction. The gauche interactions in reactant and the transition state with their relative energies are shown for **2'**, **3'** and **7'**.
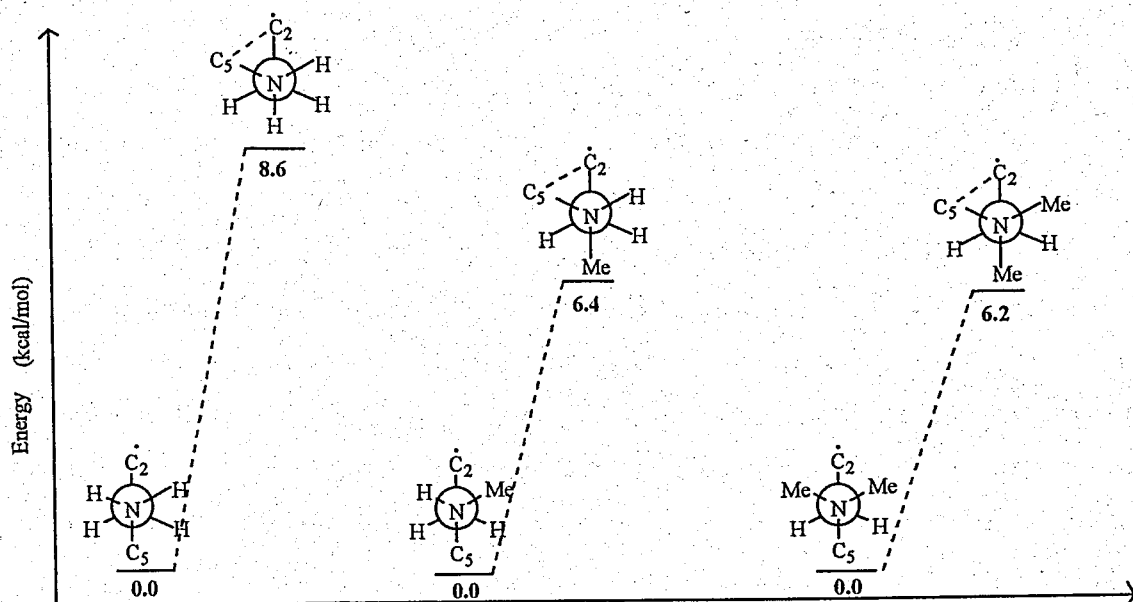
Figure 4.10. The reactants and the transition states of **2'**, **3'** and **7'**

In **2'**, the steric change is the anti to gauche change. In **7'**, the methyl substituent on N is gauche to the radical center in the reactant, whereas in the transition state it is anti, since it is an equatorial substituent on the chair-like transition state. Thus, the gauche interaction formed in reactant of **7'** is partly relieved in going to transition state. This causes a decrease in the activation barrier for the cyclization of **7'** (6.4 kcal/mol) as compared to **2'** (8.6 kcal/mol). In **3'**, one of the methyl substituents on nitrogen has the same gauche interactions as above, but the other has gauche interactions both in transition state and reactant, since it is axial on the chair-like transition state. One N-methyl accelerates cyclization since it is gauche in reactants and equatorial (anti) in the transition state while the second methyl substituent is gauche in both the transition state and the reactant and has little effect. (Figure 4.11).

Although substitution of alkyl groups for hydrogen increases slightly the population of the reactive rotamers for compounds **3** and **7**, this effect is not the main cause for the facilitation of the cyclization. In **3** and **7**, the gauche effects, which lower the energy gap between the ground state structures and the reactive rotamers are also present in the transition structures. This is a "facilitated transition state" although it could also be considered as a result of increase in the reactive rotamer that best resembles the transition state. As shown in Scheme 4.11, the reactive rotamer is consistently 4-5 kcal/mol below the transition state, as substituents have parallel effects on both species.

The calculated activation energies for cyclization are consistent with the experimental polymerizabilities of the monomers **2** and **3** [21]. The barriers to cyclization show that the cyclization reaction is energetically feasible and the methyl substituted monomer cyclizes easier as it polymerizes much more effectively. In the case of N,N-diallylamine (**1**), the cyclization reaction is calculated to be easier than its cationic analog, but the overall cyclopolymerization of the monomer is reported to be very poor, presumably due to more effective chain transfer reactions that may act to terminate its polymerization.

4.3. Concluding Remarks

The cyclization reactions of **1-3** have been studied as model intermediates in the cyclopolymerization of diallylamine monomers. The monomers are shown to produce 5-membered ring structures as suggested by experiment. The structures for transition states are also demonstrated. The 5-membered ring formation is explained by a more effective overlap possible in the 5-exo transition state as compared to the 6-endo transition state. The 5-exo preference over 6-endo is found to be mainly an enthalpic effect, as the small activation energy differences between 5-exo and 6-endo transition states show. The *cis:trans* ratio of N, N-dimethyl-N, N-diallylammonium (**3**) is calculated as 4.9:1 which is in good correlation with the experiments.
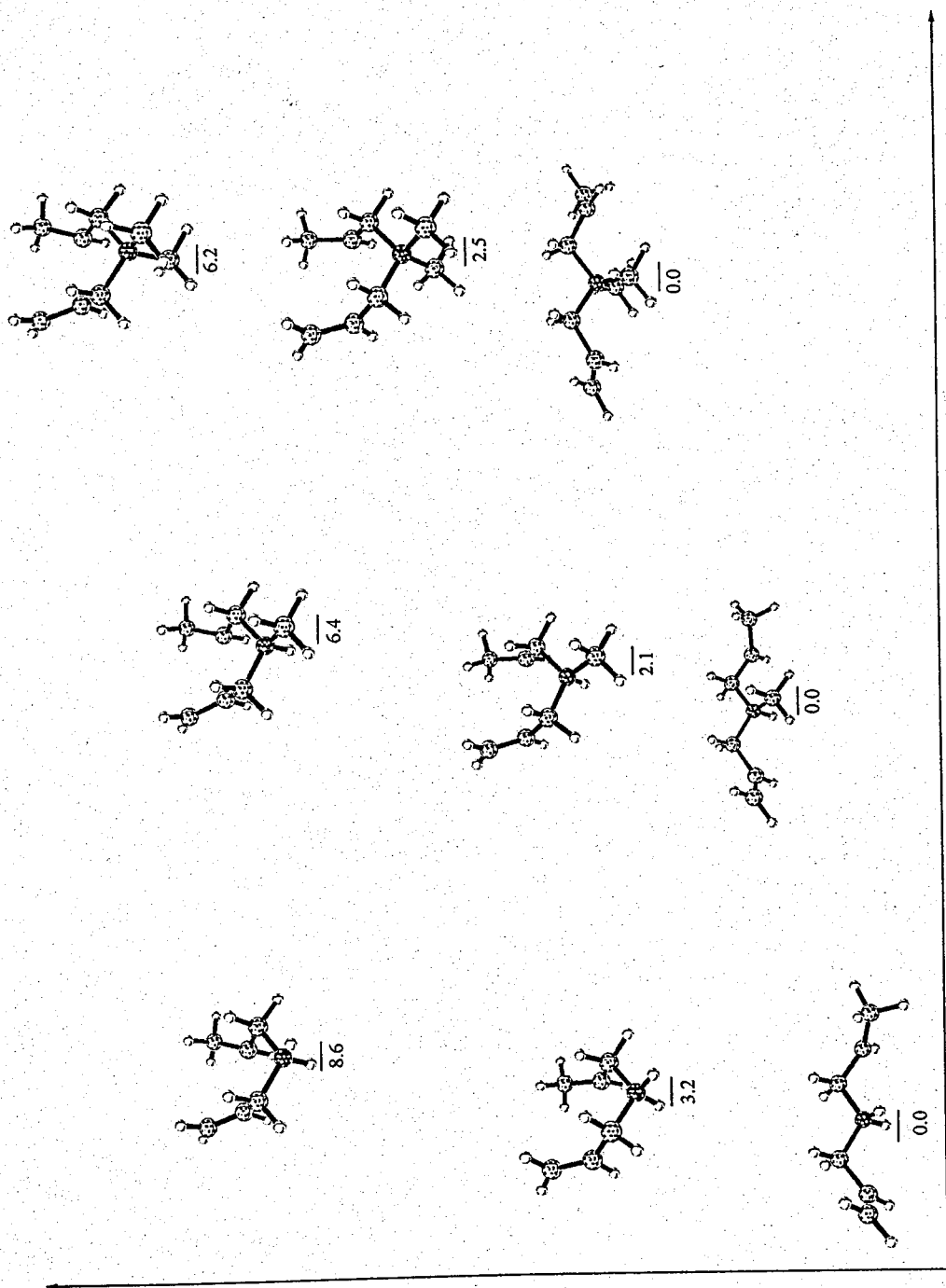
Figure 4.11. Relative energies of global minima, reactive rotamers and the transition structures for **2**, **3** and **7**

The Thorpe-Ingold effect is found to be too small to explain the energy barrier lowering by methyl substitution. Monomethyl substitution is shown to have more effect than two methyls contrary to some literature findings of gem-dialkyl effects in other systems. The "equatorial methyl" effect accounts for the acceleration, a type of "facilitated transition state."

5. MODELING THE CYCLOPOLYMERIZATION OF N-METHYL-N,N-DIALLYLAMINE, N-METHYL- N-ALLYL-2-(METHOXYCARBONYL)ALLYLAMINE AND N-METHYL-N-METHALLYL-2-(METHOXYCARBONYL)ALLYLAMINE

In cyclopolymerization, usage of monomers whose monofunctional counterparts do not homopolymerize have been found to enhance the cyclization efficiency of the monomer [13]. However, high cyclization efficiency was not always accompanied by an increase in polymerization. Thus, it became important to use monomers which have both high cyclization efficiency and high polymerization capability. In that respect, compounds 6 (N-methyl-N,N-diallylamine), 8 (N-methyl- N-allyl-2-(methoxycarbonyl)allylamine) and 9 (N-methyl-N-methallyl-2-(methoxycarbonyl)allylamine) (Figure 5.1) have drawn considerable attention. Kodaira *et al.* have reported that 8 has both high cyclization efficiency and high cyclopolymerizability [14, 15]. Monomers 6 and 8 have been found to undergo five membered cyclization whereas 9 formed six membered rings along with decreased polymerization tendency as compared to 8 [14, 15, 16]. These observations were attributed to steric and/or electronic factors due to the ester and methyl substitution on the C=C double bonds.

In the previous sections the intramolecular cyclization of a series of diallylamine and diallylammonium monomers has been studied by using quantum chemical methods [95, 96]. The steric and electronic factors that influence cylization have been explained and rationalized [95, 96]. This part of the study aims a mechanistic study of the intramolecular cyclization reactions for 6, 8 and 9 with the same methodology. The steric and electronic effects of methyl and acetate substitution on the cyclization efficiency of N-methyl-N,N-diallylamine have been discussed. The regioselectivity of ring closure has also been considered. The computational findings have been compared with the experimental polymerizabilities.
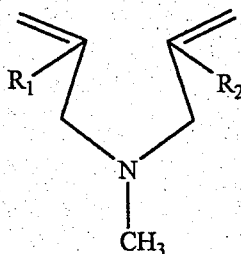
Monomers	R₁	R₂
6	H	H
8	COOCH₃	H
9	COOCH₃	CH₃

Figure 5.1. Monomers studied in this section

5.1. Methodology

The long polymer chain has been simplified and model compounds have been used for the monomers **6, 8** and **9** (Figure 3.2) in order to reduce the computational cost as in previous sections. In the models, the long polymer chain is replaced by a hydrogen atom. It has been reported that the monomers behave in the same way in cyclization in their long polymer chains as in their low molecular weight analogues, thus our model can account for the cyclization in the long polymer chains [14]. The model compounds for **6, 8** and **9** will be designated by **6', 8'** and **9'**, respectively.

The calculations have been carried out by using the density functional theory [26], with the B3LYP functional [31] and the 6-31G* basis set, using the Gaussian 98 package [61].

The model compounds of N-methyl-N,N-diallylamine (**6'**), N-methyl- N-allyl-2-(methoxycarbonyl)allylamine (**8'**) and N-methyl-N-methallyl-2-(methoxycarbonyl)allylamine (**9'**) were optimized for their global minima. The transition structures for ring formation were modeled for their various conformations depending on

4.3). They will be referred to as chair/boat as in earlier calculations of hex-5-enyl radical [66-73, 95-96]. Frequency calculations have been carried out to confirm the existence of the transition states by verifing for the one imaginary frequency belonging to the reaction coordinate.

IRC [63, 64] calculations have been performed on both five and six membered transition states for all the models of the monomers and these calculations have led to stationary local minima on both sides. The products and reactants were further optimized for their local minima.

Natural Bond Orbital (NBO) analysis [44-48] has been carried out on the stationary structures along the cyclization reaction in order to characterize the stabilizing interactions that may be present in these compounds. CHELP charges [97] for the compounds of interest will also be discussed.

The activation energies, $\Delta E^{\neq}$, free energies of activation, $\Delta G^{\neq}$, entropies of activation, $\Delta S^{\neq}$, heats of reaction, ΔE_{rxn}, and the free energies of reaction, ΔG_{rxn}, are discussed in terms of the cyclization and polymerization efficiencies of the monomers of interest (Table 5.1).

Throughout the discussion, the numbering system shown in Figure 5.2 has been used.
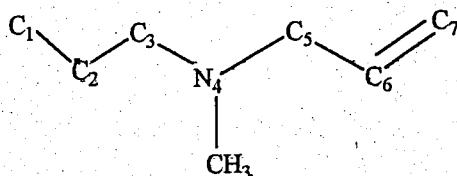
Figure 5.2. The numbering scheme used for monomers 6, 8 and 9

5.2 Discussion

5.2 Discussion

Polymerization reactions carried out on compounds **6, 8** and **9** have shown that **6** and **8** form exclusively 5-membered rings in their polymer backbones while **9** forms 6-membered ring structures [14-16]. Calculations have been carried out on models for the monomers to understand the factors that affect the regioselectivity in their cyclization reactions. The transition structures corresponding to the cyclizations have shown that **6'** and **8'** have formed exo (5-membered) rings while **9'** prefers the endo (6-membered) ring (Table 5.1). These results are consistent with the experimental findings [14-16].

Table 5.1. Energetics of **6', 8'** and **9'** in their radical cyclization reactions (in kcal/mol)

Energy	6'	8'	9'
Reactant	0	0	0
TS_{exo}	5.41	8.68	14.02
TS_{endo}	11.18	12.20	11.59
$Product_{exo}$	-11.81	-2.07	3.75
$Product_{endo}$	-18.65	-7.88	-8.87
$\Delta S^{\neq}_{exo}$	-9.38	-10.52	-11.92
$\Delta S^{\neq}_{endo}$	-9.98	-11.57	-10.82
$\Delta G^{\neq}_{exo}$	7.26	10.95	16.64
$\Delta G^{\neq}_{endo}$	13.15	14.70	14.00
ΔS_{rxn_exo}	-7.64	-3.61	-11.67
ΔS_{rxn_endo}	-11.91	-10.98	-9.24
ΔG_{rxn_exo}	-10.36	-1.60	6.44
ΔG_{rxn_endo}	-16.29	-5.53	-6.86
$\Delta\Delta E^{\neq}_{endo-exo}$	5.77	3.52	-2.43
$\Delta\Delta S^{\neq}_{endo-exo}$	-0.60	-1.05	1.10
$\Delta\Delta G^{\neq}_{endo-exo}$	5.89	3.75	-2.64

Close inspection of the difference in the activation energies, $\Delta\Delta E^{\neq}$ ($\Delta E_{endo}^{\neq}$ - $\Delta E_{exo}^{\neq}$), for the 5 and 6-membered transition states of the same monomer, shows that substitution decreases the energy difference between two paths. The $\Delta\Delta G^{\neq}$ ($\Delta G^{\neq}_{endo}$–$\Delta G^{\neq}_{exo}$) values also reflect the same trend as $\Delta\Delta E^{\neq}$ (Table 5.1). The energy differences between the exo and the endo transition structures indicate that as substitution on the parent structure, 6', increases, the exclusive exo preference decreases either due to destabilization of the exo transition structure with respect to the endo or stabilization of the endo with respect to the exo.

Capon and Rees have interpreted the unexpected exo preference of hexenyl systems in terms of the activation entropy, $\Delta S^{\neq}$ [98]. They propose that higher strain energy in the smaller ring is overcome by the more favorable activation entropy of the exo cyclization. $\Delta\Delta S^{\neq}$ ($\Delta S^{\neq}_{endo}$- $\Delta S^{\neq}_{exo}$) values for 6', 8' and 9' are -0.60 cal/mol.K, -1.05 cal/mol.K and 1.10 cal/mol.K, respectively (Table 5.1). Although the trend is similar to the one observed in the ring size preference, the changes are too small to account for ring preference. For instance, at a very high temperature of 400 K, an energy difference of 1.05 cal/mol.K in $\Delta S^{\ddagger}$, would alter the free energy change only by 0.42 kcal/mol. For compounds 6', 8' and 9', although the numerical values follow the expected trend, the small $\Delta S^{\neq}$ values are far away from behaving as driving force (Table 5.1).

Julia and co workers have explained the exo/endo preference of 1,6-ring closures in hex-5-enyl systems by referring to non-bonded interactions that may be present in the 6-membered ring [99]. The exo path is favored over the endo for cases where there are unfavorable non-bonded interactions between the pseudo-axial H on C_2 and the syn H on C_7 in the endocylic transition structure of hex-5-enyl system. This distance is 2.62 Å, 2.56 Å and 2.53 Å for 6', 8' and 9', respectively. Compound 9' has the shortest C--H distance and yet prefers the endo transition structure. Furthermore, these distances are too long for a significant destabilizing interaction to occur.

In cyclization reactions of hex-5-enyl radical, Beckwith *et al.* proposed the conformations of the transition structures to be important in determining the ring size preference [67]. Similarly, in our calculations, the conformations of the

transition structures corresponding to the cyclization of **6'**, **8'** and **9'**, are the key factors in determining the regioselectivity of the cyclization reactions. The three-dimensional orientation of the transition states will be discussed in the following section to account for the regioselectivity observed by both experiments and calculations. The transition states for the cyclization reactions of **6'**, **8'** and **9'** are similar in many ways to those involved in the cyclization of hex-5-enyl radical and N, N-diallylamine and N, N-diallylammonium monomers considered in our earlier studies as they resemble chair and boat conformations of cyclohexane-like structures (Figure 4.2 and 4.3).

5.2.1. N-methyl-N,N-diallylamine (6)

The global minimum for the ground state structure of **6'**, **R'6**, is in an extended structure with anti conformations about the C-N bonds (Figure 5.3). There is not a significant delocalization of electrons from the lone pair of nitrogen to the C-N bonds as has been reported to be present in its cationic analogues in section 4. The absence of this delocalization can be traced from the C-N bonds being equal to each other (1.465 Å).

The conformation of the transition structure has vital importance in understanding the exo preference of the monomer, which was expected from the Baldwin's Rules [74]. The exo transition structure (**TS6'**$_{exo}$) is chair-like with methyl substituent on nitrogen in the equatorial position (Figure 5.3). In the 6-membered transition structure, the skeleton of the ring is chair-like and equatorial substitution is favored, as observed in 5-membered transition structure (Figure 5.3). Axial orientation of the methyl group on nitrogen and axial methyl group on radical center destabilize the endo less than the exo because a 6-membered ring has a more extended structure and it can accomodate the axial substituents more easily. Overall, the predominant factor which determines the stability of the transition structures **TS6'**$_{exo}$ and **TS6'**$_{endo}$ over all the other transition state conformations is based on the equatorial preference of the substituent on the cyclohexane ring.
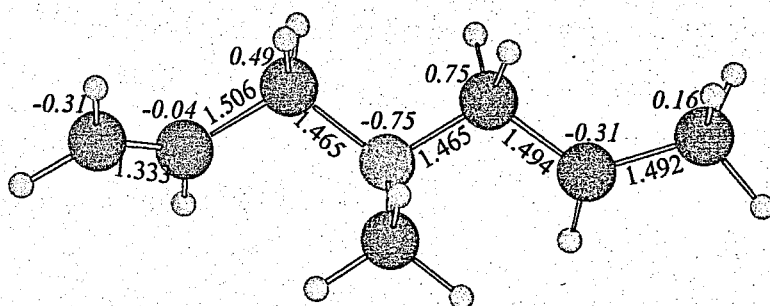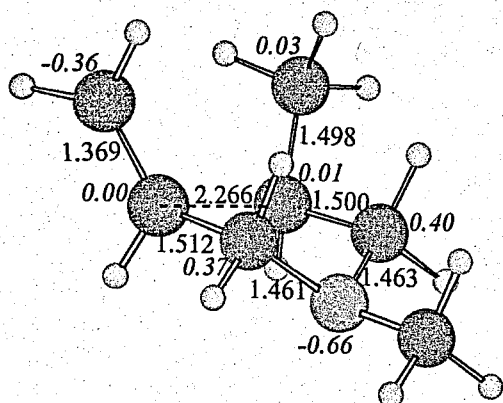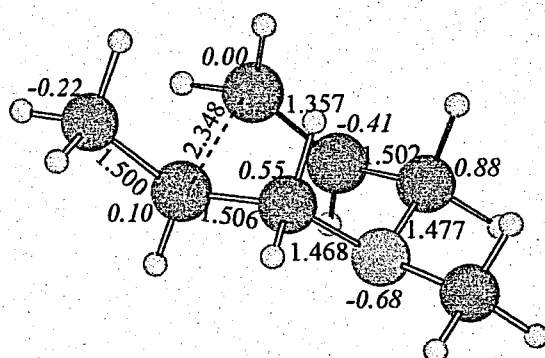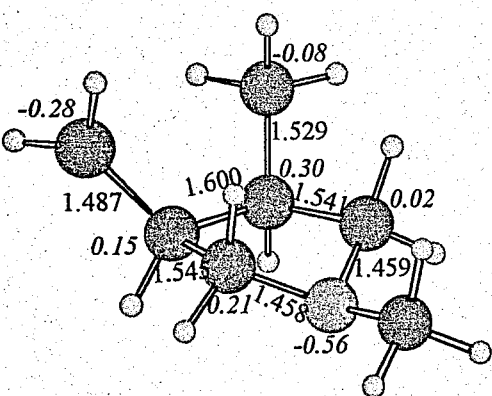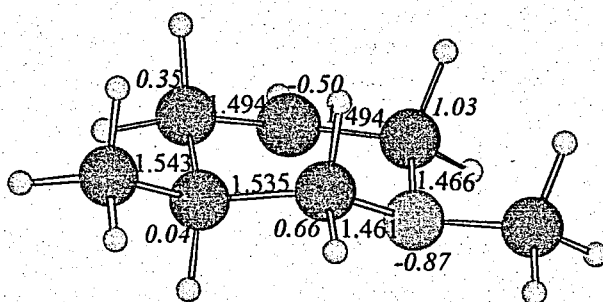
Figure 5.3. Global minimum, transition structures and the products for exo and endo cyclization of 6'

In **TS6'**$_{exo}$ and **TS6'**$_{endo}$, the C=C distances have elongated but yet the distances are more reactant-like than product-like. The carbons at the reacting centers have only partial sp^3 character in the transition state. Thus, the geometrical parameters show that both the endo and the exo transition states are early.

The Mulliken Bonding Analysis (MBA), NBO results and CHelp charges also confirm the preference for **TS6'**$_{exo}$ versus **TS6'**$_{endo}$. Mulliken bond orders indicate the bond order of the forming C---C bond to be stronger in the case of **TS6'**$_{exo}$ (Table 5.2).

Table 5.2. The Mulliken Bond Orders in the transition structures

		6'	8'	9'
TS$_{exo}$	C$_2$----C$_6$	0.105	0.145	0.163
TS$_{endo}$	C$_2$----C$_7$	0.069	0.103	0.098

CHelp electrostatic charges (Figure 5.3) show that the radical center attacks the more electrophilic site (-0.31 vs -0.04) of the C=C double bond, and leads to a 5-membered ring. The NBO delocalization energy of molecular orbitals involved in bond formation is higher in the exo transition structure than in the endo (Table 5.3). The stabilizing interactions for 5-membered ring formation are 55.79 kcal/mol in **TS6'**$_{exo}$ and 41.47 kcal/mol for **TS6'**$_{endo}$ (Table 5.3). These analyses show that steric effects as well as electrostatic effects favor exo cyclization.

In earlier reports on cyclopolymerization of diallyl monomers, the endo preference was expected because a secondary radical that forms at the endo attack is considered to be more stable than the primary radical at the exo attack [2]. Furthermore, a 6-membered ring is expected to be more stable than a 5-membered one. We have performed calculations on both 5 and 6-membered products, **P6'**$_{exo}$ and **P6'**$_{endo}$, and have observed this expectation to hold (Table 5.1). The endo product is lower in energy than the exo-product by 6.84 kcal/mol but the experimental observation and our calculations of activation energy indicate that the stability of the product has no effect on the regioselectivity.

Table 5.3. Natural Bond Orbital Analysis on the exo and endo transition structures (in kcal/mol) of 6'

TS6'$_{exo}$	Energy	TS6'$_{endo}$	Energy
α		α	
LP C$_2^{\cdot}$-->BD* C$_6$=C$_7$	24.23	LP C$_2^{\cdot}$-->BD*C$_6$=C$_7$	17.59
LP C$_2^{\cdot}$-->BD* C$_6$=C$_7$	0.28		
β		β	
BD C$_6$=C$_7$--> LP* C$_2^{\cdot}$	0.77	BD C$_6$=C$_7$--> LP* C$_2^{\cdot}$	20.93
BD C$_6$=C$_7$--> LP* C$_2^{\cdot}$	25.05	LP* C$_2^{\cdot}$--> BD* C$_6$=C$_7$	2.95
LP* C$_2^{\cdot}$--> BD* C$_6$=C$_7$	5.46		
SUM	55.79	SUM	41.47

Although the Mulliken bonding analysis and the NBO analysis can be used to rationalize the preference of **TS6'$_{exo}$** vs. **TS6'$_{endo}$**, the three-dimensional structure of the transition state is the key factor in explaining the observed regioselectivity. In the exo transition state, the p-orbital of the radical center and the π orbital of C-C double bond provide an efficient overlap geometry. On the other hand, in the 6-endo transition state, the reacting centers do not have an efficient overlap. This enhanced overlap efficiency of the 5-exo transition state overcomes the stability of the 6-membered ring structure and all other effects that may favor an endo product. The atom-atom overlap weighted natural atomic orbital analysis reveals the bond order for the forming bond to be higher in exo than in endo transition state (0.2539 in **TS6'$_{exo}$** and 0.2087 in **TS6'$_{endo}$**). Thus, our findings indicate that both the electronic and steric effects favor the formation of the exo structure.

In a ^{13}C NMR study on polymerization of **6**, the cis:trans ratio is found to be 5:1 [16], whereas, the calculated ratio is 1.6:1 at 25 °C. In our calculations, the qualitative trend is obeyed. The C=C bond, being anti with the C-N bonds provides a chair-like geometry to the system. The pseudo-equatorial substitution on C$_1$ is preferred since equatorial substitution is preferred for cyclohexane ring. In the trans transition structure, the methyl

group is in pseudo-axial orientation and this destabilizes the system by only 0.27 kcal/mol. In the real polymerization process, the long polymer chain is on C_1 and hence, this causes much more destabilization than in the model system. Thus, the calculated cis:trans ratio is lower than expected.

5.2.2. N-methyl- N-allyl-2-(methoxycarbonyl)allylamine (8)

The initiation reaction of the ester substituted diallyl compounds has been found to start from the ester side [14, 15]. This assumption has been tested by modeling the radicals formed after the initiation both from the allyl and the ester sides. The radical that formed by initiation from the ester side is found to be 7.40 kcal/mol more stable than the radical that formed by initiation from the allyl side. The stability of the radical formed by initiation from the ester side, **8'**, is obviously due to the conjugation between the C=O bond and the radical.

The structure corresponding to the global minimum of compound **8'**, **R8'**, does not adopt an all anti orientation in its backbone as in the case of **R6'** (Figure 5.4). The radical center, C=O and the oxygen of ester group are all coplanar as expected for maximum delocalization. The methyl group on the ester is syn with the C=O group. Due to the lack of symmetry in **R8'**, the C-N bonds are not equal to each other as in **R6'**.

Methyl ester substitution on N-methyl-N-N-diallylamine, **6**, did not alter the regioselectivity for the cyclization reaction and the exo cyclization is preferred over the endo (Table 5.1). In **TS8'$_{exo}$**, the skeleton of the transition state is chair-like (Figure 5.4). The ester group, being bulkier than methyl, occupies the pseudo-equatorial orientation. The methyl group on nitrogen is also in the equatorial position. **8'** has a chair-like transition structure in its 6-membered transition state, **TS8'$_{endo}$**, as in **6'** (Figure 5.4). The methyl on nitrogen and the ester substituent prefer the equatorial position as in **TS8'$_{exo}$**. As in the case of **TS6'$_{exo}$**, the axial methyl group on nitrogen destabilizes the transition state less in its endo analogue because the 6-membered ring, being more flexible than the 5-membered ring can accommodate the axial group much better.
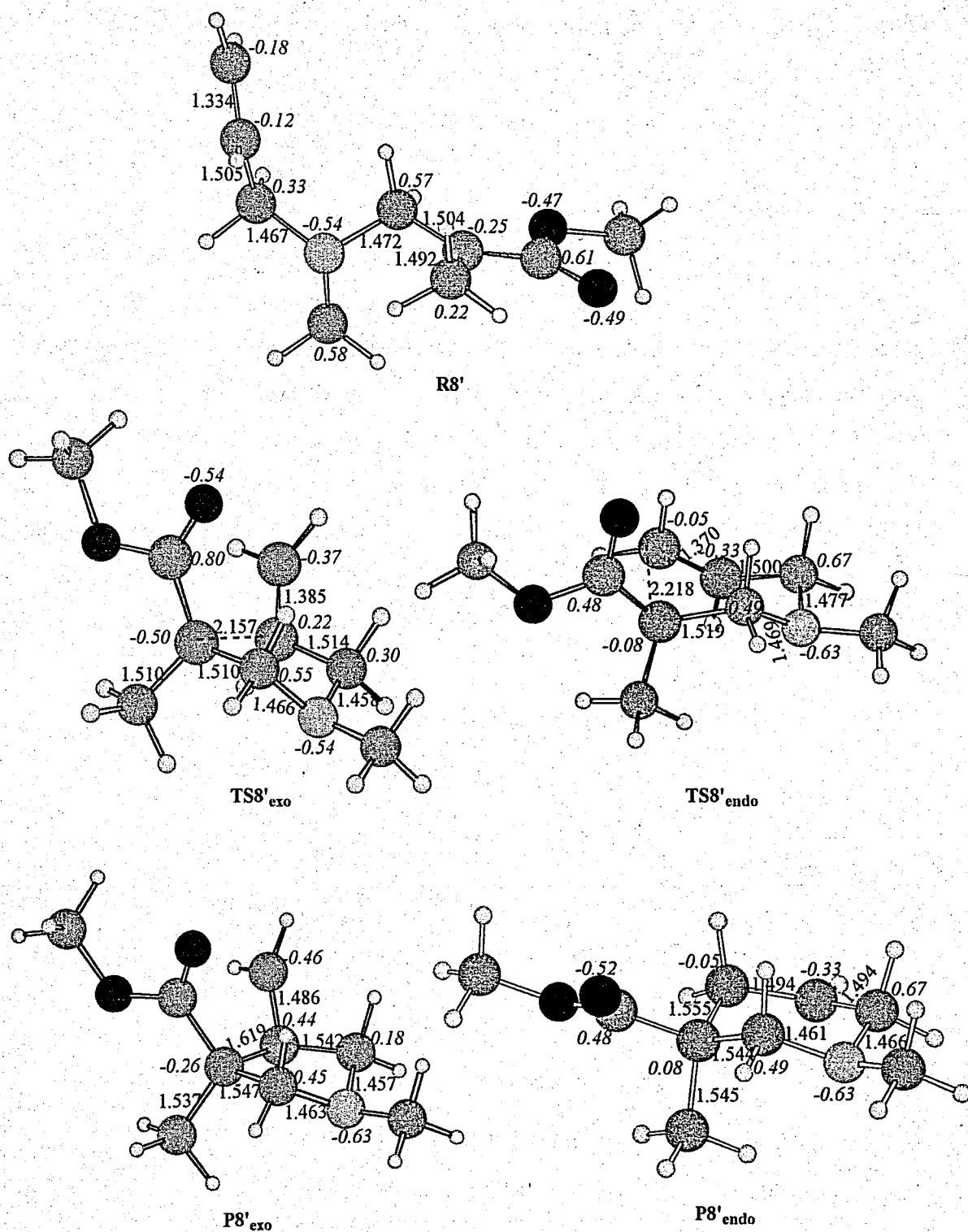
Figure 5.4. Global minimum, transition structures and the products for exo and endo cyclization of **8'**

Both the endo and the exo paths have early transition states and **TS8'$_{endo}$** is earlier than **TS8'$_{exo}$** so that the C=C bond is longer and the carbons at the reacting centers have more sp^3 character in **TS8'$_{endo}$**. The geometrical changes in **TS8'$_{exo}$** and **TS8'$_{endo}$** indicate that **8'** has a later transition state than **6'**.

The Mulliken Bonding Analysis, NBO results and the CHelp charges also confirm the experimental regioselectivity as in the case of **6'**. The Mulliken Bonding Analysis for exo and endo transition states has shown stronger bonding for 5-membered transition structure than for 6-membered (Table 5.2). NBO results show that there is a greater donor-acceptor interaction in **TS8'$_{exo}$**, than in **TS8'$_{endo}$** (Table 5.4). CHelp charges indicate that the ester group provides conjugation between the radical center and the C-O bonds. The electron density on C$_2$ is smaller in **R8'** as compared to **R6'**. As in the case of **6**, the preferred site of attack on the C$_6$=C$_7$ double bond is C$_6$, which is slightly more electrophilic than C$_7$.

Table 5.4. Natural Bond Orbital Analysis on the exo and endo transition structures (kcal/mol) of **8'**

TS8'$_{exo}$	Energy	TS8'$_{endo}$	Energy
α		α	
LP C$_2\cdot$-->BD* C$_6$=C$_7$	30.05	LP C$_2\cdot$--> BD* C$_6$=C$_7$	25.60
LP C$_2\cdot$-->BD* C$_6$=C$_7$	0.66		
β		β	
BD C$_6$=C$_7$-->LP* C$_2\cdot$	1.14		
LP C$_6$ --> LP* C$_2\cdot$	143.97	BD C$_6$=C$_7$-->LP* C$_2\cdot$	39.22
SUM	175.82	SUM	64.82

Compound **8** is reported to produce dominantly the trans product in its polymers [14]. Our calculations account for the experimentally observed stereoselectivity. The experimentally observed activation energy difference for the trans-cis cyclization is determined to be 1.07 kcal/mol [14]. We have calculated this energy difference as

1.51 kcal/mol. The cis:trans ratio is reported to vary from 10:90 to 34:66 by changing the temperature in the range of −78 to 180 °C [14]. The cis:trans ratio is calculated to be 27:73 at 180 °C. Decreasing the temperature to 25 °C increases the trans content to 13:87. Thus, our calculations produce the experimental trend qualitatively.

5.2.2.1. Steric Effect of the Ester Group in Cyclization. The ester group behaves as a bulky substituent on a cyclohexane ring. In its endo and exo transition states, it acquires the most stable orientation with respect to the ring, i.e. the equatorial orientation on C_2. This causes a change in the skeleton of the ring, such that in 6, the cis conformation is the preferred geometry but in 8 the trans orientation is preferred.

The bulky group causes steric hindrance in both exo and endo ring closures and steric crowding at the reacting sites. This increases the activation energy of cyclization because the reacting centers have to undergo more conformational change in attaining the suitable geometry for cyclization reaction at the expense of energy cost. This effect is more pronounced in the exo transition structure because a 5-membered ring is less extended than a 6-membered ring and can accommodate the ester group less easily. Thus, as a result of inclusion of the ester group in the parent structure, the activation energy for exo cyclization of 8' is higher by 3.27 kcal/mol than that of 6' whereas, this increase is only 1.02 kcal/mol in the case of endo cyclization.

Furthermore, if there is extended delocalization involving the radical center in radical addition reactions, the radical center is reported to resist pyramidalization [100]. This effect may lead to an increase in the activation energy of 8' with respect to 6'.

5.2.2.2. Electronic Effect of the Ester Group in Cyclization. According to NBO analysis, the radical on C_2 has more stabilizing interactions with the ester side of the molecule than the nitrogen. The NBO energies for the interaction of the lone pair on C_2, $LP(C_2)$ with the anti-bonding lone-pair on C of C=O (LP*) is 128.08 kcal/mol, whereas interaction of $LP(C_2)$ with the anti-bonding orbital of the C_3-N_4 bond (BD* (C_3-N_4)), is 3.52 kcal/mol and the interaction of LP (N_4) with BD* (C_2-C_3) is only 0.88 kcal/mol. The radical on C_2 is

delocalized with the ester group as expected. Due to these interactions and the decreased electron density on C_2 (-0.25 vs -0.31), the radical is reluctant to attack the C=C double bond.

5.2.2.3. <u>Effect of the Ester Group in Polymerization</u>. In the real polymerization reaction, there are a number of reactions other than cyclopolymerization, like homopolymerization or chain transfer reactions by H-abstraction from the allylic C. In our calculations, these reactions are not taken into account. The monofunctional counterpart of diallyl compounds, the allyl monomers, have low polymerization and this was attributed to chain transfer reaction by hydrogen. The secondary radical that forms by H-abstraction in chain transfer reactions is stabilized by resonance and is reluctant to polymerize. In that respect, the chain transfer reaction acts as a termination reaction. In the diallyl monomers, the cyclopolymerization takes place, overcoming the competing reactions like H-abstraction and homopolymerization.

Although the diallylamine monomer **6** has low barrier for cyclization, it is less polymerizable with respect to **8** because it still suffers from H-abstraction. The ester group may have steric and electronic effect in diminishing H-abstraction and thus, enhances cyclopolymerization. The secondary radical that forms at C_2 before cyclization is stabilized by the conjugation of the ester group and abstracts the H less readily. This is verified by the NBO delocalization energies and decreased electron density on the radical center. Secondly, the ester group may cause bulkiness in the vicinity of the hydrogens to be abstracted and this may decrease H-abstraction efficiency. Thus, chain transfer reaction by H-abstraction plays an important role and is more dominant in **6** than in **8**, although cyclization reaction is more facile with **6**. This is also conformed by the allyl C-H bond lengths in the global minimum which are 1.112 Å, 1.106 Å, 1.109 Å and 1.100 Å in **R6'**, and 1.101 Å, 1.102 Å, 1.099 Å and 1.107 Å in their analogues in **R8'**. Comparison of allylic C-H bond lengths in **6'** and **8'** shows that the C-H bonds are stronger in **8'** than in **6'**, diminishing chain transfer reaction by H-abstraction.

In addition, the ester group may suppress homopolymerization. It is known that the monomers whose monofunctional part do not have polymerization tendency increase cyclopolymerizability [13]. The functional counterparts of **8** are known to undergo poor polymerization [14-15]. Thus, the monomer with the ester group has enhanced cyclopolymerization tendency than homopolymerization, which is another competing reaction for cyclopolymerization.

5.2.3. N-methyl-N-methallyl-2-(methoxycarbonyl)allylamine (9)

Initiation in **9** can produce secondary radical on both sides of the diallyl compound and our calculations have shown that initiation takes place from the ester site as in the case of **8**. The secondary radical that forms upon initiation from the ester side (C_2) is found to be 7.06 kcal/mol more stable than the structure with a secondary radical at C_6. Thus, our calculations account for the presence of the methallyl pendant unsaturation encountered in polymers of N-methyl- N-allyl-2-(methoxycarbonyl)allylamine [15].

The global minimum for the model of N-methyl-N-methallyl-2-(methoxycarbonyl)allylamine (**R9'**) has almost the same three-dimensional structure as the global minimum for N-methyl-N-allyl-2-(methoxycarbonyl)allylamine (**R8'**). The methyl group on the double bond does not make any significant structural change in the conformation of the reactant. However, it alters the regioselectivity of cyclization reaction in **9'**. The energy barriers on the model structure of **9** have showed endo preference which is in accordance with the experimental results [15].

The Mulliken Bonding analysis indicates a stronger bonding for the exo transition structure than the endo (0.163 vs. 0.098) and likewise, the NBO stabilization energy is higher for **TS9'**$_{exo}$ (216.22 kcal/mol) than for **TS9'**$_{endo}$ (134.78 kcal/mol) (Table 5). These findings support the formation of stronger bonding in exo rather than in endo transition state, contrary to our expectations and the experimentally observed regioselectivity [15]. However, CHelp charges show that the radical prefers to attack the more nucleophilic site (C_7) of the C=C double bonds. These analyses indicate that the observed regioselectivity is

not purely directed by electronic effects. In **TS9'$_{exo}$** the reacting centers may form the C-C bond more effectively, but at a higher energy cost due to the steric effect of substituents on C=C double bond. Hence, the transition structures and their energies are much better indicators of regioselectivity.

Table 5.5. Natural Bond Orbital Analysis on the exo and endo transition structures of 9'
(Energies in kcal/mol)

TS9'$_{exo}$	Energy	TS9'$_{endo}$	Energy
α		α	
LP C$_2$-->BD* C$_6$=C$_7$	44.44	LP C$_2$-->BD* C$_6$=C$_7$	24.36
β		β	
LP C$_6$ -->LP* C$_2$	171.78	LP C$_7$ -->LP* C$_2$	110.42
SUM	216.22	SUM	134.78

The geometry of the transition state, **TS9'$_{endo}$**, is similar to **TS8'$_{endo}$**. The methyl substituent on nitrogen is in the equatorial orientation and the C=C bond is directed such that the ring has a chair-like geometry. As in the case of **TS8'$_{endo}$**, the bulkier ester group occupies the equatorial position at C$_2$. Methyl substitution on the C=C bond does not alter its axial vs. equatorial preference and the chair-like geometries of **TS6'$_{endo}$** and **TS8'$_{endo}$** are preserved in **TS9'$_{endo}$**.

In **TS9'$_{exo}$**, the geometry of the ring is boat-like, contrary to 6' and 8'. The ester group occupies the pseudo-equatorial position as in **TS8'$_{exo}$**. In **TS9'$_{exo}$**, the favored conformation of the C=O group is due to a stabilizing interaction between the oxygen of C=O and the H on C$_3$ at a distance of 2.391 Å. C$_7$ is in an axial-like orientation. In **TS6'$_{exo}$** and **TS8'$_{exo}$**, the pseudo-equatorial orientation of C=C was preferred, but in the case of **TS9'$_{exo}$**, the methyl substituent on the C=C bond occupies the equatorial position since it is slightly bulkier. This has caused a boat-like transition structure for **TS9'$_{exo}$**.
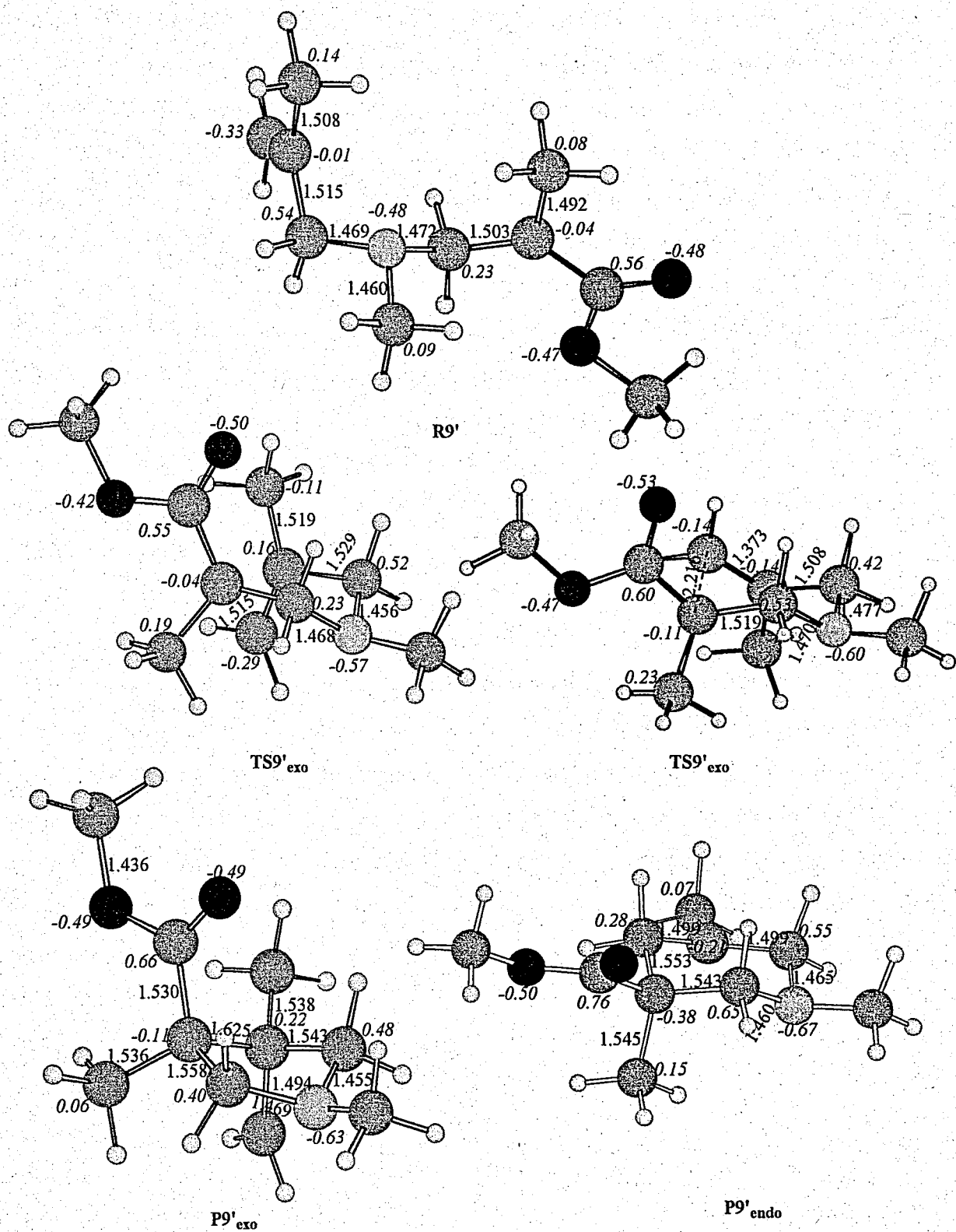
Figure 5.5. Global minimum, transition structures and the products for exo and endo cyclizations of 9'
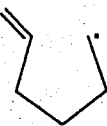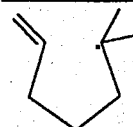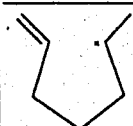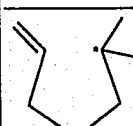
5.2.3.1 Effect of Methyl Substitution in Cyclization. We have explained the exo preference of diallylamine compounds mainly by the more favorable overlap efficiency of the reacting centers in the exo transition structure. In the literature, there are examples of compounds that undergo 6-membered ring formation as substitution on double bonds increases [67]. The five membered ring formation is explained by kinetic control of the reaction and the six membered ring formation by taking steric factors and stabilization of 6-membered radical into consideration as in experimental studies on 8 and 9. However, our calculations show that in the case of 6', 8' and 9', the experimentally observed regioselectivity is due to lower activation barrier of the cyclization reaction. Also, the 6-membered product of 9' is 12.62 kcal/mol lower in energy than the 5-membered product. Although the 6-membered products are lower in energy than the 5-membered along the polymerization of 6' and 8', the observed regioselectivity is exo and the kinetic factors dominate in the ring size preference.

The geometry of **TS9'$_{exo}$** is different than the transition structures located for hex-5-enyl [67] and diallylamine analogues modeled in our previous sections. In those cases, the reacting centers have optimum overlap efficiency in exo geometry. The favorable overlap efficiency of the exo cyclization overcomes the factors favoring the endo path, such as the stability of the 6-membered ring, the strain in the 5-membered product and the less stable primary radical that forms in the exo cyclization. However, as substituents are introduced to the parent system, as in the case of 8' and 9', the five-membered ring can hardly form, because the substituents at the reacting centers interfere and prevent cyclization. Thus, in 9', as in radical addition reactions to alkenes, the radical prefers the unsubstituted site for attack [101]. The relative rates of cyclization in hexenyl analogues show that as substituents on the C=C bond or the radical center increases, the relative rate of endo cyclization remains almost unaffected (Table 5.6). However, the rate of exo cyclization is affected much more than endo cyclization. In this study, we observe a similar effect. The geometries of the transition states **TS9'$_{exo}$** and **TS9'$_{endo}$** show that the methyl group on the double bond promotes steric interaction. In **TS9'$_{exo}$**, the five-membered ring can hardly accomodate the two substituents; methyl at C$_6$ and ester at C$_2$, thus, the destabilization is carried in the exo rather in the more extended endo transition structures. As a

result, the activation energy for the exo cyclization of 9' is much higher than that of 6' and 8', whereas the activation energy of 6', 8' and 9' in the endo cyclization is almost the same in all (Table 5.1).

Table 5.6. Relative rates for cyclization of hexenyl analogues [67]

	k_{exo}	k_{endo}
	1	0.02
	1.4	0.02
	0.022	0.04
	0.0002	0.02

5.2.3.2. Effect of Methyl Substitution in Polymerizability. In the cyclopolymerization of 8 the cyclization step is reported to be rate-determining by ESR studies [102], so the activation energies related to the cyclization step are crucial in comparing the cyclopolymerizabilities of the monomers. The polymerization of 9 is reported to be slower than 8 [14-15]. In accordance with the experimental observations, the activation energy of cyclization for 9' is higher than 8'. This is explained and demonstrated by the increased steric effect of the methyl group in cylization.

5.3. Concluding Remarks

In this study, the cyclization reactions of 6', 8' and 9' are studied as models for the cyclization reaction that takes place in the cyclopolymerization of monomers 6, 8 and

9. The calculated activation energies for cyclization have been used with success in explaining the experimental regioselectivities. The exo vs. endo preferences of the models are rationalized by taking into account different factors such as steric, electrostatic effects and entropy. The favorable entropy difference is shown to be insufficient in explaining the regioselectivity and steric effects seem to dominate the electrostatic effects.

The regioselectivity is governed mostly by the steric effects of methyl and ester substituents. Conclusively, the observed regioselectivity is mainly due to factors that cause destabilization in the exo transition states and that do not favor the exo cyclization. This conclusion is drawn by almost unchanged reaction barrier in endo cyclization and increased activation energy in exo cyclization by substitution. The experimental stereoselectivity has also been reproduced by considering the transition state geometries.

The methodology and the models used have enabled us to reproduce the experimental results whose mechanistic details had not been clarified earlier. We have been able to rationalize the substituent effect on the regioselectivity of the cyclization of diallyl derivatives. Finally, the fact that the cyclization barriers are not in agreement with the rates of the cyclopolymerization has led us to consider the expected side reactions. The strength of the α C-H bonds has been considered. It is shown that the α C-H bonds are stronger for ester substituted monomers. This prevents the effective H-abstraction, thus decreases the efficiency of degredative chain transfer, which acts as termination reaction in cyclopolymerization. The intermolecular reactions constitute the scope of Section 7 where the homopolymerization and H-abstraction reactions of diallyl monomers have been discussed.

6. MODELING THE CYCLOPOLYMERIZATION OF DIALLYL ETHER AND METHYL α-[(ALLYLOXY)METHYL]ACRYLATE

In previous sections, cyclopolymerization of various diallylamine and diallylammonium monomers have been studied. In this section, the study is extended to diallylethers, namely, diallyl ether (10) and methyl α-[(allyloxy)methyl]acrylate (11) (Figure 6.1). Experimentalists have tried different means of controlling ring size, reaction yield and cyclization efficiency, k_c/k_i, where k_c and k_i are the rate constants for cyclopolymerization and homopolymerization, respectively. As mentioned earlier, usage of monofunctional moieties that do not homolymerize is reported to facilitate cyclization by suppressing homopolymerization [13]. In most of the cases, the polymerization of non-symmetrical diallyl monomers was governed by the non-allyl counterpart [17]. The non-allyl monofunctional counterpart of methyl α-(allyloxymethyl)acrylate (11) (Figure 6.1), namely alkyl α-propoxymethylacrylate is reported to have high homopolymerization [18]. In that respect, monomer 11 was not expected to have a high cyclopolymerizability but the experiments did not confirm these predictions. Almost complete cyclization and high radical polymerizability of monomer 11 even in bulk was observed [18, 19]. The experimentalists tried to explain the high cyclization of 11 by the conformational preferences favoring cyclopolymerization [19] but their attemps have been inconclusive [6].

Monomer	R
10	H
11	COOCH₃
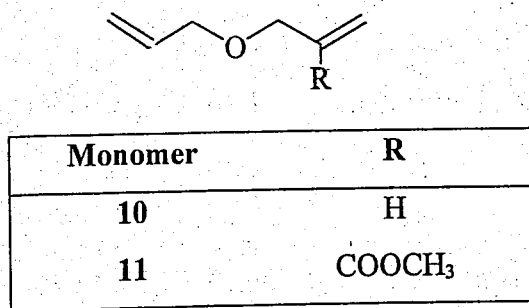
Figure 6.1. Diallylether monomers 10 and 11

In cyclopolymerization, the ring size of the cyclic species has been of interest. The regioselectivity in radical cyclization reactions is reported to depend on the substituents on

In cyclopolymerization, the ring size of the cyclic species has been of interest. The regioselectivity in radical cyclization reactions is reported to depend on the substituents on the double-bond and on the backbone [67]. Thompson *et al.* state [19] that the five-membered ring formation of **11** is not common as compared to other cyclopolymerization studies [35]. Monomer **11** is reported to form exclusively 5-membered ring in its polymerization although a 6-membered ring would be expected [18]. The diallyl ether monomer, **10** (Figure 6.1), is also reported to undergo cyclopolymerization reaction with 5-membered rings on its backbone [2].

In this study, the cyclization of monomers **10** and **11** in their cyclopolymerization mechanism has been modeled to account for their cyclopolymerizabilities. The conformational preferences of the monomers prior to cyclization have been explained and their effect in cyclization have been demonstrated. The transition structures leading to 5-membered and 6-membered rings have been located and, their energetics and three dimensional geometries have been discussed to account for the regioselectivity of cyclization of these monomers. Stereoselectivity of monomers have also been considered. The effect of ester substitution has been inquired and finally, the experimental data has been compared with the calculations.

6.1. Methodology

To model the cyclization reactions of monomers **10** and **11** in their cyclopolymerization reactions, a model compound is used to simplify the long polymer chain as in our earlier studies [95, 96, 103]. The model compounds for **10**, and **11** will be designated by **10'** and **11'**.

The calculations have been carried out by using the density functional theory [26], with the B3LYP methodology [31] and the 6-31G* basis set, using the Gaussian 98 package [61]. In the diallyl and diallylammonium analogues of **10** and **11**, we have successfully reproduced the regioselectivity and other available experimental data by using this methodology.

search is done with the semi-empirical PM3 [24, 25] method and the lowest 20 conformers have been optimized with B3LYP/6-31G*. In addition to the global minima, the reactants that are cyclic in their ground state and in a very suitable geometry for cyclization have also been located. These rotamers which resemble the transition states will be referred to as "reactive rotamers" as in previous sections.

The transition structures for the cyclization reactions of the model compounds, **10'** and **11'**, have also been modeled. Various conformations of the transition structures, depending on ring size and ring geometry have been located. One imaginary frequency belonging to the reaction coordinate has confirmed the validity of the transition state.

Intrinsic Reaction Coordinate (IRC) [63, 64] calculations have been performed on both five and six membered transition structures. The stationary points obtained in this way were further optimized. The geometries obtained by the DFT theory have been shown to be adequate [95, 96, 103] however, the energies were further improved by using higher level of calculations. MP2/6-31G* optimizations have been performed on the B3LYP/6-31G* geometries of global minimum and transition structures of **10'**.

Natural Bond Orbital (NBO) analysis [44-48] has been performed on the reactants and transition structures.

The energetics for cyclization, the activation energies, $\Delta E^{\neq}$, free energies of activation, $\Delta G^{\neq}$, entropies of activation, $\Delta S^{\neq}$, heats of reaction, ΔE_{rxn}, and the free energies of reaction, ΔG_{rxn}, have been also reported. These findings will be discussed in terms of polymerization efficiencies, regioselectivity and stereoselectivity of the monomers. The effect of ester substitution will also be explained. The calculations will be compared with the available experimental data.

The numbering system shown in Figure 6.2 will be used in the following discussion.

The numbering system shown in Figure 6.2 will be used in the following discussion.
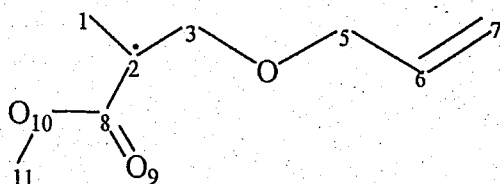
Figure 6.2. The numbering scheme used for compounds **10** and **11**

6.2 Results and Discussion

6.2.1 Diallyl Ether (10)

The model compound located as global minimum for the model of diallyl ether, **GM_10'**, (Figure 6.3) is in an extended conformation. This conformation allows strong hyperconjugative interactions from the lone-pairs of oxygen, with the partially filled p orbital of the radical and the π-bonds to the corresponding antiperiplanar antibonds. These effects are demonstrated by NBO calculations in Table 6.1. In the global minimum, the allyl sides are very much like their three-dimensional structure in the transition state but the ring-like structure is distorted by rotation around the C-O bonds. If the C5-C6 and C3-O4 bonds were anti to each other, the structure of the molecule would be more extended but the hyperconjugative interactions from the lone pairs to the antiperiplanar C2-C3 and C5-C6 bonds in the global minimum would be diminished.

The reactive rotamer of **10'**, **RR_10'**, (Figure 6.3) obtained from the IRC calculations has also been studied. The 3-dimensional structure of this rotamer is similar to its transition structure. The reactive rotamer is only 0.88 kcal/mol higher in energy than the global minimum and the barrier for rotation can easily be attained under the reaction conditions by free rotation around single bonds. The presence of oxygen as heteroatom in the ring causes the reactive rotamer to be closer in energy with respect to the global minimum and this will be demonstrated by NBO analysis done on both conformers.
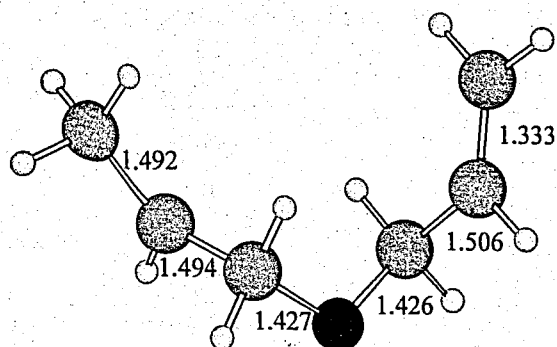
GM_10'
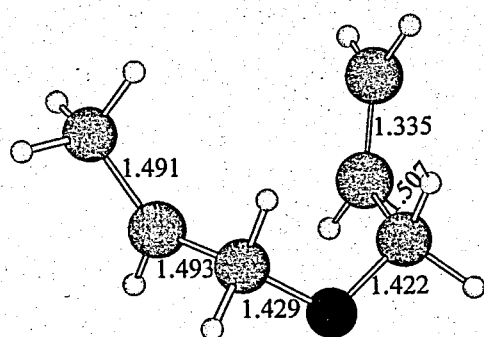
RR_10'
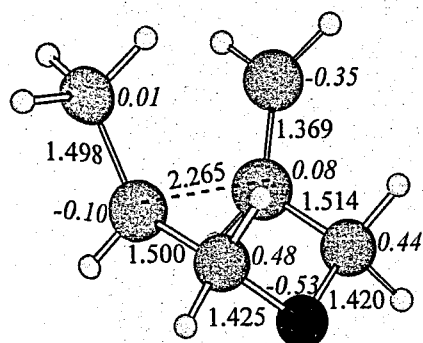
TS10'$_{exo}$
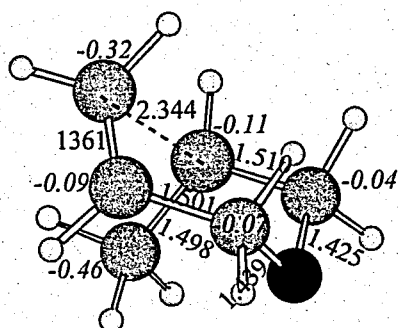
TS10'$_{endo}$
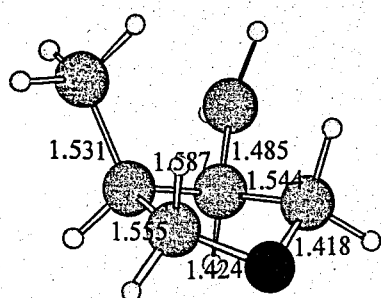
P10'$_{exo}$
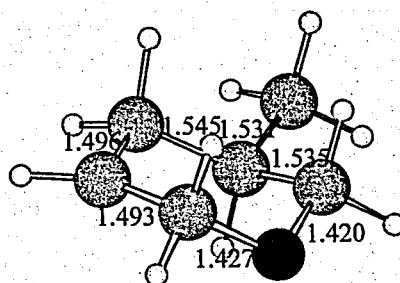
P10'$_{endo}$

Figure 6.3. The global minimum, reactive rotamer, transition structures and products for endo and exo cyclization for the model compound of diallyl ether (**10'**)

Table 6.1. The NBO stabilization energies (kcal/mol) of the reactive rotamer (**RR_10'**) and the global minimum (**GM_10'**)

Donor-Acceptor	RR_10'	GM_10'
LP_1 (O) $\rightarrow$ BD^*C_2-C_3	0.66	0.98
LP_2 (O) $\rightarrow$ BD^*C_2-C_3	6.79	6.41
LP_1 (O) $\rightarrow$ BD^*C_5-C_6	1.25	0.62
LP_2 (O) $\rightarrow$ BD^*C_5-C_6	6.93	7.16
LP_1 (O) $\rightarrow$ BD^*C_3-H_a	2.01	1.69
LP_2 (O) $\rightarrow$ BD^*C_3-H_a	4.01	5.18
LP_1 (O) $\rightarrow$ BD^*C_3-H_b	0.76	0.81
LP_2 (O) $\rightarrow$ BD^*C_3-H_b	0.62	0.68
LP_1 (O) $\rightarrow$ BD^*C_5-H_a	1.50	1.43
LP_2 (O) $\rightarrow$ BD^*C_5-H_a	5.46	-
LP_1 (O) $\rightarrow$ BD^*C_5-H_b	1.60	2.12
LP_2 (O) $\rightarrow$ BD^*C_5-H_b	-	4.47
LP C_2 $\rightarrow$ BD^*C_3-H_a	0.35	0.93
LP C_2 $\rightarrow$ BD^*C_3-H_b	4.49	4.99
LP C_2 $\rightarrow$ BD^*C_3-O_4	4.34	2.33
BD_1 C_6=C_7 $\rightarrow$ BD^* O_4-C_5	2.26	2.49
BD_2 C_6=C_7 $\rightarrow$ BD^* O_4-C_5	2.35	2.50

In Table 6.1, the hyperconjugative interactions from the lone-pairs, π-bonds and half-filled p-orbital of the radical are considered. It is important at this point to recall that a hyperconjugative interaction is maximized when the donor and acceptor molecular orbitals are on the same plane. These interactions invoke the anomeric effect where the donor is a bonding orbital and the acceptor is an antiperiplanar antibonding orbital [104]. The donor-acceptor stabilizations have shown the hyperconjugative interactions to be strong in both conformers for **10'**. However, there are two interactions in **RR_10'** that are lost in global minimum (**GM_10'**). One of them is from the lone pair of oxygen to the antiperiplanar

antibonding orbital of C5-H (LP$_2$(O)→BD* C$_5$-H$_a$) with a stabilizing interaction of 5.46 kcal/mol. In the reactive rotamer (**RR_10'**) there is an interaction of 4.34 kcal/mol from the radical center to the C3-O4 bond while the geometry of the global minimum (**GM_ 10'**) allows only a 2.33 kcal/mol of stabilization. This kind of hyperconjugation has been reported to be important in the stereoselectivity of pyranyl compounds [105, 106]. The other interactions are almost in the same order. When the whole system is considered, the total donor-acceptor interactions are higher for the reactive rotamer (197.14 kcal/mol) than for the global minimum (195.07 kcal/mol). These interactions suggest that the donor-accceptor stabilizations are maximized in the reactive rotamer and they stabilize the system, even more than the global minimum and overcome the strain energy induced by the cyclic structure to a great extent. Thus, the energy of the reactive rotamer is only 0.88 kcal/mol higher than the global minimum.

It is well known by anomeric effect that the hyperconjugation is often accompanied by changes in bond length [104]. In compounds **RR_10'** and **GM_10'**, there are hyperconjugative interactions in both directions, so there is no net bond shortening in the donor bond and bond lengthening in the acceptor.

In section 4, the diallylamine and diallylammonium monomers have been considered and their reactive rotamers as well as their global minima have been located. The reactive rotamer was found to be 1.3 kcal/mol and 2.5 kcal/mol above the global minima in N-methyl-N-N-diallylamine (**6**) and in N, N-dimethyl,N-N-diallylammonium (**3**), respectively. The total donor-acceptor interactions calculated by NBO are 218.3 kcal/mol in the reactive rotamer and 213.4 kcal/mol in the global minimum of **6**. In the N, N-dimethyl,N-N-diallylammonium (**3**), these interactions are 223.35 kcal/mol and 224.17 kcal/mol, respectively. **6** has more donor-acceptor interactions in its reactive rotamer than in its global minimum. Whereas, in **3**, the reactive rotamer has even less donor-acceptor interactions, hence a sterically unfavored ring-like conformer is at a higher level. These findings suggest that the ring strain is overcome by the more favorable conformation for hyperconjugative interactions. Hence, the relative energy of the ring-like structure with respect to the global minimum is higher in cases where this type of interactions are absent.

Later, we will demonstrate that the hyperconjugation is also important in the facilitation of transition state as well.

A semi-empirical search with PM3 has also been conducted on the dimer geometry. The structure corresponding to the global minimum for the dimer has a 3.35 Å of C--C bonding distance in cyclization. Another conformer which is only 0.15 kcal/mol higher than the global minimum has a C--C bonding distance of 3.24 Å. These results show that the presence of the oxygen in diallyl compounds allows ring-like conformers to be at a relatively lower energy level, facilitating the cyclization.

6.2.1.1. The Transition Structures for 10'. In our earlier reports, the conformations of the transition states rather than the stability of products were demonstrated to be the key points in determining the regioselectivity of the cyclization. Thus, the conformations of transition states as well as the exo vs endo closure preference of the monomers 10' and 11' have been discussed. They have been referred to as chair and boat.

10' has shown exo preference (Table 6.2). As mentioned earlier, 6-membered products are expected to form in general due to higher ring strain in 5-membered rings. Furthermore, in cyclopolymerization, the secondary radical, that forms by endo cyclization can also be expected to be more stable than the primary radical that forms by exo ring closure. Additionally, the radicals prefer to add to the least substituted carbon of the double-bond [101]. However, 10' undergo exo ring closure despite the factors favoring endo ring formation.

The difference between the activation energies of the exo and the endo transition states of 10' is 4.92 kcal/mol, demonstrating the experimental exclusive exo preference (Table 6.2). The exo preference of the diallyl monomers in cyclization was interpreted to be kinetically controlled [6].

Table 6.2 The energetics of cyclization for model compounds **10'** and **11'** in kcal/mol

	10'	11'
Global Minimum (**GM**)	0	0
Reactive Rotamer (**RR**)	0.88	0.68
TS_{exo}	5.33	9.82
TS_{endo}	10.25	12.08
Product-exo	-13.51	-2.16
Product-endo	-20.07	-8.49

The transition structure of exo ring closure, **TS10'$_{exo}$** (Figure 6.3), is an early transition structure, which is typical in cyclization reactions. Along the reaction coordinate, the C=C double bond has lengthened by 0.036 Å in **TS10'$_{exo}$** and the COC angle decreases from 113.9° in **GM_10'** to 108.9° in **TS10'$_{exo}$**. The ring in **TS10'$_{exo}$** has a chair-like geometry. C1 behaves as an equatorial substituent on a cyclohexane ring. The transition state with axial C1 is only 0.28 kcal/mol higher in energy than **TS10'$_{exo}$**. The destabilization by axial substitution is small because in the axial orientation, the methyl group is not exposed to steric interactions. In the real polymerization process, the long polymer chain can cause much more steric hindrance than the methyl group in the model and the axial substitution may be more destabilized with respect to equatorial substitution. The transition structure for endo ring closure (**TS10'$_{endo}$**) has also a chair-like geometry. It is 4.92 kcal/mol higher in energy than **TS10'$_{exo}$**.

The exo selectivity of diallyl compounds has been shown to depend on the backbone structure and on the nature of substituents on the C=C double-bond [67]. In our previous sections on diallyl amine and diallyl ammonium monomers, it has been shown that 5-membered ring formation is facilitated due to the favorable overlap efficiency and the regioselectivity is mostly governed by steric factors rather than the electronic factors. The regioselectivity of cyclization in **10'** is typical for radical cyclization of simple systems. In the exo transition structure, the p-orbital on the radical center is colinear with π-orbital of the the C=C bond, providing a very efficient overlap geometry. This colinearity in overlap

is considered to have the largest effect in regioselectivity. Electrostatic effects also direct the exo attack of the growing radical. The radical prefers to attack the more electrophilic site of the double-bond (-0.28 vs. -0.08). In this system, in addition to the electrostatic effects, there are hyperconjugative interactions in the transition states, which can be traced by the NBO stabilization energies. In the ring-like structure of the transition states, there are stabilizing hyperconjugative interactions as in the reactive rotamer (Table 6.3).

Table 6.3. The NBO stabilization energies (kcal/mol) of the transition states of **10'**

Donor-Acceptor	TS10'$_{exo}$	TS10'$_{endo}$
LP$_1$ (O) → BD*C$_2$-C$_3$	1.51	0.74
LP$_2$ (O) → BD*C$_2$-C$_3$	4.79	7.39
LP$_1$ (O) → BD*C$_5$-C$_6$	1.85	0.87
LP$_2$ (O) → BD*C$_5$-C$_6$	5.11	6.02
LP$_1$ (O) → BD*C$_3$-H$_a$	0.86	2.04
LP$_2$ (O) → BD*C$_3$-H$_a$	6.67	4.28
LP$_1$ (O) → BD*C$_3$-H$_b$	1.36	1.35
LP$_2$ (O) → BD*C$_3$-H$_b$	-	-
LP$_1$ (O) → BD*C$_5$-H$_a$	0.76	1.40
LP$_2$ (O) → BD*C$_5$-H$_a$	7.12	-
LP$_1$ (O) → BD*C$_5$-H$_b$	1.39	1.51
LP$_2$ (O) → BD*C$_5$-H$_b$	-	4.55
LP C$_2$ → BD*C$_3$-H$_a$	-	0.31
LP C$_2$ → BD*C$_3$-H$_b$	2.90	3.31
LP C$_2$ → BD*C$_3$-O$_4$	4.37	2.10
BD$_1$ C$_6$=C$_7$ → BD* O$_4$-C$_5$	0.48	-
BD$_2$ C$_6$=C$_7$ → BD* O$_4$-C$_5$	4.49	7.68
LP C$_2$ → BD* C$_6$-C$_7$	22.91	19.56
BD C$_6$-C$_7$ → LP* C$_2$	26.44	21.92

The three-dimensional geometries of **TS10'$_{exo}$** and **TS10'$_{endo}$** allow different hyperconjugative interactions to take place. The total donor-acceptor interactions are 267.57 kcal/mol and 238.38 kcal/mol in the exo and endo transition states, respectively. The NBO energies show that, in addition to the overlap efficiency of the exo transition state, it is also stabilized more by the hyperconjugative interactions allowed by the exo geometry. One of the most significant contribution to this energy difference is from the interactions at the reacting centers: LP C2→σ* (C6=C7) and σ (C6=C7) → LP* C2. The effects that lower the strain energy of **RR_10'** are also present in **TS10'$_{exo}$** and stabilizing interactions from the lone pairs of oxygen to the antibonding orbitals of C3-H and C5-C6 bonds are more significant. Thus, the hyperconjugative effects which may be expressed as a facilitation of the transition state may decrease the barrier for cyclization. Furthermore, the regioselectivity may also be affected to a great extent by the hyperconjugative effects.

In diallylamine (**1**), the barrier for cyclization has been calculated to be 7.3 kcal/mol. Comparison of this barrier with that of **10'** shows that the presence of oxygen enhances the cyclization, because the ring-like geometry in ether analogs allows more hyperconjugation.

6.2.1.2. Stereoselectivity in Cyclization. The ring closure of the model compound **10'** has been reported to favor *cis* product and the rates of *cis* product formation over *trans*, k_{cis}/k_{trans}, have been found to be experimentally 2.3 at t=65 °C [107]. Our calculations have reproduced the *cis* preference in cyclization. The *cis-trans* energy difference is 0.28 kcal/mol. This ratio is calculated to be 2.2 at t=25 °C with the B3LYP energies. The *cis* preference in cyclization can be explained on the basis of chair-like transition states. C1 behaves as a substituent on a cyclohexane ring, preferrring the sterically less hindered equatorial position. The *cis-trans* energy difference is quite small because the ring has no substituent so as to cause strong steric repulsion of the axial substituent.

6.2.1.3. Comparison of Cyclization Rate Constant with the Experiments. The activation energy for cyclization of the model compound, **10'** has been determined as 4.1 kcal/mol by experiments [108]. This barrier has been determined to be 5.33 kcal/mol with B3LYP/6-31G* calculations. The PMP2 optimizations of B3LYP geometries of the global minimum

of reactant and the exo transition state decreases the barrier to 3.82 kcal/mol. The experimental pre-exponential factor is 9.64 and the calculated value is 10.92, in good agreement with the experiment. The calculations refined by PMP2 optimizations of the B3LYP geometries with the 6-31G* basis set are successful to reproduce the experimental activation energy.

6.2.2 Methyl α-(allyloxymethyl)acrylate (11)

The site of initiation produces either a tertiary radical if the intiation takes place from the methacrylate site or a secondary radical if it proceeds from the allyl side. In the study on amine analogues of 11, namely N-methyl-N-allyl-2-(methoxycarbonyl)allylamine) (8), it is shown that initiation starts from the ester side. In the diallyl ether compounds, the initiation is assumed to take place from the methacrylate side, based on experimental observations and calculations [18, 19].

Monomer 11, methyl α-(allyloxymethyl)acrylate, has surprisingly high polymerization efficiency even in bulk. It has been stated by Thompson *et al.* that the preferred conformations of the ether linkage may play an important role in this system [19]. Many attempts have been made to identify group preassociation and/or conformational preferences favoring cyclopolymerization [19], however, the results have been inconclusive [6].

The three-dimensional structure for model of 11 has been determined for its global minimum and the reactive rotamer has been located. The conformational preferences of the monomer and the effect of oxygen in attaining the strained cyclic-like structure prior to cyclization will be discussed.

In the global minimum, GM_11' (Figure 6.4) the allylic side is in a ring-like geometry as in GM_10'. The C6-C5-O4-C3 dihedral of 71° was preferred over 180°, not satisfying the expectations of the anti being more stable than the gauche. This geometry allows gauche orientation of the lone pairs on ether oxygen with the C5-C6 and C5-H

bonds. On the other hand, one of the lone-pairs of ether oxygen is antiperiplanar to C5-H and C5-C6 bonds, respectively. The donor-acceptor interactions allowed by this geometry are 7.66 kcal/mol from the lone-pair of oxygen to the antibonding C5-C6, 6.59 kcal/mol to the antiperiplanar C5-H bond and 1.53 kcal/mol to the other C5-H bond (Table 6.4). These interactions are 1.16, 7.24 and 6.62 kcal/mol, in the anti orientation of the C6-C5-O4-C3 dihedral, respectively. The energy of this conformer is only 0.42 kcal/mol higher than **GM_11'** because in this geometry, the lone-pairs on oxygen are antiperiplanar to the C5-H bonds, thus, the interaction with the C5-C6 antibond is diminished and compensated by the C5-H interaction. The methacrylate side of the molecule is in an extended conformation, providing a very efficient geometry for delocalization of the radical center and the ester group. The C2-C3 bond is in anti orientation with the O4-C5 bond, with antiperiplanar lone-pairs with the C3-H bond. The total donor-acceptor interactions associated to these bonds are in the order of 7.31 and 7.21 kcal/mol. (Table 6.4) Gauche orientation of the C2-C3 and O4-C5 bonds would generate a ring-like geometry with steric interactions. The sum of all the donor-acceptor interactions in the global minimum is 706.77 kcal/mol.

The energy of the reactive rotamer, **RR_11'**, is only 0.68 kcal/mol higher than **GM_11'** although steric hindrance is introduced in the system by the ring-like geometry and the ester group (Table 6.2). The steric effects of the ring-like geometry are relieved to a certain extent by the hyperconjugative effects in the molecule. The allyl side of **RR_11'** has almost the same geometry and the same kind of hyperconjugative interactions as in **GM_11'**. On the methacrylate side, the lone-pairs on oxygen are almost antiperiplanar to the C3-H and C2-C3 bonds, with donor-acceptor interactions of 5.31 and 7.80 kcal/mol, respectively (Table 6.4). The methacrylate side allowed more-donor acceptor interactions between the lone-pairs of oxygen and antiperiplanar bonds. The sum of all donor-acceptor interactions is 702.95 kcal/mol in **RR_11'**, which is almost equivalent to the interactions in **GM_11'**.
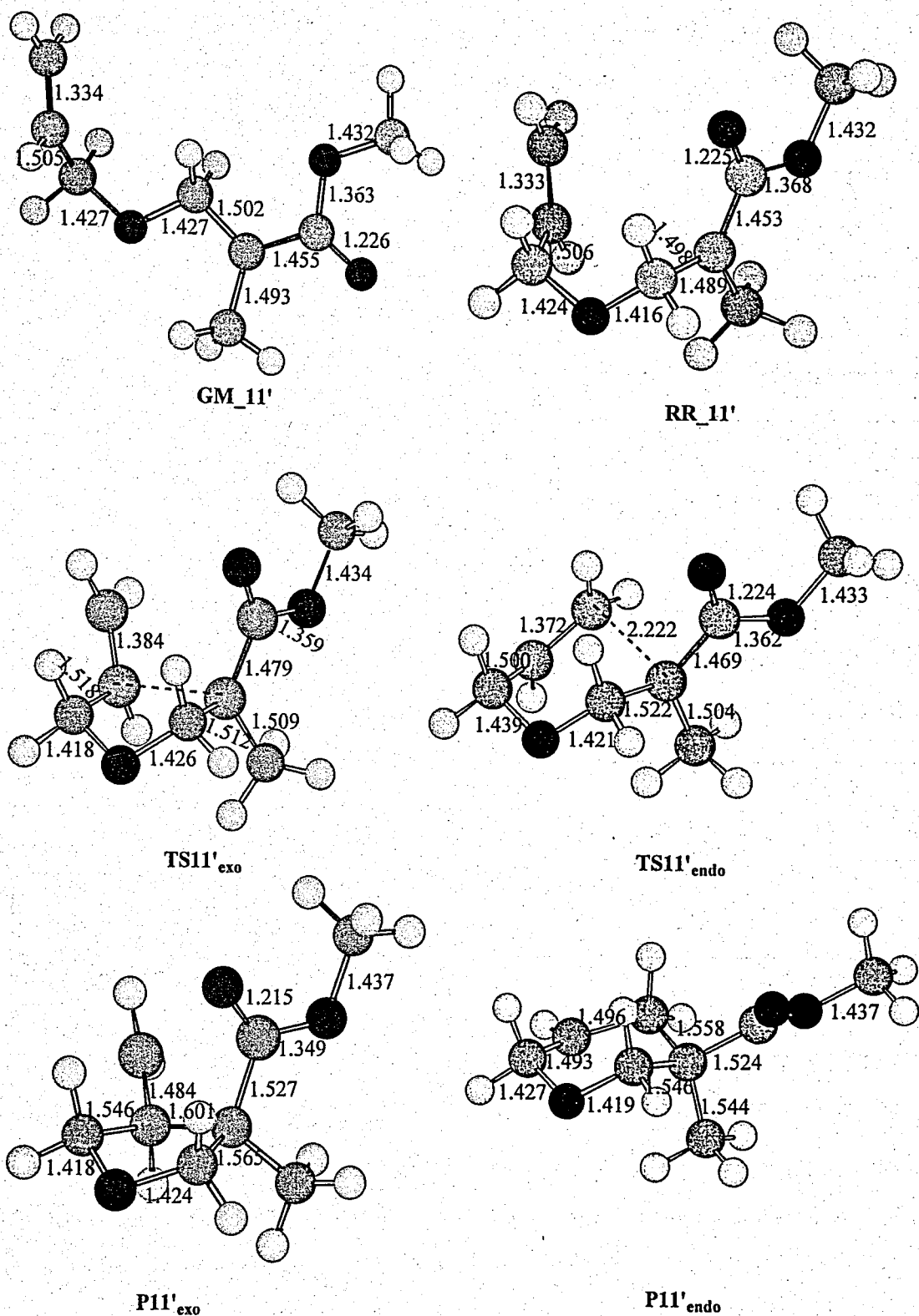
Figure 6.4. The global minimum, reactive rotamer, transition structures and products for endo and exo cyclization for the model compound 11'

Table 6.4. The NBO stabilization energies (kcal/mol) of the reactive rotamer (**RR_11'**) and the global minimum (**GM_ 11'**)

Donor-Acceptor	RR_11'	GM_ 11'
LP_1 (O) $\rightarrow$ BD*C_2-C_3	0.26	1.25
LP_2 (O) $\rightarrow$ BD*C_2-C_3	7.54	-
LP_1 (O) $\rightarrow$ BD*C_5-C_6	0.85	0.91
LP_2 (O) $\rightarrow$ BD*C_5-C_6	7.03	6.75
LP_1 (O) $\rightarrow$ BD*C_3-H_a	2.22	1.20
LP_2 (O) $\rightarrow$ BD*C_3-H_a	3.09	6.01
LP_1 (O) $\rightarrow$ BD*C_3-H_b	1.29	1.30
LP_2 (O) $\rightarrow$ BD*C_3-H_b	0.71	6.11
LP_1 (O) $\rightarrow$ BD*C_5-H_a	1.73	1.63
LP_2 (O) $\rightarrow$ BD*C_5-H_a	4.53	4.96
LP_1 (O) $\rightarrow$ BD*C_5-H_b	1.47	1.53
LP_2 (O) $\rightarrow$ BD*C_5-H_b	-	-
LP C_2 $\rightarrow$ BD*C_3-H_a	-	3.11
LP C_2 $\rightarrow$ BD*C_3-H_b	3.15	3.05
LP C_2 $\rightarrow$ BD*C_3-O_4	4.79	-
BD_1 C_6=C_7 $\rightarrow$ BD* O_4-C_5	0.27	-
BD_2 C_6=C_7 $\rightarrow$ BD* O_4-C_5	5.35	5.17
LP C_2 $\rightarrow$ LP* C_8	128.39	134.16

The three-dimensional structures of **RR_ 11'** and **GM_ 11'** allow different stabilizing interactions (Table 6.4). For example, there is an interaction of 7.54 between the lone pair on ring oxygen and C2-C3 bond (LP_2 (O) $\rightarrow$ BD* (C_2-C_3)) in **RR_ 11'** whereas such an interaction does not exist in **GM_ 11'**. The interaction from the lone pair on radical center to the antibonding C3-O4 bond (LP (C_2) $\rightarrow$ BD* (C_3-O_4)) has also diminished in **GM_ 11'** whereas it is 4.79 kcal/mol in **RR_ 11'**. On the other hand, the 3.11 kcal/mol of interaction, LP (C_2) $\rightarrow$ BD* (C_3-H_a) of **GM_ 11'** is not present in **RR_**

11'. The most striking difference is in the interaction of the radical center with the C=O of the ester group in **GM_ 11'** allowing a greater stabilization. These interactions show that the extended structure of the **GM_ 11'** has only 0.5 percent higher stabilizing interaction with respect to the sterically strained cyclic-like structure of the **RR_ 11'**.

6.2.2.1. The Transition Structures for 11'. 11 has shown exo preference over the endo in both calculations and experiment (Table 6.2). The endo preference has been expected due to several reasons mentioned earlier. Additionally, Beckwith et al. has shown an endo:exo ratio of 44:56 for ethyl ester substituted 5-hexenyl, which has a structure similar to 11 [67]. It has also been reported that the substituents that lead to stabilization in the radical center result in endo preference [109].

The overlap efficiency of the exo geometry over the endo is still effective in exo preference of 11. In general, the endo barriers calculated in previous sections are within a range of 10-12 kcal/mol. The energy of the endo transition structure of 11' is also within this range (Table 6.2). As in N-methyl-N-allyl-2-(methoxycarbonyl)allylamine) monomer, discussed in Section 5, the ester substituent destabilizes the exo transition structure much more than the endo. The six-membered ring is able to host the ester substituent without a significant increase in its barrier height for cyclization reaction. Five-membered rings, being generally more strained than the six-membered rings, cannot host the ester group as easily as the endo transition state. However, the border-line between the steric effect of substituents and the exo overlap efficiency has not been overcome yet. It has been shown previously that the electrostatic effects do not have dominance in regioselectivity. In 11', the charges on C6 and C7 are -0.25 and -0.26, respectively. Thus, the charges on double bonds show no preference over the other for a radicalic attack.

In the five-membered transition state, **TS11'$_{exo}$**, the chair-like geometry of the ring is preserved (Figure 6.4). The ester substituent is in pseudoequatorial position, as the bulkier group prefers the equatorial substitution on the cyclohexane-like ring geometries. **TS11'$_{exo}$** is an early transition state as it is typical in the cyclization reactions. **TS11'$_{endo}$** also has a

chair-like geometry, with pseudo-equatorial orientation of the bulky ester group (Figure 6.4).

Table 6.5. The NBO stabilization energies (kcal/mol) of the transition states of **11'**

Donor-Acceptor	TS11'$_{exo}$	TS11'$_{endo}$
LP$_1$ (O) → BD*C$_2$-C$_3$	1.39	0.37
LP$_2$ (O) → BD*C$_2$-C$_3$	4.98	8.01
LP$_1$ (O) → BD*C$_5$-C$_6$	1.71	0.67
LP$_2$ (O) → BD*C$_5$-C$_6$	5.16	5.98
LP$_1$ (O) → BD*C$_3$-H$_a$	0.88	2.15
LP$_2$ (O) → BD*C$_3$-H$_a$	6.01	3.94
LP$_1$ (O) → BD*C$_3$-H$_b$	1.32	1.34
LP$_2$ (O) → BD*C$_3$-H$_b$	-	-
LP$_1$ (O) → BD*C$_5$-H$_a$	0.81	1.37
LP$_2$ (O) → BD*C$_5$-H$_a$	7.04	-
LP$_1$ (O) → BD*C$_5$-H$_b$	1.35	1.66
LP$_2$ (O) → BD*C$_5$-H$_b$	-	4.23
LP C$_2$ → BD*C$_3$-H$_a$	-	0.31
LP C$_2$ → BD*C$_3$-H$_b$	2.17	2.51
LP C$_2$ → BD*C$_3$-O$_4$	4.29	1.69
BD$_1$ C$_6$=C$_7$ → BD* O$_4$-C$_5$	0.49	-
BD$_2$ C$_6$=C$_7$ → BD* O$_4$-C$_5$	1.71	7.26
LP C$_2$ → BD* C$_6$-C$_7$	27.9	26.57
BD C$_6$-C$_7$ → LP* C$_2$	1.13	39.23
LP C$_2$ → BD* C$_8$=O$_9$	30.09	36.14
LP O$_9$ → BD* C$_8$-O$_{10}$	35.06	34.72
LP O$_{10}$ → BD* C$_8$-O$_9$	53.53	52.40
LP C$_6$ → LP* C$_2$	140.12	-
LP C$_6$ → LP* C$_7$	121.04	-
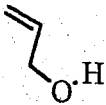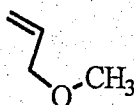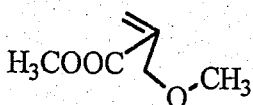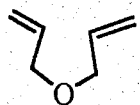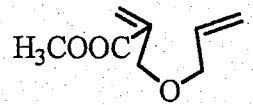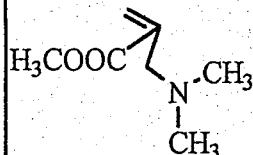
The sum of all the stabilizing interactions are 803.01 kcal/mol whereas in the endo transition state it is only 566.94 kcal/mol. The most significant difference is in the efficiency of C6=C7 bond to participate in the bonding process with an efficient delocalization extending from C7 to C6 and C2 (Table 6.5). Furthermore, in cyclization reaction the sum of all the donor-acceptor interactions increase in the exo transition state, facilitating cyclization.

6.2.2.2. Stereoselectivity in Cyclization. The ^{13}C NMR analysis of the polymers obtained from monomer 11 have shown slight dominance of *trans* forms of the repeating cyclic units [19]. Our calculations have also shown *trans* orientation of the monomer. The *trans* preference can be interpreted with a more stable equatorial substitution on cyclohexane-like structure. The calculated energy difference between *trans* and *cis* transition structures is 1.23 kcal/mol.

6.3. Comparison of Polymerizabilities

The diallyl ether monomer 10 has been reported to be a poor monomer for polymerization. In our calculations, the cyclization step has been shown to be facile, thus, the reactions that compete with the standard cyclopolymerization reaction should be more effective and cause poor cyclopolymerization of the diallyl ether monomer 10. To see the effect of the competing reactions, the model reactions for H-abstraction from the allylic carbon (Table 6.6) and the homopolymerization reactions (Figure 6.5) have been analyzed. In the models, the monofunctional counterparts or the monomer itself are considered. In the H-abstraction study, the reaction of H-abstraction by a methyl radical from the allylic carbon is studied.

Table 6.6. Energetic data on H-abstraction reaction by the CH$_3$ radical from the allylic carbon

	Ea (ϵ=1)	$\Delta G^{\neq}$
	5.45	12.50
	6.05	13.21
	6.07	13.78
	7.82	14.28
	7.78 (allyl side) 6.28 (ester side)	14.48 13.72
	6.29 (ester side)	

To verify the validity of our model systems, polymerization of allylalcohol was modeled. It is known that allylalcohol can not be polymerized efficiently [21]. This has been attributed to the degradative chain transfer by H-abstraction. The homopolymerization of allylalcohol has a free energy of activation of 18.49 kcal/mol [Figure 6.5], whereas, the barrier for H-abstraction reaction is 12.50 kcal/mol (Table 6.6). The chain transfer reaction dominates over the homopolymerization, thus decreases the polymerizability of allyl alcohol.
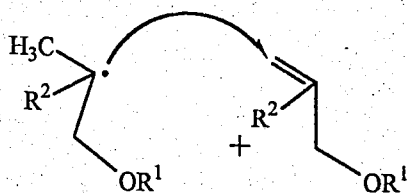
R^1	R^2	E_a ($\varepsilon=1$)	$\Delta G^{\neq}$
H	H	4.87	18.49
CH$_3$	H	3.89	16.87
CH$_3$	COOCH$_3$	4.63	19.91

Figure 6.5. Energetic data on homopolymerization of model systems

Having obtained reasonable results with our model calculations, the model compounds shown in Figure 6.5 and Table 6.6 have been investigated. After initiation, the monomer can either undergo cyclization or homopolymerization. In the gas phase, the activation energies for cyclization and homopolymerization reaction of the model system of **10'** are 5.33 kcal/mol and 3.89 kcal/mol, respectively. Although the barriers indicate a more favorable activation energy for homopolymerization, cyclization is favored entropically ($\Delta S^{\neq}=-9.77$ cal/mol K for cyclization and $\Delta S^{\neq}=-40.18$ cal/mol K for homopolymerization) and the free energy of activation is lower for cyclization. However, H-abstraction reaction is found to be more facile than homopolymerization and this explains the low polymerizability of the monomer.

Monomer **11** has been reported to undergo cyclopolymerization very efficiently, even in bulk. The barrier for cyclization has been calculated to be 9.82 kcal/mol. The free energy of activation is only 12.64 kcal/mol. The monofunctional counterpart of monomer **11** has been modeled as model for homopolymerization as in diallyl ether (Figure 6.5). The barrier for homopolymerization (4.63 kcal/mol) is lower than cyclization. However, entropy has a significant contribution ($\Delta S^{\neq}=-46.95$ cal/mol K) and free energy of activation for homopolymerization reaction is 19.91 kcal/mol (Figure 6.5). The entropic

contribution is calculated to be small in cyclization ($\Delta S^{\neq}= {}^-11.53$ cal/mol K), whereas in intermolecular reaction, it is much larger. Thus, this explains why monomer **11** undergoes cyclopolymerization although its monofunctional counterpart has high polymerizability. Although homopolymerization of the monofunctional counterpart is high, cyclization is still favorable over homopolymerization due to more favorable entropy, thus, cyclopolymerization is dominated over homopolymerization by the more favorable entropy in cyclization.

6.4. Concluding Remarks

In this section the regioselectivity and the stereoselectivity for cyclization reaction in diallyl ether (**10**) and methyl α-(allyloxymethyl)acrylate (**11**) have been determined and compared with the experimental findings. The quantitative and qualitative trend have been reproduced. The NBO analysis on model reactions has shown the hyperconjugative interactions to be effective on the molecules of interest.

In monomer **10**, the reactive rotamer of the model compound displayed stabilizing interactions, thus facilitated the cyclization of the compound, such that **1'** has an activation energy of 7.2 kcal/mol whereas **10'** has an activation barrier of 5.3 kcal/mol. The *cis:trans* ratio has also been reproduced. Although cyclization reaction has been shown to be facile ($\Delta G^{\neq}=12.50$), poor cyclopolymerization of the monomer has been demonstrated by modeling the competing reactions. H-abstraction reaction has been shown to compete very efficiently with polymerization reactions.

The calculations for monomer **11** have shown significant hyperconjugative effects to be present in both **GM_11'** and **RR_11'**. Although the reactive rotamer is very close in energy to the global minimum and has a high percent of population, the barrier for cyclization is not low as compared to its diallyl analogues without the ester group. One of the causes can be the steric effect of the ester. Besides steric, electronic effects may also be acting. The radical center may resist pyramidalization due to the effective conjugation of the radical center with the ester group when it undergoes cyclization reaction and increase

the barrier for the cyclization reaction. The transition state for cyclization reaction of **11'** has chair-like geometry with equatorial ester substituent on the ring. The trans dominance in three-dimensional geometry of transition structure is in accordance with the experiments.

Suppressing intermolecular homopolymerization reaction by use of monofunctional counterparts that do not homopolymerize has been reported to be an efficient way of cyclopolymerization. In that respect, high cyclopolymerizability of monomer **11**, although its monofunctional counterpart homopolymerized well was surprising. In our model, it has been shown that although the activation barrier for homopolymerization is lower, cyclization dominates due to more favorable entropy difference. This explains the high cyclopolymerization vs homopolymerization of monomer **11**. Thus, the main factor of enhanced cyclopolymerization is the relative rate of homopolymerization with respect to cyclization rather than the homopolymerizability of the monomer itself.

The high cyclization and high polymerization efficiency of **11** have been related to the conformational effects favoring cyclization. The energy of the reactive rotamer has been shown to be at a relatively low level due hyperconjugative effects, however, these effects did not lower the barrier for cyclization. The experimental explanation of enhanced polymerizability due to conformational effects favoring cyclization is questionable because our calculations on three-dimensional structures did not show significant conformational effects favoring cyclization. Furthermore, the cyclization barrier is slightly higher for monomer **11** than its amine analogue **8**, consistent with its slightly lower degree of cyclization [19, 102]. Although cyclization is more facile with monomer **8**, the conversion percent of **11** is slightly higher. H-abstraction barriers from the monofunctional counterparts of **8** and **11** including the ester group have shown almost the same values. This indicates that in both monomers, allylic C-H bonds have the same strength. Thus, the high cyclopolymerizability of **11** may be attributed to intermolecular reactions of the monomer rather than to the efficiency of cyclization. Furthermore, the macrostructure of the polymer may facilitate high conversion of the monomer due to enhanced H-bonding in the propagating polymer chain with the unreacted monomer.

7. A MECHANISTIC STUDY ON THE CYCLOPOLYMERIZATION OF DIALLYL MONOMERS

Control over regioselectivity, stereoselectivity and the degree of cyclization is of fundamental interest in cyclopolymerization. This can only be done by a clear understanding of the factors that govern each step of the cyclopolymerization in connection with the possible reactions that may lead monomers to different pathways other than cyclopolymerization. In previous sections, the main concern was to understand the cyclization process. In this section, the cyclization and intermolecular propagation steps in the cyclopolymerization mechanism are analyzed, based on kinetic and thermodynamic approaches. In addition to cyclization and intermolecular propagation reactions, the competing reactions and their ability to overcome the efficiency of cyclization and intermolecular propagation have also been modeled and will be discussed. Two representative monomers, N-diallylamine (1) and N,N-dimethyl-N, N-diallylamonium (3) (Figure 1.2) are chosen for this study. This choice is based on the fact that the monomers are relatively small molecules and 3 is industrially used in a variety of areas [20]. Additionally, 1 has very low polymerizability while 3 has good polymerization efficiency [21]. In general, cationic monomers polymerize better than neutrals and this has been attributed to high chain transfer efficiency of neutral monomers [5]. In compound 3, the effect of the positively charged allylic substituent has also been discussed in comparison to the neutral compound 1.

7.1 Methodology

Conformer searches have been performed and structures corresponding to the global minimum on the energy hypersurface have been located for each compound studied. The B3LYP functional [31] and the 6-31G* basis set in Gaussian 98 [61] have been used for calculations. All the structures of interest were fully optimized in the gas phase with the same methodology. In previous sections on the cyclization of diallyl monomers, Density Functional Theory [26] with the B3LYP functional has been successfull to understand the

regioselectivity and stereoselectivity of cyclopolymerization and reproduce the experimental data. Thus the same methodology has been used in this study.

Single-point calculations in water were performed with the PCM methodology [41] on the stationary structures in vacuum. Furthermore, single point solvent calculations were carried out on structures obtained from the IRC [63, 64] calculations in the gas phase in order to sketch the potential energy surface in solution.

Model compounds have been used to study the reactions involved in cyclopolymerization . In the cyclization reaction, the long propagating polymer chain was simplified and replaced with a H atom, as in our previous sections on diallyl monomers (Figure 3.2). This model has successfully reproduced the experimental regioselectivity and stereoselectivity in the cyclopolymerization reaction of diallyl monomers. To model the homopolymerization and intermolecular reactions, the long polymer chain was also replaced by H and the monomer is simplified by reducing it to a monofunctional monomer. These models have been referred to as **M1'** and **M3'** for radicalic species and **M1** and **M3** for the monomers **1** and **3**, respectively (Figure 7.1 and Figure 7.2).
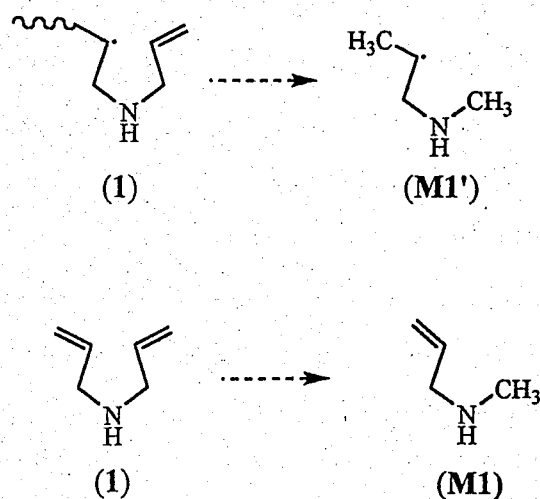
Figure 7.1. The model compounds for diallylamine monomer (1)
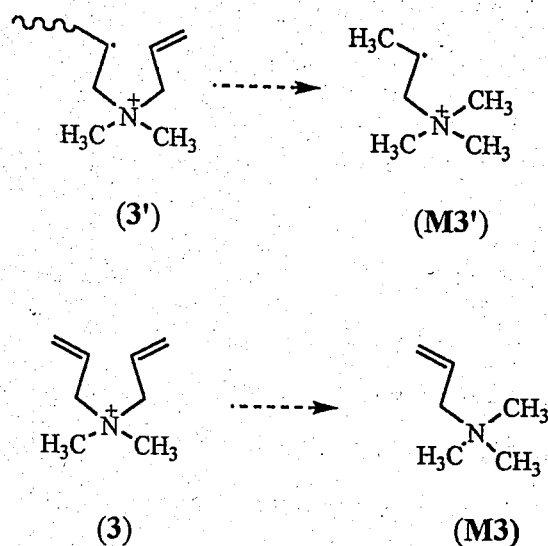
Figure 7.2. The model compounds for N,N-dimethyl-N, N-diallylamonium (3)

Four different reactions corresponding to the H abstraction from the allylic C have been considered. These are depicted in Figure 7.7, Figure 7.9, Figure 7.11 and Figure 7.15. In Figure 7.7, the H-abstraction from a series of compounds including the monofunctional counterpart of monomers 1 and 3 by the CH₃ radical is analyzed to account for the allylic C-H bond strength. The effect of allylic substituents on chain transfer reactions will be discussed by utilizing these compounds. In Figure 7.9, the intramolecular H-abstraction reactions of monomers 1 and 3 have been considered. The model displays the intramolecular H-abstraction by the propagating polymer chain prior to cyclization. In Figure 7.11, another alternative for the H-abstraction by the uncyclized propagating polymer chain has been shown. To model this reaction, the monofunctional counterparts of the monomers are considered. In Figure 7.15, the propagating cyclized ring radical abstracts the H of the incoming monomer. This reaction has been modeled by the attack of the 5-membered ring to the monofunctional counterpart of the diallyl monomer. In previous sections for 1 and 3, it has been shown that 5-membered rings form in cyclization reactions, in agreement with experiments. Thus, in intermolecular propagation reactions by the cyclized ring, the attack by 6-membered rings (endo) is not considered. The stationary structures of the 5-membered rings have been obtained by the IRC calculations on the transition states for cyclization. Along the intermolecular propagation reaction by the cyclized ring, the cyclized radical attacks another monomer (Figure 7.13). In this model,

the 5-membered ring (exo) is considered as the propagating radical, and the difunctional monomer is considered as monofunctional (Figure 7.13).

7.2. Results and Discussion

The cyclopolymerizability of a monomer can be enhanced by suppressing the reactions that compete with the standard cyclopolymerization steps, i.e. homopolymerization and degradative chain transfer. In the discussion that follows, cyclization and intermolecular propagation reactions of the cyclopolymerization will be discussed and compared with their competing reactions. The stationary geometries in the gas phase have been considered for single point energy calculations in solution. The energy barriers discussed in the text refer to the energetics in water ($\varepsilon=80$) unless otherwise stated.

7.2.1. Cyclization

The cyclization step (Figure 1.1) acts as a driving force for polymerization, such that the higher rate of cyclization as compared to homopolymerization facilitates cyclopolymerization [5]. There are different factors that determine the cyclization efficiency of a monomer, ie. the competing steps such as homopolymerization and degradative chain transfer. Using difunctional monomers whose monofunctional counterparts do not have homopolymerization tendency facilitates cyclization over intermolecular homopolymerization. The monofunctional counterparts of 1 and 3 do not have homopolymerization tendencies [17]. For example, allyltrimethylammonium cation ($CH_2CHCH_2N(CH_3)_3^+$) could not be polymerized even in conditions of complex media where allylamine could be polymerized to a certain extent [5]. However, 3, the difunctional analogue of allyltrimethylammonium monomer, could be polymerized to high molecular weights with success [20]. Thus, cyclization acts as the driving force for the polymerization of these monomers.

In the previous sections on the cyclization reactions of diallyl monomers, several compounds have been considered. In these studies, the regioselectivity and stereoselectivity of cyclization reactions have been successfully reproduced and explained

in terms of electrostatic, polar and steric effects, using molecular orbital calculations. In **1**, the exo cyclization was favored over the endo by 3.7 kcal/mol and by 4.1 kcal/mol in **3** (Figure 7.3). These results are consistent with the exclusive exo preference of these monomers [20, 21].

The energy barriers for cyclization show that cyclization is facile in both **1** and **3**, in the gas phase and in solution (Figure 7.3). It is also important to note that **3** has a lower barrier for cyclization than **1**, which is also consistent with the very good polymerization of **3** with respect to the very low polymerization of **1**.

Cyclization Reaction

Model Reaction

Monomer	E_{a_exo} ($\varepsilon=1$)	E_{a_endo} ($\varepsilon=1$)	E_{a_exo} ($\varepsilon=80$)
1	7.3	10.9	6.8
3	6.2	10.3	3.8
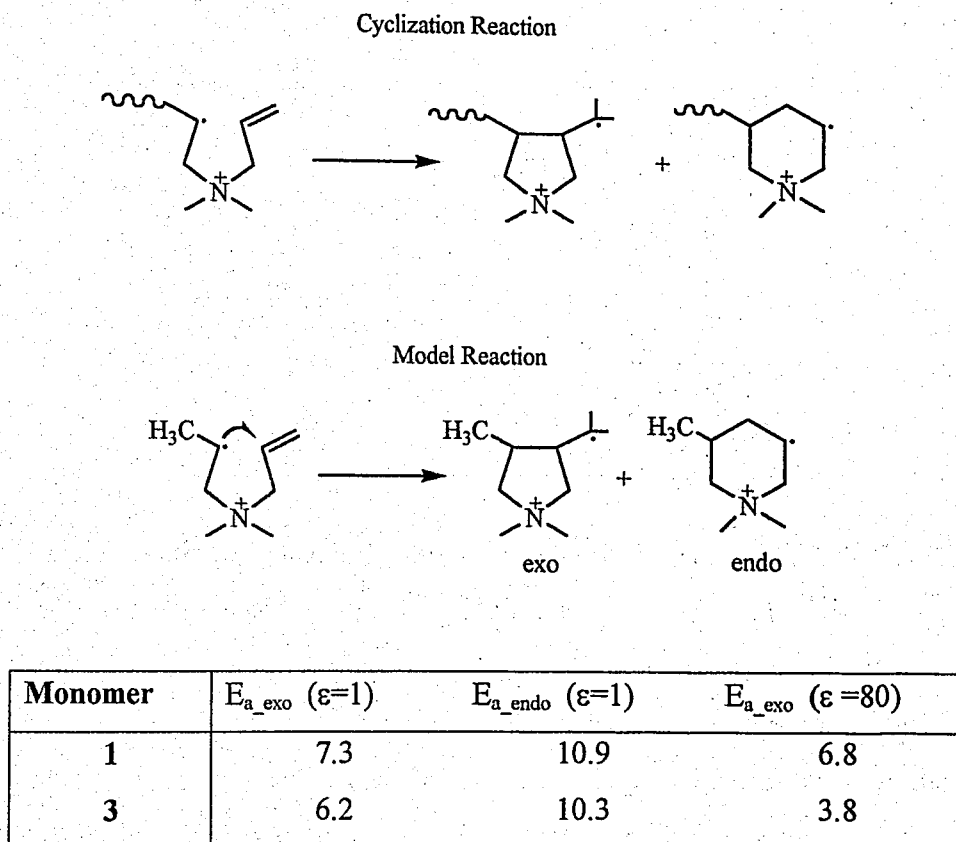
Figure 7.3. Schematic representation of cyclization reaction and B3LYP/6-31G* results (in kcal/mol) from calculations on the model reaction

7.2.1.1. Cyclization vs. Homopolymerization. To account for the higher cyclopolymerization of monomer **3** as compared to **1**, the energetics for cyclization (Figure 7.3) and homopolymerization (Figure 7.4) reactions as well as the ones for the competing

reactions have been considered. The 3-dimensional structures for model homopolymerization reactions are shown in Figure 7.5 and Figure 7.6.

Homopolymerization Reaction

Model Reaction

Monomer	E_a (ε=1)	E_a (ε =80)
1	3.9	8.9
3	52.6	10.1
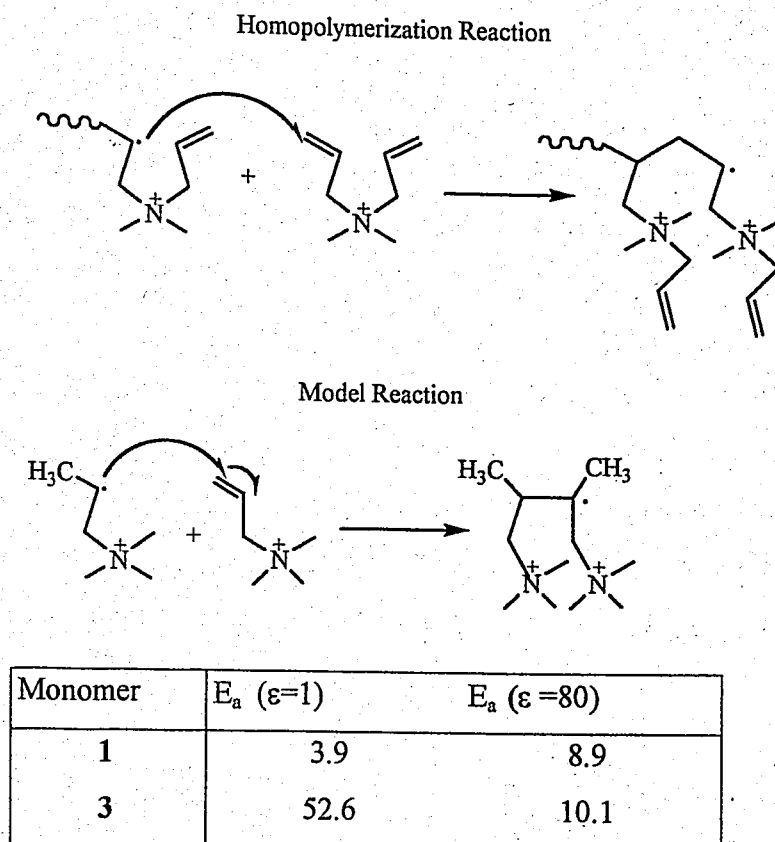
Figure 7.4. Schematic representation of homopolymerization reaction and B3LYP/6-31G* results (in kcal/mol) from calculations on the model reaction

Since the gas phase barriers for bimolecular reactions are high, the stabilizing effect of the polar medium should be considered especially for the reactions of the charged species. Single point calculations in solution have been performed to discuss the energetics of the processes investigated. In comparing the activation energies for homopolymerization and bimolecular propagation, the entropy factor has not been taken into account. With monomer 3, the difference in the energy barriers of homopolymerization and cyclization is 6.3 kcal/mol in favor of cyclization. Entropy is expected to increase the free energy barriers for both homopolymerization and cyclization reactions. However, the increase will be more significant in the case of the bimolecular reaction. In the gas phase, the entropy of

activation, $\Delta S^{\neq}$, for monomer **3** is -8.9 cal/mol K for cyclization and -40.3 cal/mol K for homopolymerization. This indicates that there is greater contribution of entropy in bimolecular homopolymerization than in cyclization, so the entropy will only increase the difference in energy between the homopolymerization and cyclization reactions.

In the case of **1**, the energy difference between homopolymerization (Figure 7.4) and cyclization (Figure 7.3) is 2.1 kcal/mol in favor of cyclization. This difference in barriers shows that in the neutral monomer, homopolymerization is much more facile than it is in the cationic monomer.

Our calculations on model reactions for homopolymerization show that for both **1** and **3**, homopolymerization (Figure 7.4) has approximately the same barriers. Additionally, cyclization reaction is faster than homopolymerization. In the ESR studies on a set of diallyl monomers, including **3**, only cyclized radicals have been observed which indicates the higher rate of cyclization as compared to intermolecular attack [110].

2.304

8.9

+

0.0
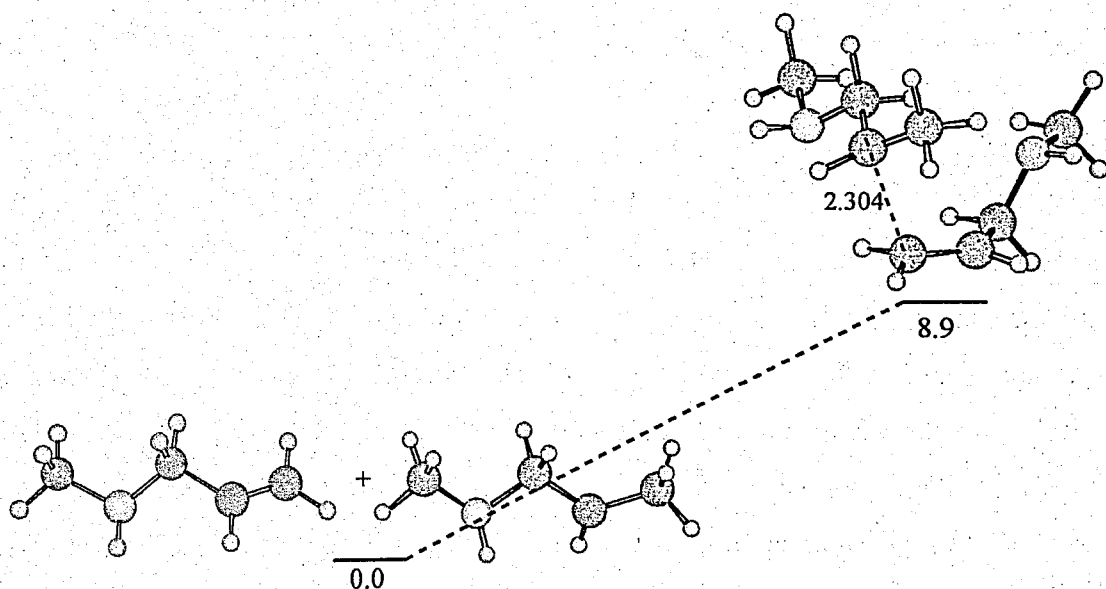
Figure 7.5 The 3-dimensional structure of model homopolymerization reaction for **1**
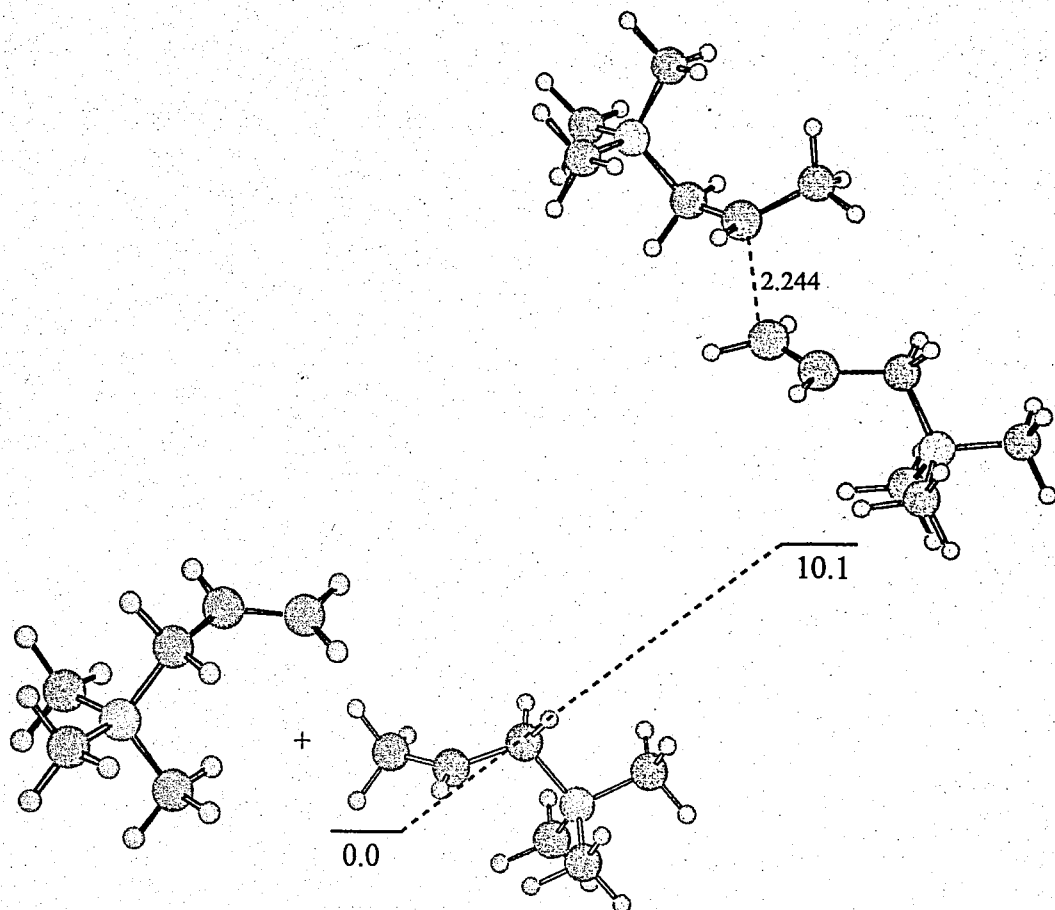
Figure 7.6. The 3-dimensional structure of model homopolymerization reaction for **3**

7.2.1.2. Cyclization vs. H-abstraction (or Chain Transfer).

The chain transfer reaction by H-abstraction from the allylic position was known to be the main cause of the poor polymerizability of allyl monomers [5]. In the chain transfer reaction, the propagating radical chain abstracts the allylic H of the incoming monomer and a resonance stabilized species, which has a lower reactivity and re-initiation capacity is obtained. In a study on allyl acetate, the allylic position was deuterium substituted and this resulted in 3 times faster polymerization of the monomer [111]. Thus, H-abstraction reaction acts as a termination reaction, and is called degradative chain transfer reaction (Figure 1.1).

The high polymerization of monomer **3** is attributed to its low chain transfer efficiency. In general, cationic monomers are known to have low chain transfer reaction than neutral ones [5]. To understand the effect of the structure of the monomer on the

allylic C-H bond strength, H-abstraction reactions with methyl radical are modeled for different monomers (Figure 7.7).

Chain Transfer Reaction
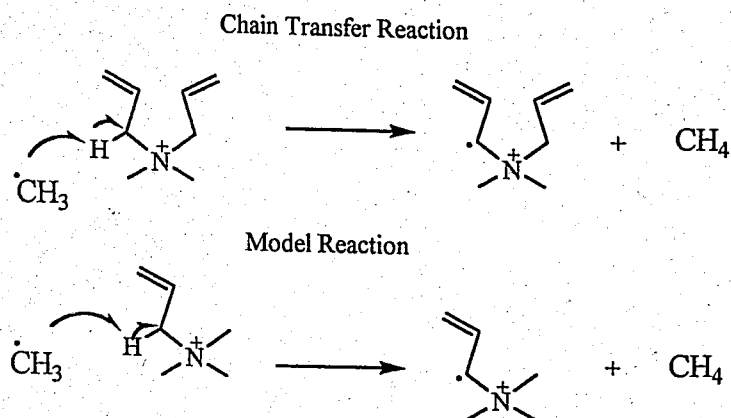
Model Reaction

	$E_a (\varepsilon=1)$	$E_a (\varepsilon=80)$
M1	4.5	6.8
M2	7.4	
M3	8.3	12.6
M4	6.8	
M5	6.7	
M6	7.1	

Figure 7.7 Models for H-abstraction reactions and B3LYP/6-31G* results (in kcal/mol) from calculations on the model reactions
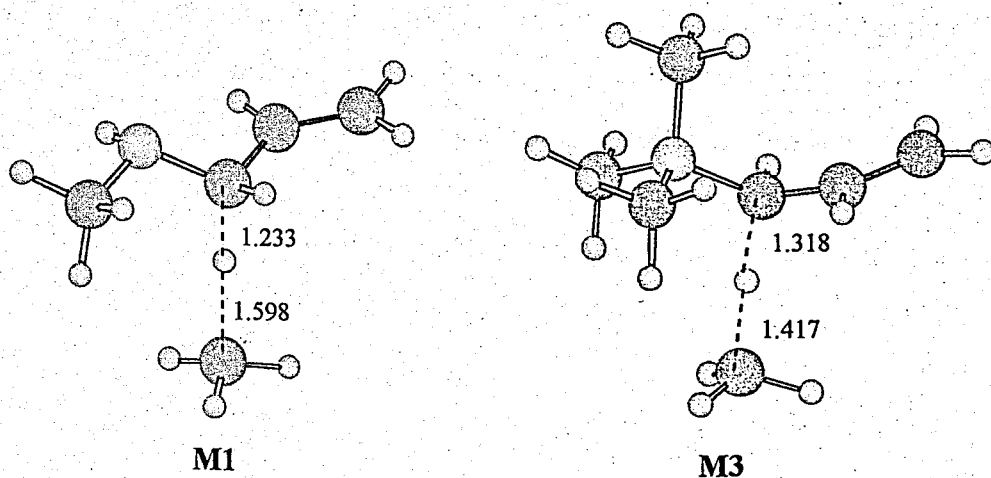
Figure 7.8 The 3-dimensional transition state structures for H abstraction reaction from **M1** and **M3** by CH_3 radical

In the models **M1-M6**, the steric effects of the approaching species are relieved to a great extent. The barriers for models **M1** and **M3** show that both in gas phase and in solution, **3** has higher barrier for abstraction (8.3 kcal/mol in the gas phase and 12.6 kcal/mol in solvent) than **1** (4.5 kcal/mol in the gas phase and 6.8 in solvent) (Figure 7.7). The allylic H in **3** is adjacent to a highly positive center which inductively increases the strength of the C-H bond, thus the barrier is increased. The -CN group on nitrogen in **M6** increases the barrier from 4.5 kcal/mol to 7.1 kcal/mol due to the inductive effect of the – CN group which does not display any steric effect. This barrier for H-abstraction is almost the same as the one in N-methyl-allylammonium monomer (**4**), which is the smallest cationic monomer among compounds **M1-M6**. Compound **M5** has a slightly lower barrier than **M6**. The inductive effect of the –CN group is slightly more effective than the steric effect of the CH_3 group. In compound **M2**, replacing one of the hydrogen groups on nitrogen of compound **M4** with the methyl group causes a small increase in the barrier due to the steric effect of methyl group. In the N-trimethylallylammonium (**M3**) case, the barrier is higher since the allylic H is sterically shielded by methyl groups and also the C-H bond is strengthened due to the positively charged nitrogen. Thus, H-abstraction is affected to a great extent by the positively charged allylic substituent as well as the bulky substituents in the vicinity of allylic C-H bond.

One of the H-abstraction reactions that competes with cyclization is the intramolecular H-abstraction prior to cyclization (Figure 7.9). The three-dimensional structures of the transition states are shown in Figure 7.10. The activation energies for this reaction in both media are much higher than the ones for cyclization of compounds **1** and **3** (Figure 7.3). This indicates that the intramolecular H-abstraction prior to cyclization has no effect so as to decrease the cyclopolymerization efficiency.

Intramolecular H-Abstraction

Model Reaction

Monomer	E_a ($\varepsilon=1$)	E_a ($\varepsilon=80$)
1	11.6	19.6
3	13.4	22.5
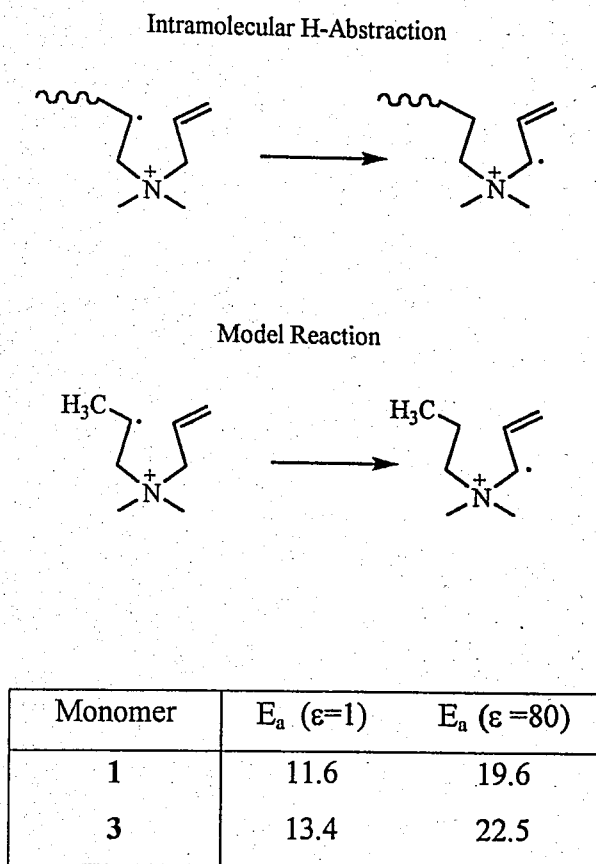
Figure 7.9. Schematic representation of intramolecular H-abstraction reaction by the propagating polymer chain and B3LYP/6-31G* results (in kcal/mol) from calculations on the model reactions

1'

3'
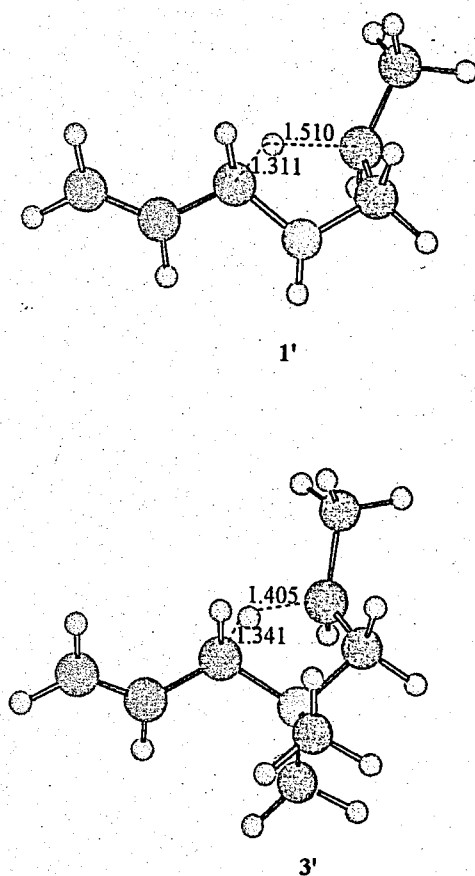
Figure 7.10 The transition state structures for intramolecular H-abstraction reactions for 1' and 3'

Another competing reaction with cyclization is the intermolecular H-abstraction by the propagating uncyclized radical (Figure 7.11). The 3-dimensional structures for transition states for this reaction are shown in Figure 7.12. For the neutral monomer, **1**, although the gas phase activation energy of intermolecular H-abstraction by the polymer chain is lower than that of cyclization, this trend is reversed in solution. For monomer **3**, cyclization dominates greatly over the intermolecular H-abstraction as these barriers in both media are much higher than the ones required for cyclization. In the intermolecular H-abstraction, the barriers reflect the steric effects of the approaching monomer chains as well. In Figure 7.7, H-abstraction reaction by the methyl group is a good indicator of allylic C-H bond strength, since the reaction is relieved from the steric effects of the attacking compound. In the model reaction of H-abstraction by the uncyclized propagating radical

(Figure 7.11), the steric effect of allyl group in the attacking radical can be observed as well. The steric effects increase the barrier by 17.2 kcal/mol in **3** and 7.4 kcal/mol in **1** as compared to their H-abstractions by the methyl radical. The cationic monomer resists H-abstraction by the presence of stronger C-H bonds and higher steric effects to approach the abstraction site.

H-Abstraction by Propagating Polymer Chain
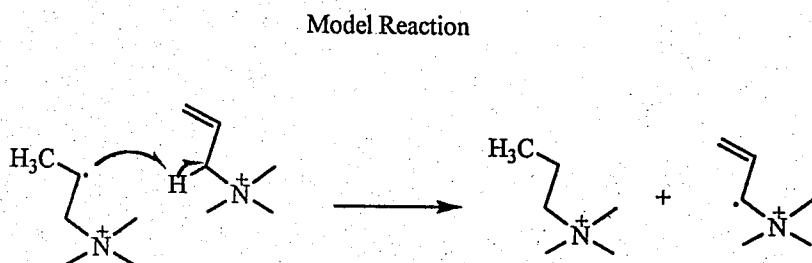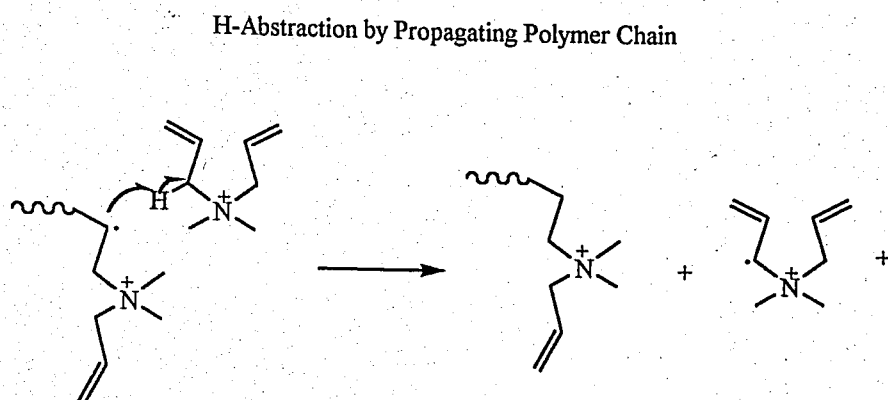
Model Reaction

Monomer	E_a ($\varepsilon=1$)	E_a ($\varepsilon=80$)
1	6.4	14.2
3	71.1	29.8

Figure 7.11. Schematic representation of H-abstraction by the propagating polymer chain and B3LYP/6-31G* results (in kcal/mol) from calculations on the model reactions
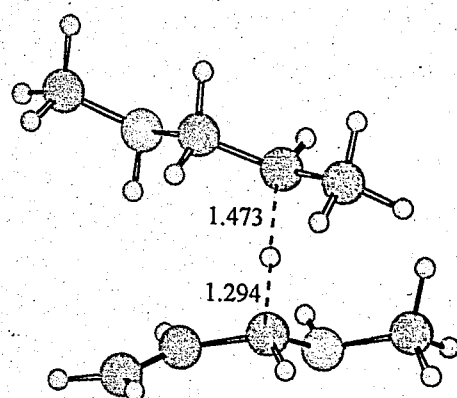
M1
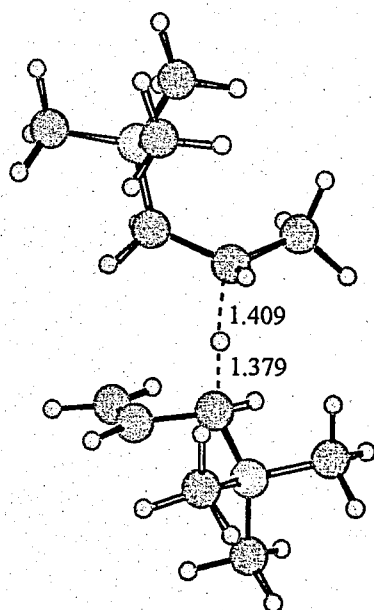
M3

Figure 7.12. The transition state stuructures for H-abstraction reaction by the propagating polymer chain of model systems **M1** and **M3**

The comparison of activation energies for cyclization versus competing reactions indicates that in **3**, the competing reactions cannot have significant effect in decreasing the cyclization efficiency. In the case of neutral monomer, the most plausible reaction besides cyclopolymerization is homopolymerization. The barriers for allylic H-abstraction

reactions indicate that the chain transfer reaction is resisted more in cationic monomer due to steric and electrostatic reasons and can be more facile in neutral monomers.

7.2.2. Intermolecular Chain Propagation

7.2.2.1. Intermolecular vs. Homopolymerization. Compounds **1** and **3** do not homopolymerize, however, the intermolecular attack of the cyclized propagating polymer chain to the incoming monomer is known to occur (Figure 7.13), especially in the case of compound **3** in cyclopolymerization [20]. The 3-dimensional structures corresponding to transition states for intermolecular propagation by the cyclized chain is shown in Figure 7.14.

Intermolecular Propagation Reaction by the Cyclized Ring

Model Reaction

Monomer	E_a ($\varepsilon=1$)	E_a ($\varepsilon=80$)
1	5.6	7.5
3	44.9	7.1
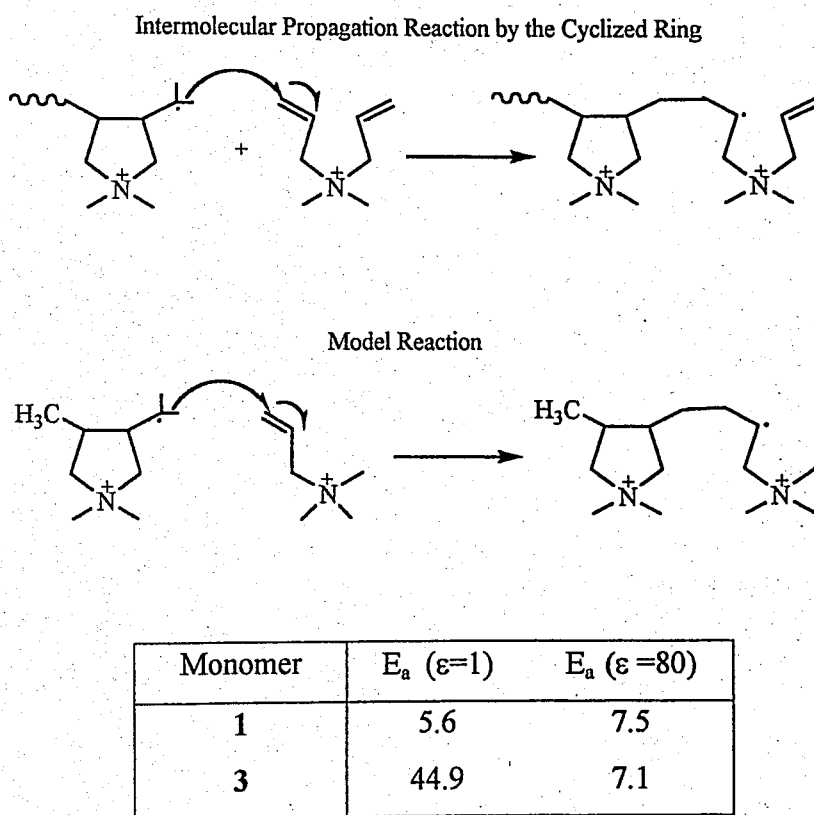
Figure 7.13. Schematic representation of intermolecular propagating reaction by the cyclized ring and B3LYP/6-31G* results (in kcal/mol) from calculations on the model reaction

Both homopolymerization and intermolecular propagation by the cyclized radical are bimolecular reactions and are similar in nature. Nevertheless, the propagation of the cyclized radical should normally be more facile than the homopolymerization because of the absence of steric hindrance in the former reaction.


M1

M3
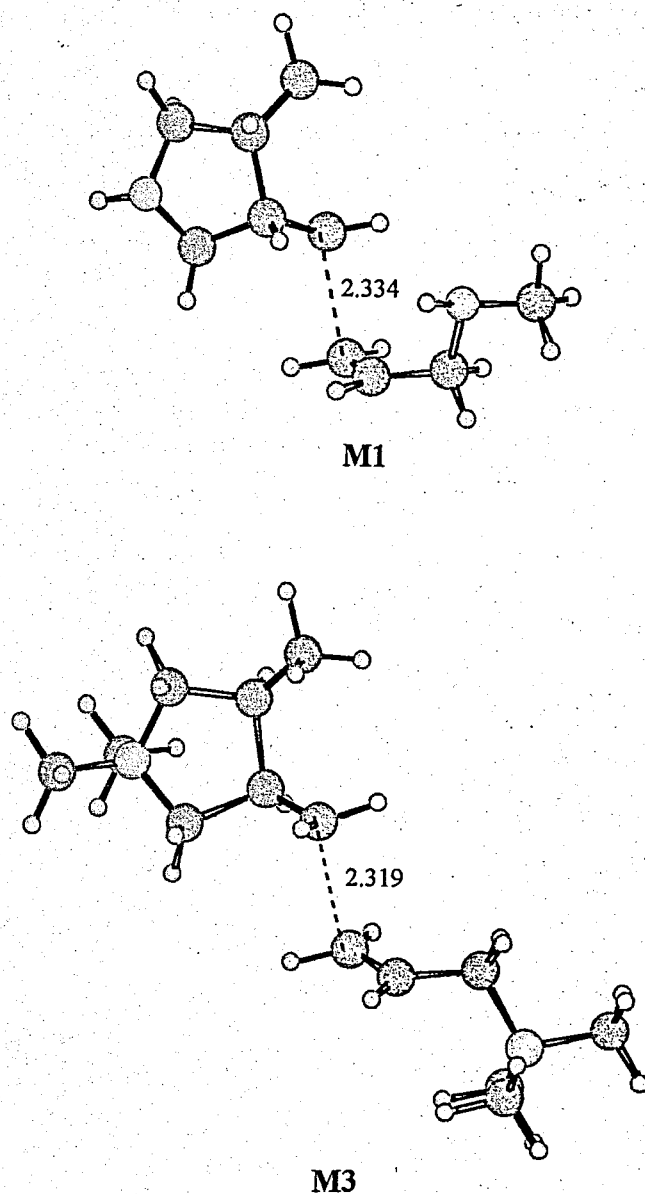
Figure 7.14. The transition state structures of intermolecular propagation reaction by the cyclized ring for **M1** and **M3**

In the case of **3**, the activation energy for homopolymerization is 10.1 kcal/mol whereas, the barrier decreases to 7.1 kcal/mol in the intermolecular propagation by the cyclized ring. In the case of **1**, these barriers are 8.9 and 7.5 kcal/mol, respectively. This indicates that cyclization facilitates the propagation of the cationic monomer **3** more than it does for the neutral **1**. Intermolecular propagation by the cyclized polymer chain radical does not have a significant efficiency with respect to homopolymerization in compound **1**.

7.2.2.2. Intermolecular Propagation vs. H-Abstraction. The competing reaction with the intermolecular propagation is H-abstraction by the propagating cyclized ring. This reaction has been modeled as shown in Figure 7.15 and the transition state structures for this reaction are shown in Figure 7.16.

H-Abstraction by the Propagating Cyclized Ring

Model Reaction

Monomer	E_a ($\varepsilon=1$)	E_a ($\varepsilon=80$)
1	7.4	14.2
3	60.3	22.3
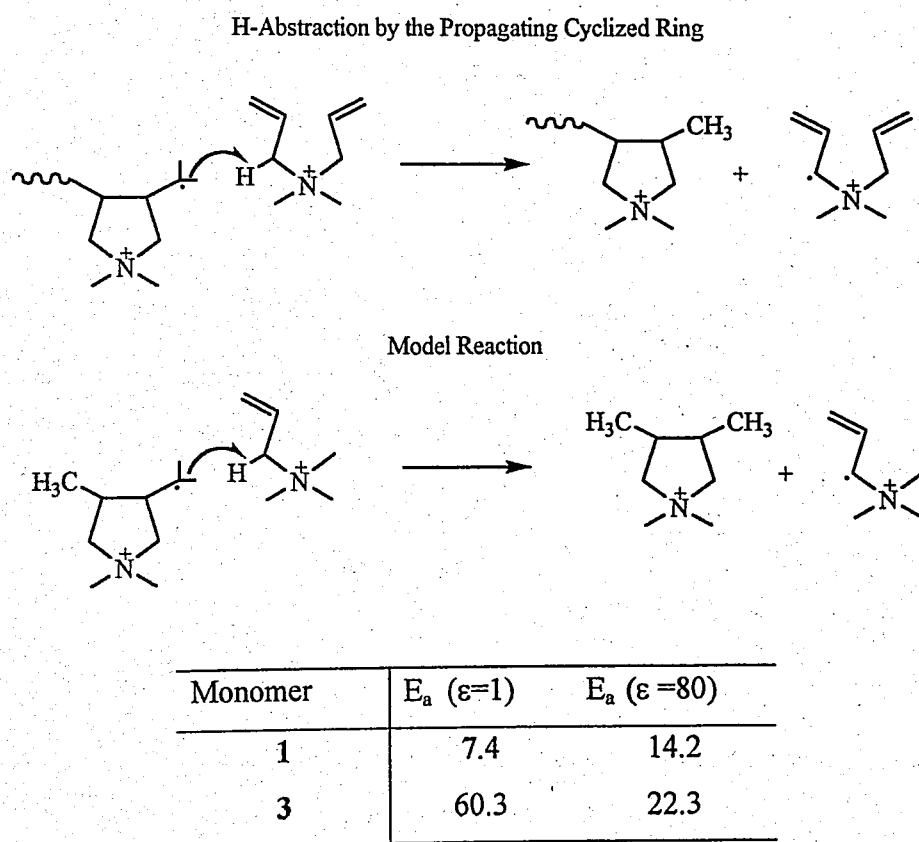
Figure 7.15. Schematic representation of H-abstraction by the propagating cyclized ring and B3LYP/6-31G* results (in kcal/mol) from calculations on the model reaction

M1

M3
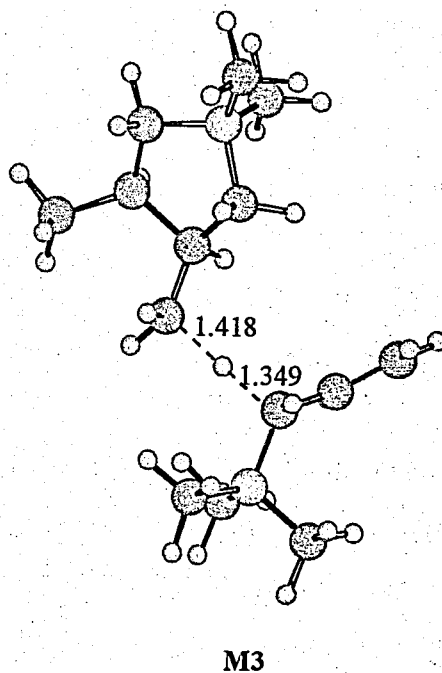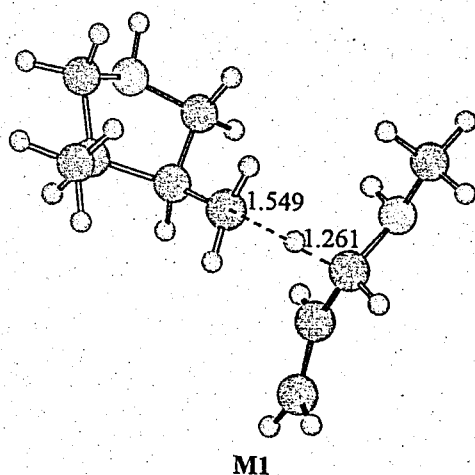
Figure 7.16. The transition structures for H-abstraction by the propagating cyclized radical from the model compounds of **1** and **3**

In monomer **1**, H-abstraction by the ring has 6.7 kcal/mol higher barrier than the intermolecular propagation reaction by the cyclized ring. In **3**, this difference is 15.2 kcal/mol. These barriers indicate that propagation by the cyclized ring is more probable than H-abstraction by the ring. Furthermore, the energy barrier to H-abstraction by the

propagating cyclized ring is 22.3 kcal/mol in **3** while this barrier is 14.2 kcal/mol in **1**. These results show that H-abstraction is more plausible in the neutral monomer **1** than it is in cationic form **3**, since the later has a much higher energy barrier.

7.3. Concluding Remarks

In this study the reactions taking place along the cyclopolymerization of compounds **1** and **3** are modeled and discussed in details.

Single point calculations in solution show that in monomer **1**, homopolymerization and cyclization have almost the same activation barriers, thus, cyclization is not faster than homopolymerization to facilitate cyclopolymerization. For **1**, intermolecular propagation by the cyclized ring is not favored over homopolymerization.

In monomer **3**, cyclization is much more facile than homopolymerization and this can justify the higher cyclopolymerization efficiency of **3**. Cyclization decreases the barrier for intermolecular attack with respect to homopolymerization. Our calculations have also shown that H-abstraction reactions are less effective in the case of monomer **3**.

The allylic hydrogen can be more easily abstracted in the neutral than in its cationic analogue. The substituents on nitrogen do not exhibit significant steric shielding to inhibit H-abstraction. Without the steric effect of the attacking compound, monomer **3** has shown a much higher barrier for H-abstraction than **1**, emphasizing the strength of the allylic C-H bond. The high barrier for H-abstraction is mainly due to the inductive effect of the positively charged neighboring nitrogen. H-abstraction reactions by the cyclized propagating ring or by the propagating polymer chain take into account the steric effect of the attacking molecule. In these cases, H-abstraction is even less efficient.

Overall, the competing reactions are more facile for monomer **1** than for monomer **3** and monomer **1** does not show strong preference for cyclization over homopolymerization.

8. CONCLUSION

The main objective of this study was to understand the relationship between the structure of the monomers and their radical cyclopolymerization efficiency.

Descriptors, extracted from the "weighted averages" obtained by spanning various conformations of the monomers have been derived from quantum mechanical calculations. The descriptors such as the C_2--C_6 bond orders, local softness values of C_6 and HOMO-LUMO gaps could be successfully used to reproduce the cyclopolymerizability of various diallylamine monomers. The ^{13}C NMR chemical shifts of the diallylamine monomers have been correlated to their polymerizabilities. A mathematical model that predicts the ^{13}C NMR chemical shifts of the vinylic carbons, based on electrostatic charges derived from quantum mechanical calculations (PM3), has been established. The validity of the model has been tested with the parameters of the various monomers.

Control over regioselectivity and stereoselectivity in cyclopolymerization has been discussed thoroughly by understanding all the factors affecting cyclization. Consideration of the cyclization reaction in details has allowed us to draw general conclusions on radical cyclizations in general. This last issue is of importance since cyclizations are of great interest in organic synthesis.

In the literature, the exo preference in radical cyclizations has been explained in various ways. A prediction based upon "the more favorable activation entropy" for the exo preference has been found to be insignificant. The $\Delta S^{\neq}$ values, although in agreement with the expected exo preference, were found to be too small to be taken into consideration. Another qualitative explanation of the exo cyclization was based upon the unfavorable non-bonded interactions between the syn H's in the endo cyclization. The distance between the H atoms was found to be too large to cause a significant destabilization through non-bonded interactions. The endo-cyclic structures have been located as the thermodynamically controlled products along the cyclization reaction. However, exo-cyclic structures have been observed experimentally confirming the preference of a kinetically controlled cyclization reaction. Endo ring closure of monomer 9 has been

explained by thermodynamic control over the reaction and stabilization of radical center by the ester group [15], but calculations have shown that 6-membered ring formation of this monomer is also kinetically controlled.

In cyclization, the more electrophilic site of the C=C bond was the preferred site of attack in the case of monomers without substituents on the backbone. However, ester substituted monomers did not follow the same trend. Thus, the explanations based on electrostatic effects have been insufficient in explaining the regioselectivity. The steric effects seem to dominate all other factors in regioselectivity. The three-dimensional geometries of the exo and endo transition states are the key features in determining the regioselectivity of cyclization. In most of the cases, the strain in the 5-membered ring and the thermodynamic stability of the 6-membered ring is overcome by the more efficient overlap of the bonding sites in the exo structure. Thus, the more efficient p-π interaction in the exo structure governs the formation of 5-membered rings. Furthermore, the substituents on the backbone have been found to destabilize the exo transition state, whereas they do not alter the activation barrier for the endo cyclization. This is due to the fact that 6-membered rings are able to host substituents more easily than 5-membered rings. Conclusively, the regioselectivity is mainly due to the steric factors that destabilize the exo ring.

The stereoselectivity in the cyclization of the monomers considered has been reproduced successfully in all cases. The B3LYP/6-31G* calculations have confirmed the preference for the experimentally more dominant isomer. The stereoselectivity is governed by the bulkier substituents favoring the more stable equatorial position in cyclohexane-like ring. The experimental *cis:trans* ratio of the model compound for monomer **10**, is perfectly reproduced in the calculations.

The substituents on the backbone have been found to affect cyclization. Monomethyl substitution on nitrogen is shown to have more effect than two methyl substitution contrary to literature findings of the gem-dialkyl effects in similar systems. The "equatorial methyl" effect -or so called facilitated transition state- has been found to account for the acceleration by a methyl group substitution on nitrogen.

The barriers for cyclization showed that the ester substituent on the double bond decreased the rate of cyclization. The main reasons may be the steric effect of the ester group in cyclization or the extended conjugation of the radical center with the ester group resisting pyramidalization. The methyl group on the double bond in monomer **9** further decreases the rate of cyclization consistent with a decrease in the degree of cyclization of the monomer [15].

Butler had indicated that cyclopolymerization might be facilitated by $\pi-\pi$ interaction of the two double bonds in 1,6-dienes. However, the reported spectroscopic evidence has been inconclusive [6, 65]. The conformational study on model compounds has shown extended structures with no significant $\pi-\pi$ interactions between the double bonds in their global minima.

The change of heteroatom from nitrogen to oxygen has shown an increase in cyclization rate (**1** vs **10**), which was attributed to hyperconjugative effects facilitating cyclization.

The very efficient polymerizability of monomer **11** has been analyzed by modeling. Compound **11** is known to cyclize easily inspite of the fact that its monofunctional counterpart undergoes efficient homopolymerization. Cyclization has been found to overcome homopolymerization because of the change in entropy which is favored during cyclization. Thus, the main factor controlling cyclopolymerization has been identified as the relative rate of homopolymerization with respect to cyclization rather than the absolute value of the homopolymerizability itself. On the other hand, conformational preferences do not facilitate the cyclization of monomer **11**. It maybe that intermolecular propagation or the macrostructure of the polymer corresponding to monomer **11** are responsible for the high polymerization efficiency of this monomer.

To understand the factors that govern cyclopolymerization, intermolecular propagation reactions and their ability to overcome the efficiency of cyclization have also been modeled. The model reactions for monomer **1** have shown that homopolymerization and cyclization have almost the same activation barriers, thus, cyclization is not faster than homopolymerization. Furthermore, intermolecular propagation by the cyclized ring is not

favored over homopolymerization. In monomer **3**, cyclization was found to be more facile than homopolymerization and this justifies the higher cyclopolymerization efficiency of **3**. Chain transfer reactions of the monomers have also been considered since they can compete with standard cyclopolymerization reactions. It has been shown that the cationic monomer **3** has a stronger allyiic C-H bond because of the inductive effect of the cation and the steric effects further decrease the H-abstraction efficiency. Competing reactions are found to be much more effective in the case of neutral monomer than the cationic.

Generally, the models and the B3LYP/6-31G* methodology used in our calculations have been successful to reproduce the experimental polymerizabilities.

The following issues can be suggested for further work:

- Geometry optimizations in solution will allow the consideration of the entropy factor in solution as well.

- The model established in Section 3 can be tested with a larger number of monomers in order to confirm its liability

- Molecular dynamic studies on polymer of **11** can provide information on its macroscopic properties

- Monomers, whose monfunctional counterparts undergo homopolymerization, can be modeled in their cyclization and intermolecular reactions. It is desirable to generalize the principles deduced from this study regarding the relative rates of cyclization versus homopolymerization.

REFERENCES

1. Butler, G. B. and R. L. Bunch, "Preparation and Polymerization of Unsaturated Quaternary Ammonium Compounds", *J. Am. Chem. Soc.*, Vol. 71, pp. 3120-3122, 1949.

2. Butler, G. B., *Cyclopolymerization and Cyclocopolymerization*, Marcel Dekker, New York, 1992.

3. Butler, G. B. and F. L. Ingley, "Preparation and Polymerization of Unsaturated Quaternary Ammonium Compounds II. Halogenated Allyl Derivatives", *J. Am. Chem. Soc.*, Vol. 73, pp. 895-896, 1951.

4. Butler, G. B., "Cyclopolymerization", *J. Polym. Sci. Part A: Polym. Chem.*, Vol. 38, pp. 3451-3461, 2000.

5. Matsumoto, A. "Polymerization of Multiallyl Monomers", *Prog. Polym. Sci.*, Vol. *26*, pp. 189-257, 2001.

6. Butler, G. B., "Cyclopolymerization and Cyclocopolymerization", *Acc. Chem. Res.*, Vol. 15, pp. 370-378, 1982.

7. Lancaster, J. E., L. Bacchei, H. P. Panzer, "The Structure of Poly(diallyldimethyl ammonium) chloride by 13C NMR Spectroscopy", *J. Polym. Sci., Polym. Lett.*, Vol. 14, pp. 549-554, 1976.

8. Ottenbride, R. M. and D. D. Shillady, *Polymeric Amines and Ammonium salts*, Pergamon Press, Oxford, pp. 143, 1980.

9. Wandrey, C., W. Jarger, G. Reinish, M. Hahn, G. Engelhard, H. Jancke, and D. Ballschuh, "Zur Chemischen Struktur von Poly(dimethyl-diallyl-ammoniumchlorid)", *Acta. Polym.*, Vol. 32, pp. 177-179, 1981.

10. Masterman, T. C., N. R. Dando, D. G. Weaver and D. Seyferth, "Investigation of the Microstructure of Poly(diallyldimethylammonium Chloride) by Nitrogen -14 (15) NMR Spectroscopy", *J. Polym. Sci., Part B:Polym Physics*, Vol. 32, pp. 2263-2270, 1994.

11. Zubov, V. P., M. V. Kumar, M. N. Masterova and V. A. Kabanov, "Reactivity of Allyl Monomers in Radical Polymerization", *J. Macromol. Sci-Chem.*, Vol. A13(1), pp. 111-131, 1979.

12. Harada, S. and S. Hasegawa, "Homopolymerization of Monoallylammonium Salts with Aza Initiators", *Macromol. Chem. Rapid Commun.*, Vol. 5, pp. 27-31, 1984.

13. Kodaira, T. and F. Aoyama, "Cyclopolymerization.II. Mechanism of the Free-Radical Polymerization of N-n-Propyldimethacrylamide", *J. Polym. Sci: Polym. Chem. Ed.* Vol. 12, pp. 897-910, 1974.

14. Kodaira, T., Q.-Q. Liu, M. Satoyama, M. Urushisaki and H. Utsumi, "Cyclopolymerization XXVI. Repeating Unit Structure of Cyclopolymers Derived from N-substituted-N-allyl-2-(methoxycarbonyl)allylamines and Mechanism of Intramolecular Cyclization", *Polymer*, Vol.40, pp. 6947-6954, 1999.

15. Kodaira, T., N. Kasajima and M.Urushisaki, "Cyclopolymerization. Part XXVII. Cyclopolymerizability of an Unconjugated Diene with Functional Groups With No Homopolymerization Tendency: Radical Polymerization of N-methyl-N-methallyl-2-(methoxycarbonyl)allylamine and Structure of the Polymers Derived Therefrom", *Polymer*, Vol. *41*, pp. 2831-2837, 2000.

16. Johns, S. R. and R. I Willing, "Cyclopolymerization. VII. The ^{13}C NMR Spectra of Cyclopolymers Obtained from N,N-Diallylamines", *J. Macromol. Sci-Chem. A*, Vol. 10, pp. 875-891, 1976.

17. Kodaira, T., "Structural Control During the Cyclopolymerization of Unconjugated Dienes", *Prog. Polym. Sci.*, Vol. 25, pp. 627-676, 2000.

18. Urushisaki, M., T. Kodaira, T. Furuta, Y. Yamada and S. Oshitani, "Cyclopolymerization. 25. Five-Membered Ring Formation Through Head-to-Head and Tail-to-Tail Additions in Radical and Anionic Polymerizations of α-(Allyloxymethyl)acrylates", *Macromolecules*, Vol. 32, pp. 322-327, 1999.

19. Thomson, R. D., W. L. Jarrett and L. J. Mathias, "Unusually Facile Cyclopolymerization of a New Allyl Ether Substituted Acrylate and Conformation of Repeat Unit Structure by INADEQUATE NMR", *Macromolecules*, Vol. 25, pp. 6455-6459, 1992.

20. Wandrey, C., J. Hernandez-Barajas and D. Hunkeler, "Diallyldimethylammonium Chloride and its Polymers", *Adv. Polym. Sci.*, Vol. 145, pp. 123-179, 1999.

21. Vaidya, R. A. and L. J. Mathias, "On Predicting Free Radical Polymerizability of Allyl Monomers. MINDO/3 and ^{13}C NMR Results", *J. Polym. Sci. Polym. Symp.*, Vol. 74, pp. 243-251, 1986.

22. Pople, J. A. and G. A. Segal, "An Approximate Self-Consistent Molecular Orbital Theory II. Calculations with Complete Neglect of Differential Overlap", *J. Chem. Phys.*, Vol. 43, pp. 136-149, 1965.

23. Dewar, M. J. S. and W. Thiel, "Ground States of Molecules, 38, The MNDO Approximations and Parameters", *J. Am. Chem. Soc.*, Vol. 99, No. 22, pp. 4899-4907, 1977.

24. Stewart, J. J. P. "Optimization of Parameters for Semiempirical Methods I. Method", *J. Comp. Chem*, Vol. 10, pp. 209-220, 1989.

25. Stewart, J. J. P., "Optimization of Parameters for Semiempirical Methods II. Applications", *J. Comp. Chem*, Vol. 10, pp. 221-264, 1989.

26. Parr, R. G. and W. Yang, *Density Functional Theory of Atoms and Molecules*, Oxford University Press, New York, 1989.

27. Flurchick, K. and J. L. Bartolotti, "An Introduction to Density Functional Theory", *Reviews in Computational Chemistry*, Vol. 7, pp. 187-189, New York, 1996.

28. Becke, D., "A New Mixing of Hartree-Fock and Local Density-Functional Theories", *J. Chem. Phys.*, Vol. 98, No. 2, pp. 1372-1377, 1993.

29. Lee, C. T., W. T. Yang and R. G. Parr, "Development of the Colle-Salvetti Correlation-Energy Formula into a Functional of the Electron-Density", *Phys. Rev. B.*, Vol. 37, No. 2, pp. 785-789, 1988.

30. Foresman, J.B. and E. Frisch, *Exploring Chemistry with Electronic Structure Methods*, pp. 118-119, Gaussian Inc., Pittsburgh, 1997.

31. Becke, D., "Density-Functional Thermochemistry. III. The Role of Exact Exchange", *J. Chem. Phys.*, Vol. 98, No. 7, pp. 5648-5652, 1993.

32. Hasaneiv, A., *Computational Methods in Quantum Chemistry*, World Scientific, pp. 158-161, New Jersey, 1995.

33. Leach A. L., *Molecular Modelling-Priciples and Applications*, Longman, Singapore, 1996.

34. Moller C. and M. S. Plesset, "Note on Approximate Treatment for Many-Electron Systems", *Phys. Rev.*, Vol. 46, pp. 618-622, 1934.

35. Baekelandt, B. G., A. Cedillo and R. G. Parr, "Reactivity Indexes and Fluctuation Formulas in Density Finctional Theory-Isomorphic Ensembles and a New Measure of Local Hardness", *J. Chem. Phys.*, Vol. 103, pp. 8548, 1995.

36. Chermette H., "Chemical Reactivity Indexes in Density Functional Theory", *J. Comp. Chem.*, Vol. 20, pp. 129-154, 1999.

37. Pearson R.G., "Maximum Chemical and Physical Hardness", *J. Chem. Edu.*, Vol. 76, pp. 267-275, 1999.

38. Parr R.G. and W. Yang, "Density functional approach to the frontier-electron theory of chemical reactivity", *J. Am. Chem. Soc.*, Vol. 106, pp. 4049-4050, 1984.

39. Berkowitz, M. and R. G. Parr, "Molecular Hardness and Softness; Local Hardness and Softness, Hardness and Softness Kernels and Relations Among These Quantities", *J. Chem. Phys.*, Vol. 88, pp. 2554-2557, 1988.

40. Onsager, L., "Electric Moments of Molecules in Liquids", *J. Am. Chem. Soc.*, Vol. 58, pp. 1486-1495, 1936.

41. Miertus, S., E.Scrocco and J.Tomasi, "Electrostatic Interactions of a Solute with a Continuum. A Direct Utilization of Ab-initio Molecular Potentials for the Prevision of Solvent Effects", *Chem. Phys.* Vol. 55, pp. 117-129, 1981.

42. Tomasi, J. and M.Persico, "Molecular-Interactions in Solution-An Overview of Methods Based on Continuous Distributions of the Solvent", *Chem. Rev.*, Vol. 94, pp. 2027-2094, 1994.

43. Cammi, R. and J.Tomasi, "Remarks on the Use of the Apparent Surface-Charges (ASC) Methods in Solvation Problems-Iterative versus Matrix-Inversion Procedures and the Normalization of the Apparent Charges", *J. Comp. Chem.*, Vol. 16, pp. 1449-1458, 1995.

44. Foster, P. and F. Weinhold, "Natural Hybrid Orbitals", *J. Am. Chem. Soc.*, Vol. 102, pp. 7211-7218, 1980.

45. Reed, A. E. and F. Weinhold, "Natural Bond Orbital Analysis of Near-Hartree-Fock Water Dimer", *J. Chem. Phys.*, Vol. 78, pp. 4066-4073, 1983.

46. Reed, A. E., R. B. Weihstock and F. Weinhold, "Natural-Population Analysis", *J. Chem. Phys.*, Vol. 83, pp. 735-746, 1985.

47. Reed, A. E. and F. Weinhold, "Natural Localized Molecular-Orbitals", *J. Chem. Phys.*, Vol. 83, pp. 1736-1740, 1985.

48. Reed, A. E., L. A. Curtiss and F. Weinhold, "Intermolecular Interactions from a Natural Bond Orbital, Donor-Acceptor Viewpoint", *Chem. Rev.* (Washington D.C.), Vol. 88, pp. 899-926, 1988.

49. Weinhold, F., "Chemical Bonding as Superposition Phenomenon", *Chem. Ed.* Vol. 76, pp. 1141-1146, 1999.

50. Weinhold, "Natural Bond Orbital Methods", in P. v. R. Schleyer, N. L. Allinger, T. Clark, J. Gasteiger, and P. A. Kollman (eds.), Encyclopedia of Computational Chemistry, Vol. 3, pp. 1792-1811, Wiley, Chichester, UK, 1998.

51. Odian, G., *Principles of Polymerization*, Wiley Interscience, 3rd ed., New York, 1991.

52. Yamada, B., A. Matsumoto and T. Otsu, "Effects of Large Ring Substituents on Radical Polymerization Behavior of 2,6-Diisopropylphenyl Methacrylate", *Makromol. Chem.*, Vol. 192, pp. 1921-1929, 1991.

53. Gallardo, A. and San Román, J, "Kinetic Behavior of Methacrylic Monomers with Large Polar Side Substituents in Free Radical Polymerization", *Macromolecules*, Vol. 25., pp.5836-5840, 1992.

54. Hatada, K, K, Nagata, T. Hasegawa and H. Yuki, "Carbon-13 NMR Spectra and Reactivities of Vinyl Compounds in Ionic and Radical Polymerizations", *Makromol. Chem.*, Vol. 178, pp. 2413, 1977.

55. Avcı, D. S. H. Küsefoğlu, R. D., Thompson and L. J. Mathias. "ESter Derivatives of a-Hydroxymethylacrylates: Itaconate Isomers Giving High Molecular Weight Polymers", *J. Polym. Sci. Polym. Chem. Ed.*, Vol. 32, 2937-2945, 1994.

56. SPARTAN Version 5.1.1, Wavefunction, Inc. 18401 Von Karmen Ave, #370 Irvine CA 92715.

57. Willkinson L, *The System for Statistics*, Evanston, I. L (Ed), SYSTAT, Inc., 1987.

58. Kodaira, T., T. Fujisawa, Q-Q. Liu and M. Urushisaki, "Cyclopolymerization. 22. Radical Polymerization of N-Methyl-N-allyl-2-(methoxycarbonyl)allylamine: Design of Unconjugated Dienes with High Polymerizability and High Cyclization Tendency Using Functional Groups of Low Polymerizabilities", *Macromolecules*, Vol. 29, pp. 484-485, 1996.

59. Matsumoto, A., Deguchi, A., Oiwa, M., *Polym. Prepr. Jpn.*, Vol. 39, pp. 1451, 1990.

60. Hahn, M. and W. Jaeger, "Kinetics of the Free Radical Polymerization of Dimethyl Diallyl Ammonium Chloride, 5", *Angew. Makromol. Chem.*, Vol. 198, pp.165-178, 1992.

61. Frisch, M. J., G. W. Trucks, H. B. Schlegel, G. E. Scuseria, M. A. Robb, J. R. Cheeseman, V. G. Zakrzewski, J. A. Montgomery, Jr., R. E. Stratmann, J. C. Burant, S. Dapprich, J. M. Millam, A. D. Daniels, K. N. Kudin, M. C. Strain, O. Farkas, J. Tomasi, V. Barone, M. Cossi, R. Cammi, B. Mennucci, C. Pomelli, C. Adamo, S. Clifford, J. Ochterski, G. A. Petersson, P. Y. Ayala, Q. Cui, K. Morokuma, D. K. Malick, A. D. Rabuck, K. Raghavachari, J. B. Foresman, J. Cioslowski, J. V. Ortiz, A. G. Baboul, B. B. Stefanov, G. Liu, A. Liashenko, P. Piskorz, I. Komaromi, R. Gomperts, R. L. Martin, D. J. Fox, T. Keith, M. A. Al-Laham, C. Y. Peng, A. Nanayakkara, C. Gonzalez, M. Challacombe, P. M. W. Gill, B. Johnson, W. Chen, M. W. Wong, J. L. Andres, C. Gonzalez, M. Head-Gordon, E. S. Replogle, and J. A. Pople, *Gaussian 98 Revision A.7*, Gaussian Inc., Pittsburgh PA, 1998.

62. Tantillo, D. J., K. N. Houk and M. E. Jung, "Origins of Stereoselectivity in Intramolecular Diels-Alder Cycloadditions of Dienes and Dienophiles Linked by Ester and Amide Tethers", *J. Org. Chem.*, Vol. 66, 1938-1940, 2001.

63. Gonzalez, C. and H. B. Schlegel, "An Improved Algorithm for Reaction-Path Following", *J. Chem. Phys.*, Vol. 90, pp. 2154-2161, 1989.

64. Gonzalez, C. and H. B. Schlegel, "Reaction Path Following in Mass-Weighted Internal Coordinates", *J. Phys. Chem.* Vol. 94, pp. 5523-5527, 1990.

65. McCormick, C. L., "Comments on 'Recent Developments in Polymerization by an Alternating Intra-Intermolecular Mechanism' by George B. Butler", *J. Polym. Sci., Part A, Polym. Chem.*, Vol. 34, pp. 911-912, 1996.

66. Spellmeyer, D. C. and K. N. Houk, "A Force-Field Model for Intramolecular Radical Additions", *J. Org. Chem.*, Vol. 52, pp. 959-974, 1987.

67. Beckwith, A. L. J., "Regioselectivity and Stereo-Selectivity in Radical Reactions", *Tetrahedron*, Vol. 37, pp. 3073-3100, 1981.

68. Beckwith, A. L. J. and C. H. Schiesser, "Regio- and Stereo-Selectivity of Alkenyl Radical Ring Closure: A Theoretical Study", *Tetrahedron*, Vol. 41, pp. 3925-3941, 1985.

69. Hartung, J., R. Stowasser, D. Vitt and G. Bringmann, "5-exo or 6-endo? Exploring Transition State Structures in Cyclizations of 4-Penten-1-oxyl Radicals", *Angew. Chem. Int. Ed., Engl.*, Vol. 35, pp. 2820-2823, 1996.

70. Canadell, E. and J. Igual, "MINDO/3 Calculations on Enthalpy and Entropy Effects in the Cyclization of the Hex-5-enyl, 2-Methylhex-5-enyl and 5-Methylhex-5-enyl Radicals", *J. Chem. Soc., Perkin Trans. II*, pp. 1331-1337, 1987.

71. Della, E. W. and A. M. Knill, "A Theoretical and Experimental Investigation of the Kinetics of Ring Closure of the 3-Methyl-3-azahex-5-enyl Radical", *Aust. J. Chem.*, Vol. 48, pp. 2047-2051, 1995.

72. Beckwith, A. L. J., C. J Easton, T. Lawrance and A. K. Serelis, "Reactions of Methyl-Substituted Hex-5-enyl and Pent-4-enyl Radicals", *Aust. J. Chem.*, Vol. 36, pp. 545-556, 1983.

73. Jursic, B. S., "Preference in Formation of Three-, Five- and Six-membered Rings in Cyclization of the Primary Unsaturated Radical Studied with the Hybrid Density Functional Theory Method", *J. Mol. Struct. (Theochem)*, Vol. 492, pp. 285-291, 1999.

74. Baldwin, J. E., "Rules for Ring Closure", *J. Chem. Soc., Chem. Commun.*, pp. 734-736, 1976.

75. Winans, R. E. and C. F. J. Wilcox, "Comparison of Stereopopulation Control with Conventional Steric Effects in Lactonization of Hydrocoumarinic Acids", *J. Am. Chem. Soc.*, Vol. 98, pp. 4218-4285, 1976.

76. Danforth, C., A. W. Nicholson, J. C. James and G. M. Loudon, "Steric Acceleration of Lactonization Reaction: An Analysis of Stereopopulation Control", *J. Am. Chem. Soc.*, Vol. 98, pp. 4275-4281, 1976.

77. Capon, B. and S. P. McManus, *Neighboring Group Participation*, Vol. 1, Plenum Press, New York, pp. 58-75, 1976.

78. Kirby, A. J., "Effective Molarities for Intramolecular Reactions", *Adv. Phys. Org. Chem.*, 17, 183-278, 1980.

79. Sternbach, D. D., D. M. Rossana and K. D. Onan, "Intramolecular Diels-Alder Reactions with Furan - The Gem-dialkyl Effect Revisited", *Tetrahedron Lett.*, Vol. 26, pp. 591-594, 1985.

80. Sternbach, D. D. and D. M. Rossana, "Intramolecular Diels Alder Reactions of the Furan Diene - Substituent and Solvent Effects", *Tetrahedron Lett*, Vol. 23, pp. 303-306, 1982.

81. Jung, M. E. and J. Gervay, "Studies on The Effect of Substituents on the Rate Enhancements in Intramolecular Diels-Alder Reactions-Reasons for the Gem-Dimethyl Effect", *Tetrahedron Lett.*, Vol. 29, pp. 2429-2432, 1988.

82. Curtin., M. L. and W. H. Okamura, "Synthetic and kinetic studies of the intramolecular Diels-Alder reactions of cycloalkenylallenylphosphine oxides Michael", *J. Org. Chem.*, Vol. 55, pp. 5278-5287, 1990.

83. De Corte., F., F. Nuyttens., S. Cauwberghs and P. De Clercq, "Rate Acceleration of the Intramolecular Diels-Alder Reaction With the Furan-Diene by Anchoring Substitution-The T-Butyl Effect Revisited", *Tetrahedron Lett.*, Vol. 34, pp. 1831-1832, 1993.

84. Jung, M. E. and J. Gervay, "Solvent Effects in Intramolecular Diels-Alder Reactions of 2-Furfuryl Methyl Fumarates: Evidence for a Polar Transition State", *J. Am. Chem. Soc.*, Vol. 111, pp. 5469-5470, 1989.

85. Jung, M. E. and J. Gervay, "Gem-Dialkyl Effect in The Intramolecular Diels-Alder Reaction of 2-Furfuryl Methyl Fumarates: The Reactive Rotamer Effect, The Enthalpic Basis for Acceleration, and Evidence for a Polar Transition State", *J. Am. Chem. Soc.*, Vol. 113, pp.224-232, 1991.

86. Walkup, R. D., N. U Obeyesekere and R. R. Kane, "Gem-Dialkyl Effect", *Chem. Lett.*, pp. 1055-1058, 1990.

87. Jung, M. E., "Substituent and Solvent effects in Intramolecular Diels-Alder Reactions", *Synlett*, pp. 186-190, 1990.

88. Jung, M. E., "New *Gem-* and *Vic*-Disubstituent Effects on Cyclization", *Synlett*, pp. 843-846, 1999.

89. Jung, M. E., R. Marquez and K. N. Houk, "The Influence of Geminal Disubstitution on Efficiencies of 4-Exo-Trig Radical Cyclizations", *Tetrahedron Lett.*, Vol. 40, pp. 2661-2664, 1999.

90. Giessner-Prettre, C., S. Huckel, J. Maddaluno and M. E. Jung, "Molecular Mechanics/Continuum Reaction Field/Quantum Mechanics Study of the Intramolecular Diels-Alder Reaction of 2-Furfuryl Derivatives", *J. Org. Chem*, Vol. 62, pp.1439-1448, 1997.

91. Jung, M. E. and R. Marquez, "Gem-disubstituent Effects in Small Ring Formation: Novel Ketal Ring Size Effect", *Tetrahedron Lett.*, Vol. 38, pp. 6521-6524, 1997.

92. Schleyer, P. v. R., "The Thorpe-Ingold Hypothesis of Valency Deviation. Intramolecular Hydrogen Bonding in 2-Substituted Propane-1,3-diols", *J. Am. Chem. Soc.*, Vol. 83, pp. 1368-1373, 1961.

93. Bruice, T. C. and U. K. Pandit, "The Effect of Geminal Substitution Ring Size and Rotamer Distribution on the Intramolecular Nucleophilic Catalysis of the Hydrolysis of Monophenyl Esters of Dibasic Acids and the Solvolysis of the Intermediate Anhydrides Thomas", *J. Am. Chem. Soc.*, Vol. 82, pp. 5858- 5865, 1960.

94. Parrill, A. L. and D. P. Dolata, "The Facilitated Transition Hypothesis as an Explanation for the Gem-dialkyl Effect", *J. Mol. Struct. (Theochem)*, Vol. 370, pp.187-202, 1996.

95. Tuzun, N. S., V. Aviyente, D. Avci and N. Ince, "A Computational Approach to the Polymerizabilities of Diallylamines", *J. Molec. Model.*, Vol. 7,pp. 257-264, 2001.

96. Tuzun N. S., V. Aviyente and K. N. Houk, "Theoretical Study of Factors Controlling Rates of Cyclization of Radical Intermediates From Diallylamine and Diallylammonium Monomers in Radical Polymerizations", *J. Org. Chem.*, Vol. 67, pp. 5068-5075, 2002.

97. Chirlian, L. E. and M. M. Francl "Atomic Charges Derived from Electrostatic Potentials: A Detailed Study", *J. Comp. Chem.*, Vol. 8, 894-905, 1987.

98. Capon, B. and C. W. Rees, "Reaction Mechanisms", *Annu. Rep. Chem. Soc.*, Vol. 61, pp. 221-298, 1964.

99. Julia, M.; C. Descoins; M. Baillarge; B. Jacquet; D. Uguen and F. A. Graeger, "Inhibition Sterique de la Formation Du Cycle", *Tetrahedron*, Vol. 31, pp. 1737-1744, 1975.

100. Héberger, K.; M. Walbiner and H. Fischer, "Addition of Benzyl Radicals to Alkenes: The Role of Radical Deformation in The Transition State", *Angew. Chem.* 1992, *104*, 651; *Angew. Chem., Int. Ed. Engl.*, Vol. 31, pp. 635-636, 1992.

101. Fischer, H. and L. Radom, "Theoretical Study of Factors Controlling the Addition of Carbon Centered Radicals to Alkenes-An Experimental and Theoretical Perspective", *Angew. Chem. Int. Ed. Engl.* Vol. 40, 1340-1371, 2001.

102. Liu Q-Q., T. Kodaira, M. Urushisaki and T. Hashimoto "Cyclopolymerization XXIII. Desing of Unconjugated Dienes with High Polymerizability Using Functional Groups with No Homopolymerization Tendency and Synthesis of Completely Cyclized Polymers Therefrom: Radical Polymerizations of N-Substituted N-Allyl-2-(methoxycabonyl)allylamines", *Polym. J.*, Vol. 28, pp. 1000-1005, 1996.

103. Tuzun, N. S. and V. Aviyente, "A Computational Study on The Substituent Effect of Diallylamine Monomers in Their Cyclopolymerization Reactions ", *J. Phys. Chem. A.*, Vol. 106, pp. 8184-8190, 2002.

104. Kirby, A. J., *The Anomeric Effect and Related Stereoelectronic Effects at Oxygen*, Springer-Verlag, Berlin, 1983.

105. Beckwith, A. L. J. and P. J. Duggan, "The Quasi-Homo Anomeric Interaction in Substituted Tetrahydropyranyl Radicals: Structure and Kinetics of Formation", *Tetrahedron*, Vol. 54, pp. 4623-4632, 1998.

106. Dupuis, J., B. Giese, D. Ruegge, H. Fischer, H. G. Korth and R. Sustmann, "Conformation of Glycosyl Radicals: Radical Stabilization by β-CO Bonds", *Angew. Chem. Int. Ed. Engl*, Vol. 23, pp. 896-897, 1984.

107. Beckwith, A. L. J., V. W. Bowry and G. Moad, "Kinetics of the Coupling Reactions of the Nitroxyl Radical 1, 1, 3, 3-Tetramethylisoindoline-2-oxyl with Carbon-Centered Radicals", *J. Org. Chem.*, Vol. 53, pp. 1632-1641, 1988.

108. Burkhard, P., E. Roduner, J. Hochmann and H. Fischer, "Absolute Rate Constants for Radical Rearrangements in Liquids Obtained by Muon Spin Rotation", *J. Phys. Chem.*, Vol. 88, 773-777, 1984.

109. Butler, G. B., *Cyclopolymerization and Cyclocopolymerization*, Marcel Dekker, New York, pp. 416, 1992.

110. Beckwith, A. L. J., A. K. Ong and D. H. Dolomon, "Cyclopolymerization 2. Electron Spin Resonance Studies of Free-Radical Reactions of Some Diolefins", *J. Macromol. Sci.-Chem. A*, Vol. 9, pp. 115-124, 1975.

111. Bartlett, P. D. and F. A. Tate, "The Polymerization of Allyl Compounds. VI. The Polymerization of Allyl-1-d_2 Acetate and the Mechanism of its Chain Termination Paul ", *J. Am. Chem. Soc.*, Vol. 75, pp.91-95, 1953.